

1996

# The CFTR (Cystic Fibrosis Transmembrane Conductance Regulator) Channel: Anion Permeation, and Regulation by Adenylyl Cyclase and ATP Hydrolysis

Athanasios G. Dousmanis

Follow this and additional works at: [http://digitalcommons.rockefeller.edu/student\\_theses\\_and\\_dissertations](http://digitalcommons.rockefeller.edu/student_theses_and_dissertations)

 Part of the [Life Sciences Commons](#)

---

## Recommended Citation

Dousmanis, Athanasios G., "The CFTR (Cystic Fibrosis Transmembrane Conductance Regulator) Channel: Anion Permeation, and Regulation by Adenylyl Cyclase and ATP Hydrolysis" (1996). *Student Theses and Dissertations*. 344.  
[http://digitalcommons.rockefeller.edu/student\\_theses\\_and\\_dissertations/344](http://digitalcommons.rockefeller.edu/student_theses_and_dissertations/344)

This Thesis is brought to you for free and open access by Digital Commons @ RU. It has been accepted for inclusion in Student Theses and Dissertations by an authorized administrator of Digital Commons @ RU. For more information, please contact [mcsweej@mail.rockefeller.edu](mailto:mcsweej@mail.rockefeller.edu).





**THE CFTR (CYSTIC FIBROSIS TRANSMEMBRANE CONDUCTANCE  
REGULATOR) CHANNEL: ANION PERMEATION, AND  
REGULATION BY ADENYLYL CYCLASE  
AND ATP HYDROLYSIS**

by

Athanasios George Dousmanis

A thesis submitted in partial fulfillment of the  
requirements for the degree of

**DOCTOR OF PHILOSOPHY**

at

**THE ROCKEFELLER UNIVERSITY**

April 1996







## DEDICATION

*To my parents, Marilyn and John, for their love and support.*



## ACKNOWLEDGMENTS

I would like to acknowledge, first and foremost, the patient, steady guidance, and thoughtful support, of my thesis advisor, Dr. David C. Gadsby. I thank him for the privilege of being his first graduate student. He has been an exemplar of a scrupulous, focused, and rigorous scientist.

I wish to express my gratitude to the other members of the thesis committee, Drs. Olaf S. Andersen, Christopher Miller, Angus C. Nairn, and Torsten Wiesel, for their very helpful suggestions and contributions. In particular, I thank Dr. Andersen for generously giving his time and expertise, providing substantial criticism and assistance in data analysis.

I am indebted to Dr. Donald W. Hilgemann for allowing me to visit his laboratory in order to benefit from his considerable expertise with the giant excised-patch technique. His brand of enthusiasm proved, improbable as it may seem, inspiring. I am also grateful to several members of the Gadsby laboratory: to Dr. Tzyh-Chang Hwang, for assistance with the early whole-cell experiments, to Dr. Georg Nagel, for his construction of the giant-patch rig, and to Drs. Young-Bae Park, Ann Sostman, Steven K. Sullivan, and Jonathan Wagg for critical reading of portions of the Thesis and for many helpful discussions.

I thank Peter Hoff for his technical assistance throughout all stages of this study, for help in the preparation of the myocytes, and for his gentle sense of humor, and Mari Kuwabara, for her assistance in the final assembly of the thesis.

I would like to thank Michael Chen, of the electronics shop, and John Doherty, of the instrument maker's shop, for their extremely kind, substantial, and timely assistance, Dr. Harry Wms. Harper, for assistance in modifying the computer systems for data acquisition and analysis, and Pat Griffin, of the faculty and student's club, for our shared avocation.

Finally, I would like to thank fellow graduate students K. Chris Min and Mark M. Wurfel, for much unreciprocated assistance, and for being models of young, committed scientists.





## TABLE OF CONTENTS

Abstract .....	1
Chapter 1: INTRODUCTION.....	3
I. Overview.....	3
II. Cystic Fibrosis.....	4
III. Characteristics of the CFTR Protein.....	5
IV. CFTR is a Regulated Chloride Channel.....	7
V. CFTR in Mammalian Heart.....	8
VI. Physiological Role of CFTR in Mammalian Heart.....	10
VII. Regulation of Whole-Cell CFTR Cl <sup>-</sup> Conductance in Mammalian Heart.....	13
A. Stimulation of adenylyl cyclase activates CFTR Cl <sup>-</sup> conductance .....	13
B. Inhibition of adenylyl cyclase diminishes CFTR Cl <sup>-</sup> conductance .....	16
C. CFTR Cl <sup>-</sup> channel phosphorylation governs the ability of nucleotide to gate channel opening and closing .....	17
VIII. CFTR Regulation by Nucleoside Triphosphate.....	20
A. CFTR Cl <sup>-</sup> channels require hydrolyzable nucleoside triphosphate to open .....	20



B.	CFTR Cl <sup>-</sup> channels require nucleoside triphosphate to close.....	21
C.	Nucleoside triphosphate action at NBD1 opens channels, and, at NBD2, closes channels.....	21
D.	Inorganic phosphate (P <sub>i</sub> ) analogs act at NBD1, and AMP-PNP acts at NBD2.....	22
IX.	Mammalian Cardiac CFTR and Human Epithelial CFTR are Functionally Identical .....	23
X.	Permeability/Selectivity .....	24
A.	Background.....	24
B.	Permeation through CFTR channels.....	30
XI.	Outline .....	32
Chapter 2: MATERIALS AND METHODS.....		33
I.	Isolation of Cardiac Myocytes.....	33
II.	Composition of Solutions.....	35
A.	Whole-cell solutions .....	35
B.	Excised-patch solutions .....	37
III.	Whole-Cell Recording.....	41
IV.	Excised-Patch Recording.....	46
V.	Channel Density.....	52
VI.	Junction Potentials .....	53



VII.	Data Analysis.....	53
A.	Whole-cell experiments .....	53
B.	Excised-patch experiments .....	55
VIII.	Statistics.....	57
Chapter 3:	UPSTREAM REGULATION OF THE CARDIAC CFTR Cl <sup>-</sup> CHANNEL .....	58
I.	Introduction.....	58
II.	Results .....	58
III.	Discussion .....	70
A.	Cl <sup>-</sup> conductance provides a convenient monitor of adenylyl cyclase activity .....	70
B.	Is cardiac CFTR Cl <sup>-</sup> conductance activated without hormone stimulation? .....	71
C.	Do G <sub>s</sub> , and G <sub>i</sub> , and forskolin bind to independent sites on adenylyl cyclase?.....	72
Chapter 4:	PERMEATION THROUGH THE CARDIAC CFTR Cl <sup>-</sup> CHANNEL PORE .....	76
I.	Introduction.....	76
II.	Results .....	76
A.	Cl <sup>-</sup> accumulation/depletion .....	76
B.	Anion selectivity of the cardiac CFTR channel.....	80



C.	Single channel Cl <sup>-</sup> conductance and permeability coefficient.....	85
D.	Relative anion permeability determined by shifts in whole-cell bi-ionic reversal potentials .....	88
E.	Gating and regulatory effects on relative permeability measurements .....	94
F.	Sizing the pore.....	101
III.	Discussion .....	104
A.	E <sub>rev</sub> deviation from E <sub>Cl</sub> .....	104
B.	Inferences about the anion binding site in the pore .....	109
C.	Estimate of minimum pore diameter.....	113
D.	Single channel Cl <sup>-</sup> conductance and permability coefficient.....	114
Chapter 5: ROLE OF THE NUCLEOTIDE BINDING DOMAINS IN CFTR CHANNEL REGULATION .....		
I.	Introduction.....	116
II.	Results .....	116
A.	[ATP] dependence of channel P <sub>o</sub> .....	116
B.	[Mg <sup>2+</sup> ] dependence of channel opening rate.....	124
C.	[Mg <sup>2+</sup> ] dependence of channel closing rate.....	132
D.	AMP-PNP can substitute for ATP at NBD2.....	141
E.	Phosphorylation level of a single channel molecule governs channel open time.....	145
III.	Discussion .....	150
A.	Simplified gating scheme for CFTR channels.....	150





B.	Dependence of channel gating on phosphorylation status .....	154
C.	Influence of free $[Mg^{2+}]$ on channel gating.....	155
D.	Stoichiometry of coupling of ATP hydrolysis to channel closing.....	156
E.	Resemblance of NBD function to that of G proteins .....	157
F.	High affinity binding of ATP at NBD2 .....	158
Bibliography .....		160



## LIST OF FIGURES

<i>Number</i>	<i>Page</i>
1. Proposed topological model of CFTR.....	6
2. Regulatory pathway of the CFTR Cl <sup>-</sup> channel in a mammalian ventricular myocyte .....	14
3. Inward shift in holding current observed when bath [Mg <sup>2+</sup> ] is lowered is associated with a decrease in seal resistance (R <sub>s</sub> ).....	42
4. Whole-cell configuration.....	45
5. Inside-out, excised-patch configuration.....	50
6. Channel density in excised membrane patches .....	51
7. Activation and deactivation of the whole-cell CFTR Cl <sup>-</sup> conductance ..	60
8. Carbachol inhibition of the Iso-activated Cl <sup>-</sup> conductance cannot be overcome by maximal concentrations of Iso .....	63
9. Carbachol inhibition of the Fsk-activated Cl <sup>-</sup> conductance can be overcome by maximal concentrations of Fsk .....	66
10. Dose-response relations for Iso- and Fsk-activated currents in the absence and presence of CCh .....	69
11. Effects of Cl <sup>-</sup> accumulation and Cl <sup>-</sup> depletion on E <sub>rev</sub> measurements.	79
12. Anion selectivity of the cardiac CFTR channel .....	83



13. Single channel conductance and permeability coefficient of the locked open cardiac CFTR Cl <sup>-</sup> channel .....	87
14. Relative anion permeability determined by the shift in bi-ionic reversal potential of the Iso- or Fsk-activated Cl <sup>-</sup> conductance.....	90
15. Relative permeability of six anions through the cardiac CFTR channel .....	93
16. Nitrate permeability is unaffected by locking open the cardiac CFTR channel.....	97
17. Iodide permeability is unaffected by locking open the cardiac CFTR channel.....	100
18. Dependence of relative anion permeability on mean ion diameter....	105
19. [ATP] dependence of relative channel open probability .....	120
20. Summary of [ATP] dependence of relative channel open probability.	121
21. Increase in P <sub>o</sub> as [ATP] is raised reflects a decrease in channel closed time.....	123
22. Complete removal of bath Mg <sup>2+</sup> prevents channel opening.....	126
23. Channel opening and closing rates both depend on [Mg <sup>2+</sup> ].....	127
24. Latency to first channel opening depends on [Mg <sup>2+</sup> ].....	130
25. Summary of [Mg <sup>2+</sup> ] dependence of channel opening rate.....	131
26. Channel closing depends on [Mg <sup>2+</sup> ] .....	135
27. [Mg <sup>2+</sup> ] dependence of channel closing rate.....	136



28.	Ability of low $[Mg^{2+}]$ to slow channel closing depends on degree of channel phosphorylation .....	140
29.	The ATP analog AMP-PNP can lock channels open.....	142
30.	Channel locking and unlocking rates using the ATP analog AMP-PNP.....	143
31.	Open time of a single channel molecule depends on degree of channel phosphorylation.....	147
32.	Summary of phosphorylation dependence of open times of a single CFTR channel.....	148
33.	Schematic model of the regulation of the two NBDs by incremental phosphorylation.....	152





## LIST OF TABLES

<i>Number</i>	<i>Page</i>
1. Composition of whole-cell solutions.....	36
2. Composition of excised-patch solutions.....	38
3. Anion selectivity of the cardiac CFTR channel .....	84
4. Permeability ratios of anions in the cardiac CFTR channel.....	102



## ABBREVIATIONS

AMP-PNP.....	5'-adenosine( $\beta,\gamma$ -imino)triphosphate
Asp <sup>-</sup> .....	DL-aspartate
ATP.....	adenosine 5'-triphosphate
CCh.....	carbachol (carbamylcholine)
CDTA.....	trans-1,2-diaminocyclohexane-N,N,N',N'-tetraacetic acid
CFTR.....	Cystic Fibrosis Transmembrane conductance Regulator
EGTA.....	ethylene glycol-bis( $\beta$ -aminoethyl ether)N,N,N',N'-tetraacetic acid
Fsk.....	forskolin
Glc.....	D-(+)-glucose
GTP.....	guanosine 5'-triphosphate
HEPES.....	N-[2-hydroxyethyl]piperazine-N'-[2-ethanesulfonate]
Iseth <sup>-</sup> .....	2-hydroxyethane sulfonate
Iso.....	isoproterenol
NBD.....	nucleotide binding domain
NMG <sup>+</sup> .....	N-methyl-D-glucamine
MeSO <sub>3</sub> <sup>-</sup> .....	methanesulfonate
PKA.....	cyclic AMP-dependent protein kinase
P <sub>o</sub> .....	open probability
Pyr <sup>-</sup> .....	pyruvate ( $\alpha$ -ketopropionate)
TEA <sup>+</sup> .....	tetraethyl-ammonium



# THE CFTR (CYSTIC FIBROSIS TRANSMEMBRANE CONDUCTANCE REGULATOR) CHANNEL: ANION PERMEATION, AND REGULATION BY ADENYLYL CYCLASE AND ATP HYDROLYSIS

by

Athanasios George Dousmanis

Submitted on April 11, 1996, in partial fulfillment  
of the requirements for the degree of  
Doctor of Philosophy

## Abstract

CFTR Cl<sup>-</sup> channel function and regulation were studied in guinea-pig ventricular myocytes, using either the whole-cell or excised inside-out patch configurations of the patch clamp technique. A typical myocyte cell membrane contained a total of ~1400 CFTR channels; channel density was ~0.11  $\mu\text{m}^{-2}$ . Using whole-cell CFTR Cl<sup>-</sup> conductance as an on-line assay of cAMP levels, we examined the interaction of the adenylyl cyclase (AC) modulators forskolin (Fsk), and the GTP-binding proteins G<sub>s</sub> and G<sub>i</sub>. In the presence of GTP, maximal activation of G<sub>i</sub> using the muscarinic acetylcholine receptor agonist carbachol (CCh) reduced the efficacy with which the  $\beta$ -adrenoceptor agonist isoproterenol (Iso) activated AC, with little effect on potency, whereas CCh decreased the potency but not the efficacy of Fsk, a direct activator of AC. Thus, G<sub>i</sub> appeared to act like a competitive inhibitor of Fsk's stimulatory action on AC, but like a non-competitive inhibitor of Iso's stimulatory action.

Anion selectivity of CFTR channels was determined by shifts of the reversal potential ( $E_{\text{rev}}$ ) for CFTR channel current on changes in extracellular [Cl<sup>-</sup>] ([Cl<sup>-</sup>]<sub>o</sub>):  $E_{\text{rev}}$  shifted roughly linearly with  $\log [\text{Cl}^-]_o$ , with a slope of  $-57 \pm 3$  mV, close to the Nernst prediction of -61.5 mV, implying that CFTR channels are relatively anion selective. Relative permeability to several anions was determined by shifts of whole-cell bi-ionic reversal potential, both with normal channel gating, and with channels locked open using the ATP analog AMP-PNP. The sequence of relative permeabilities was unaffected by channel gating, and was: **NO<sub>3</sub><sup>-</sup>** ( $1.74 \pm 0.04$ ) > **Br<sup>-</sup>** ( $1.51 \pm 0.06$ ) > **I<sup>-</sup>** ( $1.30 \pm 0.07$ ) > **Cl<sup>-</sup>** (1.0) > **F<sup>-</sup>** ( $0.25 \pm 0.03$ ) > **Aspartate<sup>-</sup>** ( $0.07 \pm 0.01$ ) >> **Isethionate** (0.05), **HEPES** (0.03). Although I<sup>-</sup> was more permeant than Cl<sup>-</sup>,



it reduced current both at positive and at negative potentials, indicating that  $I^-$  ions readily enter CFTR channels, but leave them more slowly than  $Cl^-$  ions. This sequence suggests that the anion binding site within the pore is a relatively weak site (Eisenman sequence II). The minimum pore diameter appears to be  $\sim 7$  Å. The single channel conductance ( $\gamma$ ) in symmetric 160 mM  $Cl^-$ , determined with single channels isolated in excised patches and locked open with AMP-PNP, was  $10.3 \pm 0.4$  pS; the permeability coefficient for  $Cl^-$  ( $P_{Cl}$ ) was  $2 \times 10^{-17} \pm 9 \times 10^{-19}$  cm<sup>3</sup>s<sup>-1</sup>.

Protein kinase A (PKA)-phosphorylated CFTR  $Cl^-$  channels require hydrolyzable nucleoside triphosphate to open and close normally. Individual CFTR channels were studied in excised membrane patches to examine how nucleoside triphosphate action at one or both of the nucleotide binding domains (NBDs) controls channel activity. At 1.2 mM free  $[Mg^{2+}]$ , channel open probability ( $P_o$ ) increased hyperbolically with  $[ATP]$  ( $K_{0.5} \sim 35$   $\mu$ M  $[ATP]$ ), largely due to an increase in opening rate. That ATP hydrolysis governs channel opening is almost certain, since all ATPases require  $Mg^{2+}$ , and  $Mg^{2+}$  ions were absolutely required for channel opening by ATP. Thus, at 2 mM  $[ATP]$ , the mean opening rate at 20-22 °C was  $\sim 0$  at  $\sim 0$   $[Mg^{2+}]$ ,  $\sim 0.03$  s<sup>-1</sup> at 5  $\mu$ M  $[Mg^{2+}]$ , and  $\sim 0.22$  s<sup>-1</sup> at 1.2 mM  $[Mg^{2+}]$ . This suggests that both ATP and  $Mg^{2+}$  must be bound before a channel can open. Free  $[Mg^{2+}]$  levels also regulate closing. At 5  $\mu$ M  $[Mg^{2+}]$ , channels can stay open for tens of s, even after rapid ( $\sim 1$  s) ATP washout, but close promptly on raising  $[Mg^{2+}]$ : the mean closing rate rises with  $[Mg^{2+}]$ , from  $\sim 0.05$  s<sup>-1</sup> at 0 or 5  $\mu$ M  $[Mg^{2+}]$ , to  $\sim 0.3$  s<sup>-1</sup> at 1.2 mM  $[Mg^{2+}]$ . This confirms that hydrolysis of a second ATP prompts channel closure. Evidently, that second ATP stays tightly bound, stabilizing the open conformation, without  $Mg^{2+}$ . The closing rate on  $Mg^{2+}$  readdition then reflects the probability that a  $Mg^{2+}$  ion will bind and catalyze hydrolysis of that ATP, leading to channel closure.

The level of channel phosphorylation governs access to the NBDs and hence their ability to modulate channel activity. Partially phosphorylated channels can bind and hydrolyze ATP only at NBD1, resulting in exclusively brief channel openings. Fully phosphorylated channels can bind and hydrolyze ATP at both NBD1 and NBD2: hydrolysis at NBD1 opens channels, and binding of ATP at NBD2 stabilizes the channel in the open conformation, until that ATP is hydrolyzed, resulting in channel closure.





# Chapter 1

## INTRODUCTION

### I. Overview

The scope of this introduction is designed to provide a framework for the present study. In particular, it will describe the rapid advances in our understanding of the function of the Cystic Fibrosis Transmembrane conductance Regulator (CFTR) gene since its cloning in 1989 (Riordan et al., 1989). Mutations of this single gene are believed responsible for the plethora of debilitating symptoms of Cystic Fibrosis (CF; e.g., Welsh et al., 1992). A detailed understanding of how the CFTR protein normally functions should shed light on how its dysfunction can lead to CF, and upon possible methods of circumventing or compensating for the deficiency. The introduction will commence with a review of what is known about CF and the general characteristics of the CFTR gene product. Following this is a review of our present understanding of how CFTR functions in mammalian heart, and an overview of our still rather incomplete understanding of how CFTR channel activity is regulated by protein phosphorylation and nucleoside triphosphate. The introduction concludes with a discussion of the biophysics of ion permeation through membrane channels, and what is known about ion permeation through the CFTR channel.

The experimental work will then be presented in three parts. The first part deals with the regulation of an early step in the activation pathway of CFTR  $\text{Cl}^-$  channels in mammalian cardiac myocytes, i.e., the regulation of adenylyl cyclase. The second part focuses on ion permeation within the



pore of the channel itself; how well the channel discriminates between anions, the nature of the pore's selectivity filter, and the minimum dimensions of the pore. The third and final part will deal with the complex mechanism by which CFTR channels, once they are phosphorylated, can be opened and closed by the energy harnessed from the hydrolysis of ATP, a feature which distinguishes CFTR from all other known channels.

## II. Cystic Fibrosis

CF, the most common lethal inherited disease among Caucasians, is characterized by defects in  $\text{Cl}^-$  ion transport, most significantly across epithelia (Boat, Welsh & Beaudet, 1989; Quinton, 1990). Progressive lung dysfunction, resulting from pulmonary obstruction and recurrent *Pseudomonas* infection (Taussig, Landau & Marks, 1984), presumably due to impaired  $\text{Cl}^-$  (and hence water) transport across airway epithelia, is responsible for ~95% of CF mortality (Boat et al., 1989). However, diverse organ impairment, including exocrine pancreatic insufficiency, intestinal dysfunction, and male infertility, is common (Hanosh & Cutting, 1993). CF is an autosomal recessive disease, carried by ~1/20 Caucasians, and affects ~1 in 3000 live births in North America (Boat et al., 1989). Life expectancy has improved steadily with new modes of treatment, such as aggressive antibiotic, anti-inflammatory, and mucolytic therapy, and pancreatic enzyme replacement, but it is still short; in 1990 the median life expectancy was ~28 years (CF Foundation data).

A major hurdle in the battle to cure CF was cleared with the cloning, in 1989, of a single gene, alterations of which caused CF (Riordan et al., 1989). The protein product was named the cystic fibrosis transmembrane



conductance regulator (CFTR), as it was at first unclear whether it was a modulator of ion channels or an ion channel itself (Riordan et al., 1989). It is now firmly established, however, that CFTR itself is a  $\text{Cl}^-$  channel (e.g., Collins, 1992b; Welsh & Smith, 1993). Moreover, it is generally believed that the ensuing dysfunction in  $\text{Cl}^-$  ion movement across membranes leads to the plethora of abnormalities seen in patients with CF.

### **III. Characteristics of the CFTR Protein**

Figure 1 shows the proposed topological structure of CFTR. Coded by a 6.5 kb mRNA transcript, CFTR is a very large protein, of ~1500 amino acids, comprising two roughly homologous halves. Each half contains six putative transmembrane alpha helices, and one intracellular nucleotide binding domain (NBD), and the halves are connected by an ~200 amino acid hydrophilic regulatory domain (R), which contains several consensus sites for phosphorylation by cyclic AMP-dependent protein kinase (PKA) and ( $\text{Ca}^{2+}$  and) phospholipid-dependent protein kinase (PKC; Picciotto et al., 1992; Berger, Travis & Welsh, 1993; Dulhanty & Riordan, 1994). Of the > 400 mutations of the gene that have to date been identified, it is interesting that the highest density of mutations are within the NBDs (Tsui et al., 1993), pointing to a key role for the NBDs in normal channel function. Indeed, a single mutation, which leads to the deletion of three nucleic acids that encode the amino acid phenylalanine at position 508 ( $\Delta\text{F508}$ ), is present in over 90% of patients with Cystic Fibrosis (Kerem et al., 1990; Tsui, 1992), and it occurs in NBD1.



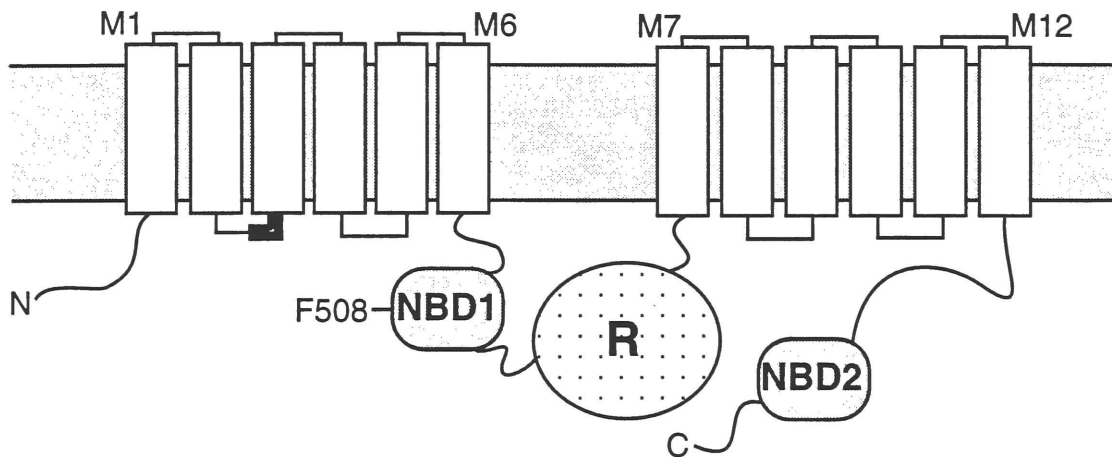


**Fig. 1. Proposed topological model of CFTR.** CFTR is a large (~1500 amino acid), membrane-bound protein, with 12 membrane-spanning sequences (M1-M12), 2 intracellular nucleotide binding domains (NBD1, NBD2), and a regulatory (R) domain containing multiple sites for phosphorylation by PKA and PKC. F508 marks the site of the predominant mutation in CF patients. The darkened section of the M2-M3 cytoplasmic loop represents the portion of the protein encoded by exon 5, believed spliced out of the cardiac isoform of CFTR.





CFTR bears substantial similarity to members of a protein family, called the ATP-binding cassette transporters, whose members share a common domain organization of two membrane-spanning and two cytosolic ATP-binding domains, and whose members include the protein believed to be responsible for multidrug resistance, P-glycoprotein, the yeast  $\alpha$  mating factor exporter STE6, and the MHC-linked peptide transporter (Ames & Lecar, 1992; Higgins, 1992). For members of this family, the two NBDs are believed to be sites of ATP hydrolysis (e.g., Urbatsch, Al-Shawi & Senior, 1994; Urbatsch et al., 1995), the energy of which is said to fuel the transport of the substrate. Unlike those other members, however, in CFTR the two halves of the molecule are connected by the additional cytoplasmic regulatory domain.

#### **IV. CFTR is a Regulated Chloride Channel**

It is now generally believed that CFTR is itself a chloride channel (Collins, 1992b; Welsh et al., 1992). Heterologous expression of CFTR in a wide variety of non-epithelial cells which express little if any endogenous CFTR, including Sf9 insect cells (Kartner et al., 1991), Chinese hamster ovary (CHO) cells (Tabcharani et al., 1991), fibroblasts (Anderson et al., 1991a; Berger et al., 1991; Dalemans, Barbry & Champigny, 1991), and *Xenopus* oocytes (Bear et al., 1991; Drumm et al., 1991), yields small conductance, ohmic  $\text{Cl}^-$  channels which are activated via the cAMP-PKA signaling cascade. Either all of these cells express a channel which is only unmasked by expression of exogenous CFTR, or CFTR is itself a  $\text{Cl}^-$  channel. Additional confirmation that CFTR is itself a channel comes from experiments examining single amino acid mutations: the charge-



reversing point mutations K95D (in M1) and K335E (in M6) altered anion permeability sequences (Anderson et al., 1991b), and the charge-reversing mutation R347D (in M6) halved the single channel conductance and abolished the anomalous mole-fraction effect (indicative of a multi-ion pore) observed in wild-type CFTR (Tabcharani et al., 1993). Strikingly, by replacing the arginine residue with a histidine (R347H), which is positively charged at low pH and neutral at high pH, channel behavior could be switched from that resembling the R347D mutant to that of a wild-type channel simply by raising the pH from 5.5 to 8.7 (Tabcharani et al., 1993).

Recently, fusion of purified overexpressed recombinant CFTR into planar lipid bilayers gave small ohmic  $\text{Cl}^-$  channels which could be activated by PKA and ATP (Bear et al., 1992), unequivocally establishing that CFTR functions as a regulated  $\text{Cl}^-$  channel.

## **V. CFTR in Mammalian Heart**

Concurrent with the cloning of human epithelial CFTR, a  $\text{Cl}^-$  conductance was isolated in mammalian cardiac myocytes, using the whole-cell voltage-clamp technique, which was activated by hormonal stimulation, and which was regulated by protein phosphorylation by cyclic AMP-dependent protein kinase (PKA) (Bahinski et al., 1989a; Harvey & Hume, 1989; Matsuoka, Ehara & Noma, 1990). The single channel currents underlying this whole-cell conductance were soon isolated, both in cell-attached patches on myocytes exposed to epinephrine (Ehara & Ishihara, 1990), and in excised inside-out (Nagel et al., 1992) and outside-out (Ehara & Matsuura, 1993) patches. It became clear that this cardiac  $\text{Cl}^-$  conductance showed remarkable similarity to human epithelial CFTR, including



similar Cl<sup>-</sup> selectivity (Bahinski et al., 1989a; Ehara & Ishihara, 1990), single channel conductance (Ehara & Ishihara, 1990), insensitivity to block by stilbenes (Hwang et al., 1992b), voltage-independent gating (Ehara & Ishihara, 1990), a requirement for phosphorylation by PKA (Nagel et al., 1992), and a requirement for hydrolyzable nucleoside triphosphate (Nagel et al., 1992). Strengthening the already substantial functional similarities, it was shown by Northern blot analysis that mRNA coding for CFTR was present in guinea-pig and rabbit ventricle, and human atrium (Levesque et al., 1992; Nagel et al., 1992).

Although the full sequence of the cardiac CFTR gene has not yet been published (but cf., Collier et al., 1996), it is now clear that there is a very high degree of homology between human epithelial CFTR and cardiac CFTR. A rabbit ventricular amplification product corresponding to 180 amino acids within NBD1 showed 98% identity with human epithelial CFTR (Levesque et al., 1992). Sequencing of amplification products corresponding to the two putative membrane-spanning domains (M1-M6, M7-M12) revealed > 95% identity to epithelial CFTR (Horowitz et al., 1993), except for a deletion of 30 amino acids in the first cytoplasmic loop (corresponding to exon 5), leading to the suggestion that mammalian cardiac CFTR is likely an alternatively spliced isoform of epithelial CFTR (Horowitz et al., 1993). Moreover, recently it has been shown that injection of antisense oligodeoxynucleotide directed against the first 23 base pairs of the human epithelial CFTR gene product into guinea-pig ventricular myocytes resulted in an ~50% reduction in cAMP-dependent Cl<sup>-</sup> current, with no change in the augmentation of L-type Ca<sup>2+</sup> currents (Warth et al., 1996). This provides direct evidence that a channel either identical to or



closely resembling CFTR is responsible for the cAMP-dependent  $\text{Cl}^-$  current in mammalian heart.

Cardiac expression of human epithelial-type CFTR and the exon 5 deletion variant seems to vary across species. Neither gene is expressed in dog or rat heart, nor in rabbit or guinea-pig atria (Horowitz et al., 1993); however, in rabbit and guinea-pig ventricle, the exon 5 deletion variant, exclusively, is expressed (Horowitz et al., 1993). Interestingly, in human and simian heart both genes are possibly expressed, in both the atrium and the ventricle (Warth et al., 1996b).

## **VI. Physiological Role of CFTR in Mammalian Heart**

As a result of hormonal stimulation, e.g., by activation of  $\beta$ -adrenoceptors, it is expected that a voltage-independent and sustained  $\text{Cl}^-$  conductance would be activated. Since the normal intracellular  $\text{Cl}^-$  concentration in ventricular myocytes is  $\sim 20$  mM (Vaughn-Jones, 1979) and extracellular  $\text{Cl}^-$  is  $\sim 150$  mM, opening CFTR  $\text{Cl}^-$  channels would drive the membrane voltage towards the  $\text{Cl}^-$  equilibrium potential ( $E_{\text{Cl}}$ ,  $\sim -50$  mV; Vaughn-Jones, 1979; Desilets & Baumgarten, 1986). This would result in a repolarizing force during periods of strong membrane depolarization, and could thus be expected to accelerate action potential repolarization. Therefore, it has been suggested that this  $\text{Cl}^-$  conductance might protect the heart from possible arrhythmogenic conditions expected upon  $\beta$ -adrenoceptor stimulation, due to the increased heart rate and increases in calcium entry into cells (Bahinski et al., 1989a). It is unclear whether cardiac, or indeed epithelial, CFTR  $\text{Cl}^-$  channels are active in the absence of hormonal stimulation (see Chapter 3, Discussion).





Determining the precise effects of this conductance on action potential duration and shape has been hampered by the lack of a direct, specific, potent CFTR channel blocker (Hwang & Gadsby, 1994). However, in support of this protective role of CFTR in mammalian heart, application of the  $\beta$ -adrenoceptor agonist isoproterenol (Harvey & Hume, 1989), or histamine (Harvey & Hume, 1990), with  $\text{Ca}^{2+}$  currents blocked by nisoldipine, halved the duration of action potentials of current-clamped ventricular myocytes. But, since these studies were carried out at room temperature, to prevent activation of delayed rectifier  $\text{K}^{+}$  channels, the combined physiological contribution of these two currents to the shape and duration of the action potential is unclear. In another study, carried out at 36 °C, the stilbene derivative 4,4'-dinitro-2,2'-stilbene disulfonic acid (DNDS), which appears to block CFTR  $\text{Cl}^{-}$  conductance under certain conditions (Bahinski et al., 1989a; Matsuoka et al., 1990), likely by an indirect effect on channel regulation (Hwang & Gadsby, 1994), was used to diminish CFTR  $\text{Cl}^{-}$  conductance. Using nystatin-perforated patches to monitor membrane voltage, so that the intracellular milieu was minimally disrupted, exposure to isoproterenol reduced action potential duration only slightly, but subsequent addition of DNDS, which in the same cells had no effect on action potential duration without isoproterenol, caused a marked prolongation of the action potential (Takano & Noma, 1992). Although weakened by the likelihood that DNDS exerts its inhibitory effect on CFTR  $\text{Cl}^{-}$  conductance via an indirect pathway (Hwang et al., 1992b; Harvey, 1993), this result suggests that the cardiac CFTR  $\text{Cl}^{-}$  current does indeed counteract increases in action potential duration due to the enhanced  $\text{Ca}^{2+}$  current resulting from  $\beta$ -adrenergic stimulation (Takano & Noma, 1992). This suggestion has been given more support by a recent study which



showed that the sulfonylurea glibenclamide, known to inhibit epithelial-type CFTR currents (Sheppard & Welsh, 1992), can block the shortening of action potentials in current-clamped ventricular myocytes exposed to forskolin (Tominaga et al., 1995). In contrast to this postulated role of CFTR as a safeguard against arrhythmia, it has also been postulated that activation of CFTR in heart might be *harmful*, since although its activation normally would result in only a small membrane depolarization from the resting membrane potential, under certain conditions (e.g., hypokalemia) its activation may lead to a more pronounced depolarization and abnormal automaticity; thus, defective CFTR might, in heart, be protective (Levesque et al., 1993).

Studies on the cardiac function of CF patients are rare. And, although reports of ventricular dysfunction during stress (Benson et al., 1984) and arrhythmias (Sullivan et al., 1986) have been published, cardiac abnormalities typically have been regarded as secondary to pulmonary dysfunction, viz., *cor pulmonale*. Detailed electrophysiological studies are warranted to determine whether CF patients exhibit cardiac dysfunction. In particular, young CF patients who are nowadays kept relatively free of pulmonary disease could be given stress electrocardiograms to examine the role of the CFTR channel in cardiac function. Additionally, new populations of CF patients now exist which have received CF-free lungs, as well as hearts and lungs, as a result of transplants and cotransplants. All of these patients could be fruitfully studied to examine how CFTR functions in normal heart, and if its dysfunction leads to measurable cardiac conduction abnormalities (Hwang & Gadsby, 1994).



## **VII. Regulation of Whole-Cell CFTR Cl<sup>-</sup> Conductance in Mammalian Heart**

### **A. Stimulation of Adenylyl Cyclase Activates CFTR Cl<sup>-</sup> Conductance**

Figure 2 summarizes the sequential steps in the cycle of activation of the CFTR Cl<sup>-</sup> ion channel in mammalian heart (for review, see Gadsby, Nagel & Hwang, 1995). In the absence of channel phosphorylation CFTR channels are inactive (Fig. 2, **i**). Channels are activated by phosphorylation, which is regulated by hormonal activation of the classical receptor-adenylyl cyclase (AC)-cyclic AMP (cAMP)-PKA cascade. To activate CFTR channels, the natural hormone agonists epinephrine and norepinephrine bind to  $\beta$ -adrenoceptors, which act through a GTP-binding protein to stimulate AC, an enzyme which catalyzes the formation of cAMP from ATP. Raised intracellular cAMP levels then activate PKA by binding to its regulatory subunit and releasing the active catalytic subunit (Fig. 2, PKA\*). Activated PKA then catalyzes the phosphorylation of a variety of cellular proteins at serine and threonine residues (Cohen, 1988), including the CFTR Cl<sup>-</sup> channel (Fig. 2, **ii**; Picciotto et al., 1992). Subsequent to this phosphorylation of CFTR by PKA, ATP (binding, presumably, at one or both of the putative nucleotide binding domains of the channel protein) can then permit the opening and closing of the channel (Fig. 2, **iii**; Hwang & Gadsby, 1994).

Isoproterenol (Iso), a  $\beta$ -adrenoceptor agonist, modulates mammalian CFTR Cl<sup>-</sup> conductance exclusively by binding to  $\beta$ -adrenoceptors, with subsequent activation of AC, since propranolol (a specific  $\beta$ -adrenoceptor antagonist) completely abolishes its effect, and its effect is mimicked by intracellular application of cAMP (Hwang et al., 1992c). As with the



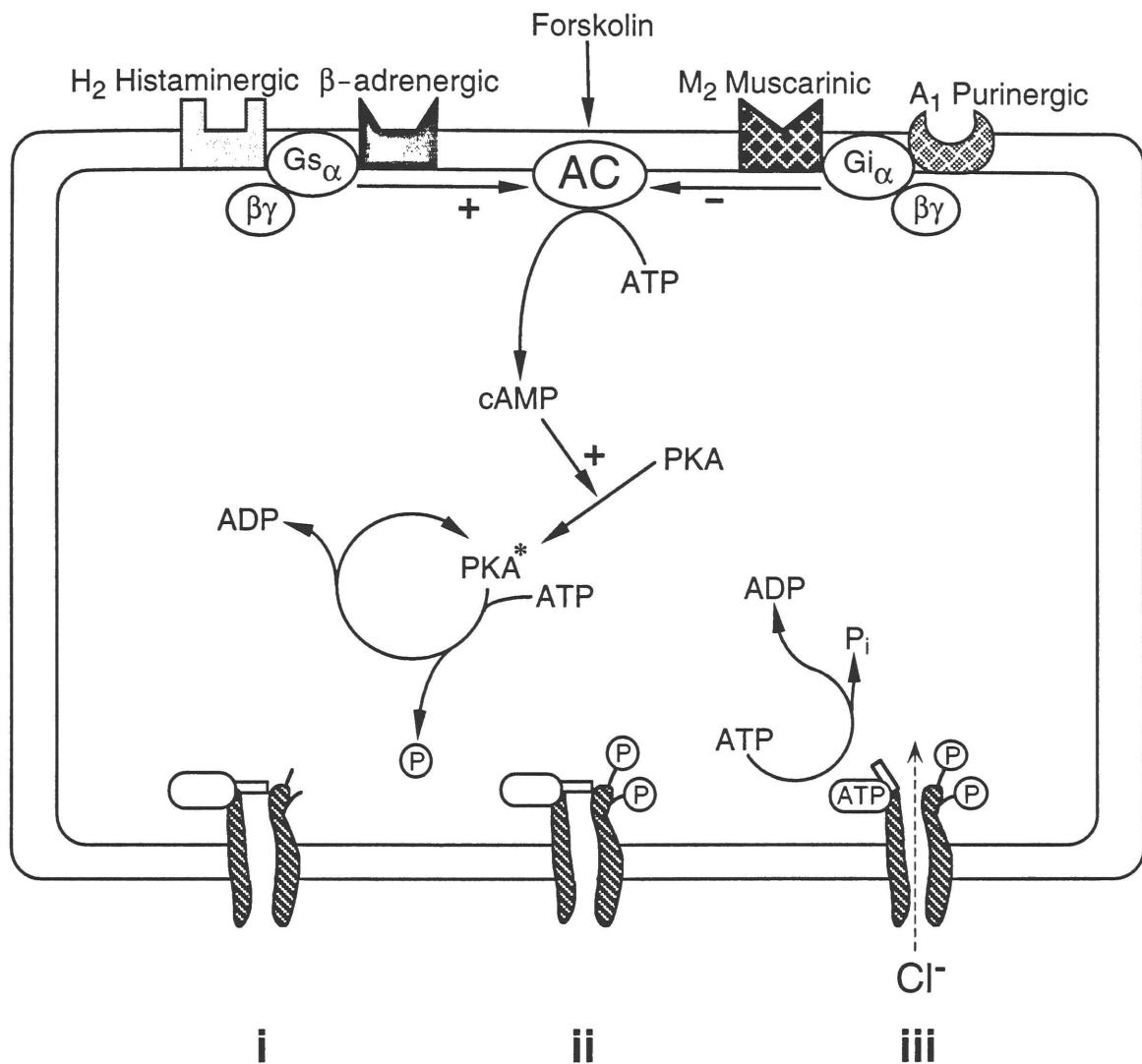


**Fig. 2. Regulatory pathway of the CFTR Cl<sup>-</sup> channel in a mammalian ventricular myocyte.** Channels remain inactive in the absence of phosphorylation (i). Stimulation of the GTP-binding protein-coupled β-adrenoceptor or the H<sub>2</sub> histaminergic receptor leads to activation of adenylyl cyclase (AC), a membrane-bound enzyme which catalyzes the formation of cyclic AMP (cAMP). Raised cAMP levels activate the cytosolic cAMP-dependent protein kinase (PKA), which phosphorylates the CFTR channel at serine residues on the channel's R domain (ii). Once stably phosphorylated, the channel can then be opened and closed by application of MgATP, presumably by successive cycles of ATP hydrolysis (iii). Dephosphorylation, presumably by phosphatases 2A and 2C, returns channel to the inactive state (ii→i).





cardiac dihydropyridine-sensitive  $\text{Ca}^{2+}$  conductance,  $\beta$ -adrenoceptor activation of cardiac CFTR  $\text{Cl}^-$  conductance is effected by receptor coupling to AC via a stimulatory heterotrimeric GTP-binding protein ( $G_s$ ; Gilman, 1987); receptor stimulation encourages the formation of the active, GTP-bound  $G_\alpha$  subunit of  $G_s$ , since, in the presence of  $\text{GTP}\gamma\text{S}$  (which binds tightly to  $G_\alpha$ , and, since the terminal phosphate of  $\text{GTP}\gamma\text{S}$  cannot be hydrolyzed, leads to persistently activated  $G_\alpha$ ), Iso leads to a persistently activated current, and since a high concentration  $\text{GDP}\beta\text{S}$  (which competes with GTP for the nucleotide binding site on  $G_\alpha$ , but does not activate  $G_\alpha$ ) prevents Iso activation of the conductance (Hwang et al., 1992c). Furthermore, in the absence of pipette GTP, the ability of Iso to activate cardiac CFTR  $\text{Cl}^-$  conductance progressively diminishes, but can be restored by the addition of micromolar amounts of GTP to the pipette solution (Horie, Hwang & Gadsby, 1992).

The stimulatory G-protein  $G_s$  stimulates cardiac CFTR  $\text{Cl}^-$  conductance exclusively through the classic cAMP-mediated pathway since PKI, a specific peptide inhibitor of PKA (Cheng et al., 1986), completely abolished Iso-activated  $\text{Cl}^-$  current, and Iso does not elicit a larger  $\text{Cl}^-$  current after maximal stimulation via Fsk or cAMP (Hwang et al., 1992c). Furthermore,  $\text{Cl}^-$  current persistently activated by  $\text{GTP}\gamma\text{S}$  was completely abolished by PKI. This contrasts with the muscarinic inwardly-rectifying  $\text{K}^+$  current, which flows via GIRK channels that can be directly modulated by G-protein subunits (e.g., Wickman et al., 1994).

Histamine, like Iso, acts via  $G_s$  to stimulate AC, since the magnitudes of the currents elicited by maximal concentrations of histamine and Iso are similar, and, as with the Iso response,  $\text{GTP}\gamma\text{S}$  leads to a persistently



activated current, while excess GDP $\beta$ S prevents current activation (Hwang et al., 1992c).

Forskolin (Fsk), a hydrophilic compound capable of stimulating AC directly (Seamon & Daly, 1986), can also activate cardiac CFTR Cl<sup>-</sup> conductance (Hwang et al., 1992c). Its action is independent of a GTP-binding protein, since Fsk reversibly activates a current which in the presence of GTP $\gamma$ S or excess GDP $\beta$ S, and current activation by Fsk is not diminished by sustained lack of pipette GTP (Horie et al., 1992; Hwang et al., 1992c). Furthermore, Fsk activates Cl<sup>-</sup> conductance solely by stimulating AC, since its effects are abolished by pipette application of PKI (Hwang, Horie & Gadsby, 1993).

Each of these upstream activators of cardiac CFTR Cl<sup>-</sup> conductance result in the stimulation of AC, yielding increased levels of intracellular cAMP which activates PKA, since the magnitudes of currents elicited with maximal concentrations of Iso, His, Fsk and cAMP are similar (Hwang et al., 1992c). Furthermore, pipette application of the catalytic subunit of PKA can mimic their effect (Bahinski et al., 1989a), and a peptide inhibitor of PKA (PKI) can completely abolish their effect (Bahinski et al., 1989b; Hwang et al., 1992c; Hwang et al., 1993).

## **B. Inhibition of Adenylyl Cyclase Diminishes CFTR Cl<sup>-</sup> Conductance**

Stimulation of muscarinic acetylcholine receptors inhibits cardiac CFTR Cl<sup>-</sup> conductance by inhibiting AC (Fig. 2). Thus carbachol (CCh), a muscarinic acetylcholine receptor agonist, inhibits cardiac CFTR Cl<sup>-</sup> conductance activated by Iso and Fsk, but not by cAMP (Hwang et al., 1992c). As with the cardiac Ca<sup>2+</sup> conductance, the muscarinic effects are mediated by a GTP-binding protein, since the inhibition is abolished by



depletion of intracellular GTP, by inclusion of GDP $\beta$ S, or by treatment with pertussis toxin (Hwang et al., 1992c). Muscarinic agonists have been shown to diminish Fsk-activated Ca<sup>2+</sup> current in guinea-pig (Hescheler, Kameyama & Trautwein, 1986) and in frog (Parsons et al., 1991) myocytes.

### **C. CFTR Cl<sup>-</sup> Channel Phosphorylation Governs the Ability of Nucleotide to Gate Channel Opening and Closing**

It is widely accepted that human epithelial (Berger et al., 1991; Tabcharani et al., 1991) and mammalian cardiac (Nagel et al., 1992) CFTR Cl<sup>-</sup> channels fail to open unless they are first phosphorylated, and that PKA is the most efficacious kinase. Indeed, phosphorylation at multiple sites is observed in 2-dimensional phosphopeptide maps of activated human epithelial CFTR (Cheng et al., 1991; Picciotto et al., 1992). In agreement with this, the upstream regulators of cardiac CFTR Cl<sup>-</sup> conductance all act exclusively by phosphorylating cardiac CFTR through stimulation of PKA, since pipette application of PKI can abolish their effects (Bahinski et al., 1989a; Hwang et al., 1993). Furthermore, once the stimulatory drive is removed, e.g., by application of the  $\beta$ -adrenoceptor antagonist propranolol to cells exposed to Iso (Hwang et al., 1992c), by withdrawal of bath-applied Iso (Bahinski et al., 1989a), or by pipette application of PKI (Hwang et al., 1993), whole-cell CFTR Cl<sup>-</sup> conductance is abolished within 1-2 min. The implication is that rapid channel dephosphorylation, by active endogenous phosphatases, deactivates the channel. Indeed, pipette application of okadaic acid or microcystin, both inhibitors of phosphatases 1 and 2A (Takai et al., 1987; Honkanen, 1990), enhanced steady-state Cl<sup>-</sup> conductance during exposure to Fsk, slowed its deactivation on Fsk removal, and led to an incomplete deactivation, the remaining conductance being insensitive to



PKI (Hwang et al., 1993). The simplest conclusion is that the channel can exist in at least two functionally distinct phosphorylation states, as revealed by this differing ability to be dephosphorylated by phosphatases sensitive to okadaic acid and microcystin.

That CFTR Cl<sup>-</sup> channel activity can be modulated by the level of protein phosphorylation has been confirmed in studies of unitary currents in excised membrane patches, where a single channel molecule can exhibit a slow decrease in open probability ( $P_o$ ) after withdrawal of PKA catalytic subunit, but an abrupt increase in  $P_o$  upon reapplication of PKA (Hwang et al., 1992b). This, combined with the observation of predominantly a single conductance amplitude in unitary currents in inside-out (Nagel et al., 1992), or outside-out membrane patches (Ehara & Matsuura, 1993), shows that phosphorylation level regulates channel  $P_o$  rather than channel conductance.

PKA appears to be the primary kinase regulating the activity of CFTR. The cDNA sequence of human epithelial CFTR reveals that the R domain contains multiple potential phosphorylation sites (Riordan et al., 1989), nine of which are classical dibasic consensus sites for PKA phosphorylation (Pearson & Kemp, 1991). Of these, five serines on the R domain are the principal physiological sites of phosphorylation by PKA (Cheng et al., 1991; Picciotto et al., 1992); crude measurements in CFTR mutants suggested that there might be redundancy between these sites (Cheng et al., 1991).

PKC, another serine/threonine kinase, appears to modulate the ability of PKA to activate CFTR, since it can only weakly activate recombinant CFTR Cl<sup>-</sup> channels expressed in CHO cells or 3T3 fibroblasts (Berger et al., 1993; Chang et al., 1993; Tabcharani et al., 1991), yet can strongly potentiate subsequent activation by PKA of CFTR Cl<sup>-</sup> channels in cell-attached or





excised patches (Tabcharani et al., 1991; Bajnath et al., 1993; Chang et al., 1993). PKC has been shown to phosphorylate the CFTR R domain, both *in vivo* and *in vitro*, at ~2 mol/mol, primarily at Ser 686 and Ser 790 (Picciotto et al., 1992; Berger et al., 1993). However, unlike recombinant R domain phosphorylated by PKA, R domain phosphorylated by PKC shows no conformational change, as inferred from changes in CD spectra upon phosphorylation (Dulhanty & Riordan, 1994). Furthermore, PKA-phosphorylated R domain shows altered mobility on SDS-polyacrylamide gels, suggesting a structural/conformational change in the R domain, which is not observed in PKC-phosphorylated R domain (Picciotto et al., 1992; Dulhanty & Riordan, 1994).

There is some evidence that cyclic GMP-dependent protein kinase (PKG) can also activate CFTR. In particular, purified PKG type II activated CFTR Cl<sup>-</sup> channels from 3T3 and IEC-CF9 cells nearly as well as PKA (French et al., 1995), but PKG type I did not (Berger et al., 1993; French et al., 1995). The suggestion that PKG-mediated phosphorylation can directly regulate CFTR is tempered by the finding that in T84 (Chao et al., 1994), Caco-2 (Tien et al., 1994), or guinea-pig myocytes (Ono et al., 1992), in which channel activation by cGMP has been confirmed, the effect of cGMP is sensitive to the specific PKA inhibitor PKI, implying that its action is indirect and through the PKA-stimulatory pathway, possibly through inhibition of a phosphodiesterase. In another T84 cell line, however, CFTR channels could be activated by cGMP in the presence of PKI (Lin, Nairn & Guggino, 1992). The role of cGMP in the regulation of CFTR is further complicated by the suggestion that cGMP may *directly* stimulate activity of CFTR channels by binding to a specific site in the third cytoplasmic loop (Sullivan, Agellon & Schick, 1995).



## VIII. CFTR Regulation by Nucleoside Triphosphate

### A. CFTR Cl<sup>-</sup> Channels Require Hydrolyzable Nucleoside Triphosphate to Open

Although phosphorylation of CFTR Cl<sup>-</sup> channels by PKA is required for channel activity, it is certainly not sufficient; recombinant epithelial (Anderson et al., 1991b; Berger et al., 1993) and native (Nagel et al., 1992; Hwang et al., 1994) CFTR Cl<sup>-</sup> channels, having been phosphorylated by PKA, close abruptly upon withdrawal of nucleoside triphosphate, but can be promptly reopened by their reapplication. PKA-phosphorylated CFTR Cl<sup>-</sup> channels require hydrolyzable nucleoside triphosphate for channel opening, since channels close upon ATP withdrawal, but can be reopened by ATP, GTP, UTP, ITP, CTP, or AMP-CPP, yet ATP analogs which lack the terminal phosphate, such as cAMP or ADP, or which contain a poorly hydrolyzable terminal phosphate, such as ATP $\gamma$ S, AMP-PNP and AMP-PCP, cannot open channels (Anderson et al., 1991a; Nagel et al., 1992). The fact that AMP-PNP, an analog which closely resembles ATP in molecular structure but which has a poorly hydrolyzable  $\beta$ - $\gamma$  bond (Yount, 1975), could not open channels which could be opened by ATP, provides the strongest evidence that ATP hydrolysis is required to open PKA-phosphorylated CFTR Cl<sup>-</sup> channels, although this conclusion is still not universally accepted (Gunderson & Kopito, 1995; Quinton & Reddy, 1992).

Further recent evidence that hydrolysis of ATP controls the opening of CFTR Cl<sup>-</sup> channels comes from experiments which show that the inorganic phosphate (P<sub>i</sub>) analogs orthovanadate and beryllium fluoride, which halt further cycles of ATP hydrolysis and inhibit ATPases by tightly binding to the site vacated by P<sub>i</sub>, after hydrolysis of the terminal phosphate



bond (Chabre, 1990), can dramatically stabilize the open conformation of channels opened by ATP (Baukrowitz et al., 1994).

## **B. CFTR Cl<sup>-</sup> Channels Require Hydrolyzable Nucleoside Triphosphate to Close**

AMP-PNP can profoundly stabilize the open conformation of CFTR Cl<sup>-</sup> channels already opened by ATP (Gunderson & Kopito, 1994; Hwang et al., 1994; Carson, Travis & Welsh, 1995; Gunderson & Kopito, 1995). Since the CFTR Cl<sup>-</sup> channel contains two putative nucleotide binding domains, the simplest interpretation is that AMP-PNP acts only at one of the NBDs, and only after ATP has acted at the other NBD to open the channel. The most parsimonious explanation for AMP-PNP's ability to stabilize the open channel conformation is that hydrolysis of ATP at that site normally leads to channel closure.

## **C. Nucleoside Triphosphate Action at NBD1 Opens Channels, and, at NBD2, Closes Channels**

It has been postulated that hydrolysis of ATP at NBD1 leads to channel opening, and that hydrolysis of ATP at NBD2 leads to channel closure (Hwang et al., 1994), based partly on studies of naturally-occurring mutations which indicate that mutations in NBD1 are both more numerous (Tsui, 1992) and more severe (Gregory et al., 1991) than the equivalent mutations of NBD2. Further evidence comes from site-directed point mutations which are believed to impair nucleotide hydrolysis. For instance, channels can still open with a severe mutation in NBD2, K1250M, which should compromise ATP hydrolysis at that site (Anderson & Welsh, 1992). Recently, it has been shown that mutation of lysine 464 in NBD1,



which should impair ATP hydrolysis, resulted in an increase in channel closed time (reflecting a decrease in channel opening rate), as would be expected if hydrolysis at NBD1 were required for channel opening (Gregory et al., 1991; Carson et al., 1995). Comparable mutations in NBD2, at lysine 1250, stabilized the open conformation of the channel, as would be expected if ATP action at NBD2 governs channel closure (Carson et al., 1995; Gunderson & Kopito, 1995).

#### **D. Inorganic Phosphate ( $P_i$ ) Analogs Act at NBD1, and AMP-PNP Acts at NBD2**

The inorganic phosphate analogs orthovanadate and beryllium fluoride, and the ATP analog AMP-PNP, all stabilize the channel in the open conformation, which might suggest that they act at the same site. However, crucial differences in their ability to stabilize open channels allow their sites of action to be differentiated. First, AMP-PNP cannot open highly phosphorylated channels in the absence of MgATP (Anderson et al., 1991a; Nagel et al., 1992). However, in excised patches AMP-PNP can readily stabilize the open conformation of freshly phosphorylated channels which exhibit a relatively high open probability ( $P_o$ ), but fails to do so when channels are partially dephosphorylated, and in a low  $P_o$  mode (Hwang et al., 1994). These AMP-PNP results are confirmed by experiments in intact myocytes; during PKA stimulation by Fsk, i.e., with the channels in a strongly phosphorylated, high  $P_o$  state, AMP-PNP plus ATP substantially increased CFTR  $Cl^-$  conductance. However, after treatment with microcystin or okadaic acid and subsequent withdrawal of Fsk, i.e., with the channels in a partially dephosphorylated, low  $P_o$  state, AMP-PNP plus ATP had no effect on CFTR  $Cl^-$  conductance (Hwang et al., 1994). Thus,





since AMP-PNP stabilizes channels already opened by ATP, and since channel opening likely occurs as the result of ATP hydrolysis at NBD1 (see above), it is likely that AMP-PNP exerts its effect at NBD2, by binding to it and preventing the normal action of ATP at that site. The inability of AMP-PNP to stabilize the open conformation of partially dephosphorylated channels contrasts with the ability of the  $P_i$  analogs to stabilize the open conformation of all CFTR  $Cl^-$  channels, regardless of their level of phosphorylation (Baukrowitz et al., 1994). The simplest interpretation is that the  $P_i$  analogs act by interfering with the cycles of ATP hydrolysis at NBD1.

## **IX. Mammalian Cardiac CFTR and Human Epithelial CFTR are Functionally Identical**

In addition to the significant genetic similarity between cardiac and human epithelial CFTR, there is overwhelming biophysical and biochemical evidence indicating that mammalian cardiac CFTR, and human epithelial CFTR, are functionally and essentially identical. First, both channels exhibit a low, ~10 pA single channel conductance (Anderson et al., 1991a; Kartner et al., 1991; Nagel et al., 1992) and linear unitary current-voltage relation in symmetrical high  $Cl^-$  (Anderson et al., 1991a; Nagel et al., 1992). Second, both cardiac and epithelial CFTR  $Cl^-$  channels exhibit voltage-independent gating (Kartner et al., 1991; Tabcharani et al., 1991; Nagel et al., 1992), and have an absolute requirement for PKA-mediated phosphorylation to open (Berger et al., 1991; Cheng et al., 1991; Tabcharani et al., 1991; Nagel et al., 1992). Once phosphorylated by PKA, both require ATP to open (Anderson et al., 1991a; Nagel et al., 1992; Hwang



et al., 1994). Finally, both human epithelial CFTR and mammalian cardiac CFTR  $\text{Cl}^-$  conductance, in well-buffered, dialyzed ventricular myocytes, remain unblocked by the stilbenes DNDS and SITS (Bahinski et al., 1989a; Cliff, Schoumacher & Frizzell, 1992; Hwang et al., 1992b), but both are inhibited by the sulfonylurea glibenclamide (Sheppard & Welsh, 1992; Tominaga et al., 1995).

## **X. Permeability/Selectivity**

### **A. Background**

A membrane protein which mediates the transfer of ions from one side of the membrane to the other, just like an enzyme, must exhibit some specificity, and preferentially transfer particular ions, to the practical exclusion of others. Some channels are poorly selective, such as the nicotinic acetylcholine receptor channel, which selects only for cations over anions (Andersen & Koeppe, 1992; Hille, 1992). In many other cases, however, and especially in the case of channels regulating resting membrane potentials, propagated action potentials, and the repetitive changes of membrane potential in the heart, fine discrimination between ions of the same charge is a necessity. Selectivity refers to the preferred transport of one species over another (Eisenman & Dani, 1987). How do membrane channels, while providing a low energy, (pseudo-) aqueous polar pathway for ion translocation, maintain such high selectivity yet permit very rapid transport rates? The detailed molecular basis for ion selectivity by naturally occurring pore-forming membrane proteins is still not fully understood, although much has been learned even without detailed structural information (e.g., Hille, 1975b; Cukierman, Yellen &



Miller, 1985). The study of permeation through small pore-forming proteins of known structure has yielded insights (Andersen & Koeppe, 1992). Several approaches have been developed to quantify selectivity, and have given rise to theoretical formulations describing ion selectivity.

In the simplest terms, permeability is a measure of the ease with which ions can traverse the membrane, or, if a particular membrane channel is isolated, the ease with which ions can pass through that channel. The simplest mode of selectivity is based on a sieve-like exclusion of ions (Eisenman & Dani, 1987; Andersen & Koeppe, 1992; Hille, 1992). Steric forces prohibit the passage of ions (or other charged species) which are too large, yet will allow passage of smaller ions. The concept of a cut-off size for permeation, determined using reversal potential shifts in solutions of test and control ion, has been used to size pores at their narrowest point. Early work by Hille on Na<sup>+</sup> and K<sup>+</sup> channels in myelinated frog axons, measuring permeability ratios with metal and organic cations, demonstrated that the selectivity filter can be, for the Na<sup>+</sup> channel, no smaller than 3x5 Å, and for the K<sup>+</sup> channel, no smaller than 3x3 Å (Hille, 1972; Hille, 1973; Eisenman & Dani, 1987; Andersen & Koeppe, 1992). The concept of a selectivity filter within the channel pore does not, however, rule out the possibility that the pore is narrow for a larger portion of its length. In addition, a narrow pore does not preclude a high throughput rate (Almers & McCleskey, 1984; Hess & Tsien, 1984; Andersen & Koeppe, 1992; but cf. Yellen, 1987).

Given that an ion is small enough to fit through the narrowest region of the pore, what then is the selection process? Other measures of ionic permeability can shed light on this phenomenon, which must invoke specific interactions between the ion and the channel (Eisenman & Dani,



1987; Andersen & Koeppe, 1992). Equilibrium affinity binding, in particular the difference in equilibrium affinities for two ions, in which each ion's affinity for the channel is determined by the difference between the free energy of interaction with the channel and the ion's energy of hydration, yields one measure of ion selectivity (Andersen & Koeppe, 1992). Conceptually, this is the simplest measure of selectivity, but probably the least relevant physiologically, since binding affinity is related to the depth of the energy wells in a rate theory model of ion permeation. This formulation implies that the ion which binds with the highest affinity (i.e., is best "selected" for) will prefer to remain bound (at the site corresponding to the energy well), and thus will have the slowest throughput rate, i.e., the lowest conductance, and might even be a channel blocker (Eisenman & Dani, 1987; Andersen & Koeppe, 1992). Better would be a measure of the rate at which ions enter and leave the pore, not a measure of how tightly the ion is bound within the pore. Ultimately, then, one would like a measure of permeability which reflects the relative rates of ion movement through the pore.

One method of determining selectivity is to quantify the single channel conductance ( $\gamma$ ; current/driving force) in pure solutions of a single test ion at a given potential (Bormann, Hamill & Sakmann, 1987; Eisenman & Dani, 1987; Andersen & Koeppe, 1992), given by:

$$\gamma = \gamma_{\max} \frac{[A]}{(K_A + [A])} \quad (\text{eqn. 1})$$

where  $K_A$  is the ion's dissociation constant with the channel, and  $\gamma$  is a saturating function of the ion concentration. If the channel holds only one ion at a time (when there can be no flux coupling), then the ratio of





conductances of ions A and B ( $\gamma_A/\gamma_B$ ) is comparable in meaning to  $P_A/P_B$  (see below). The conductance ratio will vary as a function of ion concentration, and will reach a maximum (Bormann et al., 1987; Andersen & Koeppe, 1992). At low concentrations, one assumes independence of ion flow is maintained, and the conductance ratio  $\gamma_A/\gamma_B$  approaches the ions' limiting permeability ratio, yielding a good measure of the channel's ability to discriminate amongst different ions (Andersen & Koeppe, 1992), since it is determined, in the simplest case, by the largest well-to-peak energy difference felt by each ion (Eisenman & Dani, 1987; Hille, 1992). Since conductance is measured in symmetric solutions of a single ion, it is also a measure of the absolute permeability of that ion.

Permeability ratios can also be measured by observing the reversal potential of the induced current with known concentrations of permeant ions on each side of the membrane. This yields a direct measure of the relative rates of ion movement through the channel (Andersen & Koeppe, 1992). The simplest method is to consider a bi-ionic situation, with a single different permeant ion on each side of the membrane. If the ions are of equal valence, and assuming equal activity coefficients, then by measuring the zero current potential ( $V_{rev}$ ) one calculates the permeability ratio of the two permeant ions by:

$$V_{rev} = \frac{RT}{zF} \ln \left( \frac{K_A[A]}{K_B[B]} \right) \quad (\text{eqn. 2})$$

where  $K_A/K_B$ , the ratio of rate coefficients for each ion's movement through the channel, approximates the permeability ratio  $P_A/P_B$  (Andersen & Koeppe, 1992; Begenisich, 1992). So, for example, if the permeability of A is twice that of B, then the concentration of B will need to be twice A to obtain



zero electromotive force. This equation describes a steady interdiffusion of ions away from equilibrium (Hille, 1992). The ratio  $K_A/K_B$  *approximates* the permeability ratio, since the rate coefficients can vary with voltage; this can be obviated by manipulating the ion concentrations so that  $V_{rev}$  is 0 mV (Andersen & Koeppe, 1992).

If one assumes the intracellular milieu is constant, permeability ratios can be calculated by examining the change in zero-current potential upon replacing ion A with an equal concentration of ion B in the external solution.  $P_A/P_B$  is approximated by  $K_A/K_B$  and is given by:

$$\Delta E_{rev} = \frac{RT}{zF} \ln \left( \frac{P_A}{P_B} \right) \quad (\text{eqn. 3})$$

(Hille, 1972; Hille, 1973; Begenisich, 1992). Either of these calculations leads to a permeability ratio which is relatively robust, especially considering that they ignore the pore structure altogether. They are insensitive to channel block, which reduces channel number but does not change  $V_{rev}$  (Begenisich, 1992; Hille, 1992; Andersen & Koeppe, 1992). For a singly occupied channel, the ratio  $P_A/P_B$  depends solely on the ratio of the rate constants for ion A and ion B to traverse the major rate-limiting energy barrier (i.e., the highest barrier peak) in the energy profile along the pore (Hille, 1975a). Even if the pore holds more than one ion at a time, the calculation provides a decent estimate, if one assumes the narrow region of the pore is the rate-limiting step, and that it is singly occupied (Eisenman & Dani, 1987). If the channel is a multi-ion pore, the permeability ratios are complex functions of the rate constants for ion permeation and of ion concentration, and depend on both the well depths and the barrier heights (Hille, 1992).



These measures of ionic selectivity have been used to develop theories on the mechanism of ion permeation. It is assumed that ions must be partially or completely dehydrated by the selectivity filter to allow it to discriminate between ions, otherwise the selectivity would simply (and only) follow the ionic mobilities. Eisenman has developed a theory of selectivity based on the ease with which water molecules are shed from an ion and the strength of the binding site within the pore (Eisenman & Dani, 1987; Eisenman & Horn, 1983). Both of these forces depend (inversely) on the size of the ion (Yellen, 1987). So, for example, for a weak field-strength site the barrier to ion passage will be determined by the hydration energies; small ions will hold their waters tightly and will pass with more difficulty than larger ions, which can easily shed waters (Yellen, 1987). This suggests a reason for selecting  $K^+$  over the smaller  $Na^+$  ion in  $K^+$  channels.

Rate theory has also been used to model the permeation pathway as a series of energy wells and peaks, with the selectivity filter represented by the highest peak; different peak heights for the various permeant ions result in varying permeabilities, and the lower the relative peak height the higher the relative permeability (Hille, 1992). This can be reconciled with Eisenman's theory, since (e.g., for a  $K^+$  channel) the highest peak will be lower for  $K^+$  than for  $Na^+$ , which in Eisenman's treatment is due to the closer approach of the  $K^+$  ion to the proposed negative charge comprising the selectivity filter (and the resulting larger electrostatic attraction felt), since the  $Na^+$  will not shed its shell of water molecules and so will be less stabilized by interaction with the selectivity filter (Hille, 1992). These theories, however, are great simplifications; neither take into account the complexities of water coupling to ion flow or the movement of portions of the protein (Hille, 1992), nor do they consider the three-dimensional array of



chemical groups (seen as energies of attraction or repulsion) encountered by the ion as it traverses the membrane from one side to the other. Nevertheless, each has proven extremely useful in elucidating the mechanism of ion permeation.

## **B. Permeation Through CFTR Channels**

Since CFTR functions as a regulated anion channel, a detailed understanding of how it discriminates among anions must be considered a crucial component of its function. The relative permeability of anions through the epithelial CFTR channel has been examined by several laboratories. There is general agreement with the following sequence of relative permeabilities:  $\text{NO}_3^- > \text{Cl}^- > \text{F}^-$ . The relative permeability of  $\text{NO}_3^-$  to  $\text{Cl}^-$ , through the human epithelial CFTR channel, measured in excised inside-out patches of CHO cells stably expressing CFTR, is  $\sim 1.7$  (Tabcharani & Hanrahan, 1993).  $\text{Br}^-$  is also more permeant than  $\text{Cl}^-$ ; the relative permeability of  $\text{Br}^-$  to  $\text{Cl}^-$ , whether through CFTR endogenous in the apical membranes of T84 epithelial, or expressed in NIH 3T3, HeLa (Anderson et al., 1991) or CHO (Tabcharani & Hanrahan, 1993) cells, is  $\sim 1.3$ . Fluoride is much less permeant than  $\text{Cl}^-$ ; its relative permeability is  $\sim 0.3$  (Anderson et al., 1991; Tabcharani & Hanrahan, 1993). The relative permeability of  $\text{I}^-$ , however, is controversial; when CFTR is expressed in Sf9 insect cells and relative permeability is measured by extracellular substitution of I for Cl, it is  $\sim 1.1$  (Kartner et al., 1991). When similarly measured in HeLa, T84, or NIH 3T3 cells, it is  $\sim 0.6$  (Cliff & Frizzell, 1990; Anderson et al., 1991), yet with intracellular substitution of  $\text{I}^-$  for  $\text{Cl}^-$ , the relative permeability of  $\text{I}^-$  is  $\sim 2$ , and complicated by apparent block of currents by iodide (Tabcharani et al., 1992; Tabcharani & Hanrahan, 1993).





Because of this discrepancy, these results have been used to suggest both a low affinity, weak field strength anion binding site (Tabcharani & Hanrahan, 1993), and a moderately high affinity site for anion binding (Anderson et al., 1991).

Cardiac CFTR shows a similar progression of relative permeabilities to anions. Overholt, Hobert & Harvey (1993) found the following sequence of relative permeabilities:  $\text{NO}_3^-$  (2.1) >  $\text{Br}^-$  (1.3) >  $\text{Cl}^-$  (1) >  $\text{I}^-$  (0.9), largely in agreement with others (Dousmanis & Gadsby, 1994); however, in the latter study,  $\text{I}^-$  was found to be more permeant than  $\text{Cl}^-$  (relative permeability  $\sim 1.3$ ), in agreement with Walsh and Long (1992).  $\text{I}^-$  clearly has complex effects on channel permeation. It decreases both inward current at negative potentials, and outward current at positive potentials (Overholt & Harvey, 1992; Dousmanis & Gadsby, 1994), suggesting that iodide may act as a permeant blocker of the channel. Walsh and Long (1992) found that extracellular NaI inhibited both cAMP-dependent  $\text{Cl}^-$  and  $\text{Ca}^{2+}$  channels, and thus inferred a direct effect on the phosphorylation level of the channel itself or an associated regulatory protein.



## **XI. Outline**

The experimental results will be divided into three sections, each dealing with a different aspect of the function and regulation of CFTR Cl<sup>-</sup> channels. In the first (Chapter 3), I examine how three modulators of adenylyl cyclase activity,  $G_s$ ,  $G_i$ , and forskolin, interact at adenylyl cyclase to exert their effects at this key early component in the activation pathway of cardiac CFTR. The second section (Chapter 4) addresses ion permeation through the CFTR channel pore. The relative ease with which the CFTR channel passes a variety of anions is examined, by measuring shifts of bi-ionic reversal potential; the relative permeabilities yield information about the nature of the selectivity filter within the pore. An estimate of the minimum pore diameter is also made. Furthermore, the permeability coefficient and single channel conductance of the CFTR channel to Cl<sup>-</sup> is estimated using individual channels locked in the open state with AMP-PNP. In the final section (Chapter 5), the complex role of the nucleotide binding domains in channel gating is examined. Evidence is presented which strongly suggests that hydrolysis of an ATP molecule at NBD1 governs channel opening, that binding of an ATP molecule at NBD2 stabilizes the channel in the open conformation, and that channel closure is governed by the hydrolysis of that second ATP. Finally, we show in a single-channel patch that the ability of ATP to bind to NBD2 and prolong channel opening depends on the extent of channel phosphorylation.



## Chapter 2

### MATERIALS AND METHODS

#### I. Isolation of Cardiac Myocytes

Single ventricular myocytes were isolated by collagenase digestion of guinea pig hearts using a Langendorff perfusion system (Isenberg & Klöckner, 1982). Guinea pigs of either sex (300-550 g; Camm Research) were fully anesthetized with pentobarbital (50-100 mg/kg, i.p.; Abbott Labs). To minimize blood clot formation, heparin (~6000 U/kg; Elkins-Sinn Inc.) was injected, i.p., either ~15 min prior to anesthetization, or simultaneously with the pentobarbital injection. The heart was exposed by making a single long U-shaped incision running from under one forelimb to the other, along the lateral aspects of the ribcage and under the sternum. The pericardium was carefully cut, to expose the heart. The great vessels at the base of the heart were clamped and cut in one smooth step, excising the heart. The beating heart was then placed in a small disposable culture dish (60x15 mm; Corning) containing normal Tyrode's solution (~20 °C), to promote the ejection of any remaining blood. Excess tissue was cut away, to expose the aorta, the aorta was promptly cannulated with a glass tube, and retrograde coronary perfusion was begun, at ~36 °C, with oxygenated normal Tyrode's solution. Typically, the time from the initial incision to commencement of coronary perfusion was not longer than 1.5 min. After 0.5-2 min, the perfusate was switched to a  $\text{Ca}^{2+}$ -free Tyrode's solution, in which contraction stopped. After 1-5 min, perfusion was commenced of  $\text{Ca}^{2+}$ -free Tyrode's solution containing 0.1-0.3 mg/ml (Yakult Pharmaceutical Ind. Corp.) or 0.5-1.0 mg/ml (Sigma Type 1, or



Worthington CLS 2) collagenase, or an admixture of Yakult and one of the other two enzymes (all at ~36 °C). Occasionally, 10-20  $\mu\text{M}$   $\text{Ca}^{2+}$  was added to the enzyme solution, to attempt to better control the digestion process. Collagenase digestion was halted, after 7-20 min, by perfusion of *kraftbrühe* (KB) solution, a high  $[\text{K}^+]$  low  $[\text{Ca}^{2+}]$  nutrient solution used to maintain  $\text{Ca}^{2+}$ -tolerant, viable cells (Isenberg & Klöckner, 1982), first at 36 °C, then at room temperature, to rinse away the collagenase. The partially digested heart was then removed from the Langendorf set-up and placed in a culture dish containing KB. A transverse cut was made, to remove the atria, and a longitudinal cut was made down the lateral wall of the left ventricle, exposing the interior of the left ventricle, including the anterior and posterior papillary muscles and the ventricular wall of the septum. Small, ~3x3 mm chunks of ventricular tissue were excised, comprising portions of the anterior and posterior papillary muscles and associated wall, parts of the septum, and a piece of the right ventricular wall, and placed in 5 ml disposable polystyrene micro beakers (Fisher Scientific) filled with KB solution. The small chunks were snipped into small bits using fine scissors, the resultant dispersed tissue was shaken gently for 0.5-1 min, then filtered through 210  $\mu\text{m}$  nylon mesh (Small Parts Inc.) to yield a myocyte suspension which was stored at 4 °C. Whole-cell recordings were typically made within 12 hours, and excised-patch recordings, within two days of cell isolation.





## II. Composition of Solutions

### A. Whole-Cell Solutions

Tyrode's solution used during the myocyte isolation contained (mM): 145 NaCl, 5.4 KCl, 1.8 CaCl<sub>2</sub>, 0.5 MgCl<sub>2</sub>, 5.5 Glc, and 5 HEPES (pH 7.4 with NaOH). KB solution contained (mM): 80 L-glutamic acid, 20 taurine, 10 oxalic acid, 10 KH<sub>2</sub>PO<sub>4</sub>, 10 HEPES, 25 KCl, 0.5 EGTA, 5 pyruvic acid, 10 Glc (pH 7.4 with KOH).

The solutions used for the whole-cell experiments are listed in Table 1, and are referred to by number in the figure legends [e.g. E1/I4 denotes extracellular (bath) solution 1 and intracellular (pipette) solution 4]. The standard bath solution (1) contained 150 mM Cl<sup>-</sup>. Solutions 2 and 3 contained 125 and 24 mM Cl<sup>-</sup>, respectively. In solutions 4 and 5, all Cl<sup>-</sup> was replaced by either isethionate (4) or HEPES (5). Solution 6 (along with 2) was used in the experiments testing the relative permeability of anions (test anion represented by X<sup>-</sup>). The standard pipette solution (1) contained 24 mM Cl<sup>-</sup>, solution 2 contained 0 Cl<sup>-</sup>, solution 3 was the standard solution for the experiments testing relative anion permeability, and solutions 4 and 5 were used for the experiments in which relative permeability was determined with channels locked open using a mixture of MgATP and Li<sub>4</sub>AMP-PNP. Stock solutions of isoproterenol-HCl (0.8 mM in isotonic lactate buffer; Winthrop Pharmaceuticals) forskolin (10 mM in ethanol; Calbiochem Corp.), carbachol (10 mM in water; Aldrich Chemical Co.), and GTP (10 mM in water; Sigma) were diluted to the desired final concentration in bath solution daily before use. Tris<sub>2.5</sub>GTP (100 μM) was included in pipette solution for experiments whenever isoproterenol was used to activate whole-cell Cl<sup>-</sup> conductance, or whenever carbachol was



**Table 1. Composition of whole-cell solutions (mM)**

External (Bath) Solutions									
	Na <sup>+</sup>	Mg <sup>2+</sup>	Cd <sup>2+</sup>	Cl <sup>-</sup>	X <sup>-</sup>	Iseth <sup>-</sup>	SO <sub>4</sub> <sup>2-</sup>	HEPES	Glc
<b>1</b>	150	2	1	150	-	-	-	5	5.5
<b>2</b>	150	2	0,1	125	-	25	2	5	5.5
<b>3</b>	154	2	0,1	24	-	130	2	5	5.5
<b>4</b>	150	2	1	-	-	150	3	5	5.5
<b>5</b>	90	2	1	-	-	-	3	205	5.5
<b>6<sup>#</sup></b>	150	2	0,1 <sup>*</sup>	-	125	25	2,3 <sup>*</sup>	5	5.5

Internal (Pipette) Solutions									
	Cs <sup>+</sup>	TEA <sup>+</sup>	Li <sup>+</sup>	Mg <sup>2+</sup>	Cl <sup>-</sup>	SO <sub>4</sub> <sup>2-</sup>	Asp <sup>-</sup>	MeSO <sub>3</sub> <sup>-</sup>	Pyr <sup>-</sup>
<b>1</b>	100	20	-	12	24	-	85	-	5
<b>2</b>	100	20	-	12	-	2	85	20	5
<b>3</b>	100	20	-	12	125	-	-	-	5
<b>4</b>	100	20	8	6	125	-	-	-	5
<b>5</b>	100	20	12	6	125	2	-	-	5

	AMP-PNP	ATP	EGTA	HEPES	Glc	Tris <sub>2</sub> -Cr phosphate
<b>1</b>	-	10	10	10	5.5	5
<b>2</b>	-	10	10	10	5.5	5
<b>3</b>	-	10	10	10	5.5	5
<b>4</b>	-	4	10	10	5.5	-
<b>5</b>	2	2	10	10	5.5	-

Bath solutions pH balanced to 7.40 with NaOH.

Pipette solutions pH balanced to 7.40 with CsOH.

All solutions ~300 mOsm/kg.

<sup>#</sup>For experiments testing the relative permeability of HEPES, 205 mM HEPES was added.

<sup>\*</sup>For most experiments of relative anion permeability, Cd<sup>2+</sup> was left out of external solutions, with no discernable effect; occasionally, 1 mM CdSO<sub>4</sub> was added.

100 μM Tris<sub>2.5</sub>GTP was added to pipette solution whenever isoproterenol was used to activate Cl<sup>-</sup> conductance.

Pipette solutions 4 and 5 contained, in addition, 6 and 3 mM sucrose, respectively.

Free [Mg<sup>2+</sup>] for all pipette solutions ~1 mM (Bers, 1994).



used to inhibit whole-cell  $\text{Cl}^-$  conductance, to maintain GTP-binding-protein-mediated signal transduction (Horie, Hwang & Gadsby, 1992).

## **B. Excised-Patch Solutions**

The solution used to induce sarcolemmal blebs (Hilgemann, 1990) contained (mM): 134 KCl, 2-3  $\text{MgCl}_2$ , 20 glucose, 20 HEPES, 5 EGTA (pH 7.0 with KOH), and was diluted ~1:1 with distilled water, to enhance membrane separation from the myofilaments and bleb formation, and supplemented with  $\text{MgCl}_2$  to a final concentration of 2 mM to encourage seal formation (Collins, Somlyo & Hilgemann, 1992).

The solutions used for the excised patch experiments are listed in Table 2, and are referred to by number in the figure legends. The standard extracellular (pipette) solution contained 160 mM  $\text{Cl}^-$  (1). The standard intracellular (bath) solution contained 6.4 mM  $\text{Cl}^-$  (1). For the experiments on the [ATP] dependence of channel open probability, [ATP] was varied, while free  $[\text{Mg}^{2+}]$  was maintained at 1.2 mM, by varying added  $\text{Mg}^{2+}$  (solutions 2-7).  $\text{Mg}^{2+}$  was eliminated from solutions 8 and 9. EGTA was used in solutions 10-13 to weakly buffer  $\text{Mg}^{2+}$ . For the experiments to examine the  $[\text{Mg}^{2+}]$  dependence of channel opening and closing rates, free  $[\text{Mg}^{2+}]$  was adjusted by varying the amount of  $\text{Mg}^{2+}$  added to solutions containing 2 mM CDTA (solutions 8, 15-18). CDTA was the chosen buffer because of its large binding constant for  $\text{Mg}^{2+}$  (stability constant  $\sim 10^{11} \text{ M}^{-1}$  at 20 °C; Martell & Smith, 1989) and, hence, its suitability for controlling  $[\text{Mg}^{2+}]$  at very low concentrations. Consequently, only the solutions with 0, 5  $\mu\text{M}$ , and 40  $\mu\text{M}$  free  $[\text{Mg}^{2+}]$  (8, 15, 16) were reasonably well buffered but, since that is the concentration range over which  $\text{Mg}^{2+}$  markedly altered channel gating, the buffer type was not varied to improve buffering at

**Table 2. Composition of excised-patch solutions  
(mM)**

External (Pipette) Solutions									
	NMG <sup>+</sup>	Cs <sup>+</sup>	Ba <sup>2+</sup>	Mg <sup>2+</sup>	Cd <sup>2+</sup>	Cl <sup>-</sup>	HEPES	ATP	free Mg <sup>2+</sup>
1	145	5	2	2.3	0.5	159.6	10		

Internal (Bath) Solutions									
	NMG <sup>+</sup>	TEA <sup>+</sup>	Cs <sup>+</sup>	Mg <sup>2+</sup>	Cl <sup>-</sup>	Asp <sup>-</sup>	HEPES	EGTA	CDTA
1	140	20	-	3.2	6.4	140	10	-	2
2	140	20	-	3.2	6.4	140	10	-	2
3	140	20	-	3.2	6.4	140	10	-	2
4	140	20	-	3.24	6.4	140	10	-	2
5	140	20	-	3.38	6.4	140	10	-	2
6*	140	20	-	4.13	6.4	140	10	-	2
7	140	20	-	5.06	6.4	140	10	-	2
8	140	20	-	0	6.4	140	10	-	2
9	140	20	-	0	6.4	140	10	-	2
10	140	20	-	2	4	140	10	10	-
11	140	20	-	4	4	140	10	10	-
12	140	20	4	0	4	140	10	10	-
13	140	20	4	0	4	140	10	10	-
14	140	20	-	1.609	6.4	140	10	-	2
15	140	20	-	1.497	6.4	140	10	-	2
16	140	20	-	1.96	6.4	140	10	-	2
17	140	20	-	2.18	6.4	140	10	-	2
18	140	20	-	3.2	159.6	-	10	-	2

Pipette solutions pH balanced to 7.40 with NMG<sup>+</sup>.

Bath solutions pH balanced to 7.40 with Asp<sup>-</sup> or NMG<sup>+</sup>.

\*0.5 mM AMP-PNP substituted for ATP, and 2 mM Li<sup>+</sup> in all solutions, for experiment in Fig. 29; 2 mM only in AMP-PNP/ATP solution, in Fig. 13.

PKA catalytic subunit, kept as a 1 mg/ml stock solution, was diluted directly into bath solution, to yield a final concentration of ~100 nM.

Microcystin (0.4-0.5  $\mu$ M) added to all bath solutions, to maintain channel phosphorylation.

Free [Mg<sup>2+</sup>] calculated with the software program MAXC (Bers, 1994)

Mg<sup>2+</sup> stability constants, at 20 °C: EGTA ~10<sup>5</sup>, CDTA ~10<sup>11</sup> M<sup>-1</sup> (Martell & Smith, 1989).

All solutions ~300 mOsm/kg.





higher free  $[Mg^{2+}]$ . Solution 18 was used in the experiments examining the single channel conductance, after the channels had been locked open using an equal mixture of ATP and AMP-PNP. Free  $[Mg^{2+}]$  was calculated using the program MAXC (Bers, 1994).

Stock solution of microcystin-LR (200  $\mu M$  in water; Calbiochem), a potent membrane-impermeant inhibitor of phosphatases 1 and 2A (Honkanen et al., 1990) which has been shown to slow deactivation of cardiac CFTR  $Cl^-$  conductance (Hwang, Horie & Gadsby, 1993), was diluted to 0.4  $\mu M$  in all bath solutions daily before use. PKA catalytic subunit ( $\sim 1$  mg/ml in 150 mM  $K^+$  phosphate, 1 mM EDTA, pH 6.3) was prepared as described (Kaczmarek et al., 1980) and diluted to  $\sim 100$  nM in the appropriate bath solution.

Since CFTR  $Cl^-$  channels require both phosphorylation and hydrolyzable nucleoside triphosphate to open and close (e.g., Tabcharani et al., 1991; Nagel et al., 1992), PKA and ATP was applied together, at the outset of each experiment, to activate any CFTR channels in the patch. However, in 3 of 10 patches in which ATP was applied without a previous or concurrent application of PKA, channels were activated, which suggests that some channels were at least partially phosphorylated in the absence of agonists, and that they could maintain this phosphorylation during the blebbing procedure and upon patch excision. The small ( $\sim 0.1$  pA) dc outward current baseline shift observed when solution containing PKA is applied (see, e.g., Figs. 23, 31) is due to diluted buffer ( $\sim 0.6$  mM), since it was mimicked by perfusion of control solution to which was added  $K^+$ -phosphate at the same concentration; similarly, the inward shift typically observed when PKA solution was withdrawn was prevented by inclusion of the buffer in the control solution.  $K^+$ -phosphate buffer had little effect on



channel behavior. In two experiments, the behavior of PKA-phosphorylated channels was examined in the presence of 1 mM ATP, and of 1 mM ATP plus 0.6 mM K<sup>+</sup>-phosphate buffer. In each case, both mean channel open time (1.44 s *versus* 1.58 s, and 1.05 *versus* 0.95 s), and channel P<sub>o</sub> (0.23 vs. 0.25, and 0.17 vs. 0.21) were little affected. When bath [Mg<sup>2+</sup>] was reduced to the low micromolar range, a reversible inward shift in holding current developed (see, e.g., Figs. 22, 23). To determine whether this shift was due to a decrease in seal resistance (R<sub>s</sub>), bath [Mg<sup>2+</sup>] was lowered to 5 μM (buffered with CDTA), and 20 mV hyperpolarizing pulses (duration ~10 s) were applied, and compared to similar pulses before and after bath [Mg<sup>2+</sup>] was lowered (Fig. 3). Concurrent with the inward shift in holding current, there is an ~3-fold decrease in R<sub>s</sub>, likely due to the slow leaching of Mg<sup>2+</sup> from the membrane-glass interface.

### III. Whole-Cell Recording

Approximately 100 μl of the solution containing the dispersed cells was pipetted into a custom built recording chamber (~4x10 mm) mounted on the microscope stage (Diaphot; Nikon Inc.). After the cells settled on the bottom of the chamber (1-2 min), superfusion was begun with Tyrode's solution. This Ca<sup>2+</sup> challenge caused Ca<sup>2+</sup>-intolerant, unhealthy cells to contract, leaving scattered, single, Ca<sup>2+</sup>-tolerant myocytes. All superfusion solutions were heated to ~36 °C with heating coils connected to either input of a two-position valve (Hamilton Co.), whose output was connected by a 3 cm length of narrow (i.d. 1 mm) silastic tubing to one end of a glass capillary tube (i.d. 1 mm) mounted at one end of the recording chamber. Solutions flowed along the recording chamber, and were removed by suction from a small



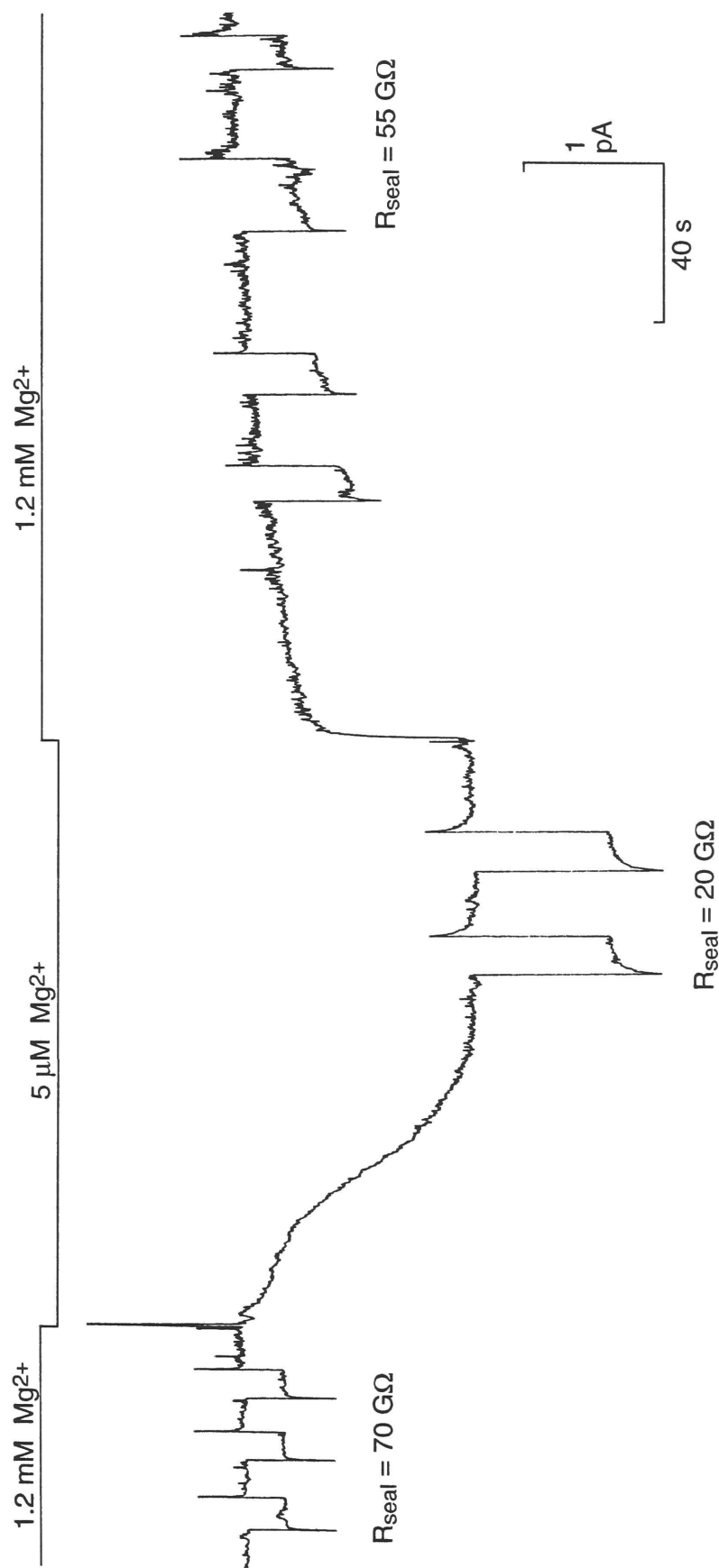


**Fig. 3. Inward shift in holding current observed when bath [Mg<sup>2+</sup>] is lowered is associated with a decrease in seal resistance (R<sub>S</sub>). Membrane current in a patch. V<sub>h</sub>=+10 mV. Current steps in response to 20 mV hyperpolarizing voltage steps, to 0 mV, to monitor R<sub>S</sub>. Upper bars denote changes in bath [Mg<sup>2+</sup>]. When bath [Mg<sup>2+</sup>] is lowered to 5 μM, an inward current develops, which is associated with a decrease in R<sub>S</sub>, and which reverses as [Mg<sup>2+</sup>] is returned 1.2 mM (E1/I1,15).**



well at the opposite end. Solutions could be changed within  $\sim 10$  s (see, e.g., Figs. 14, 15). Wide-tipped pipettes [ $\sim 5$   $\mu\text{m}$  inner diameter, initial pipette resistance ( $R_{\text{pip}}$ )  $\sim 1$   $\text{M}\Omega$ ] were pulled from borosilicate glass capillary tubes (i.d. 1.0 mm, o.d. 1.4 mm; Mercer Glass Works). Once filled with Tyrode's solution, they were connected to a pipette perfusion device which allowed alteration of the pipette solution during the experiment (Soejima & Noma, 1984). After nulling any pipette potential offset with the amplifier, the pipette tip were apposed to the membrane of an isolated myocyte using a Leitz micromanipulator, and a gigaohm seal was formed by gentle suction ( $-20$  to  $-40$  mm  $\text{H}_2\text{O}$ ). Before rupturing the membrane with more vigorous suction ( $-60$  to  $-100$  mm  $\text{H}_2\text{O}$ ), the Tyrode's solution in the pipette was exchanged for the intracellular recording solution. After patch rupture and equilibration of the pipette solution with the cell interior (taking  $\sim 1$  min), the holding potential was set to 0 mV, and the cell was superfused with a  $\text{Ca}^{2+}$ -free extracellular solution. Recordings typically commenced 3-5 min after breakthrough.

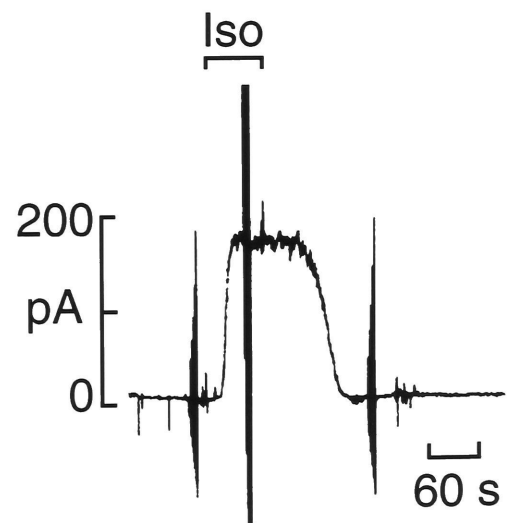
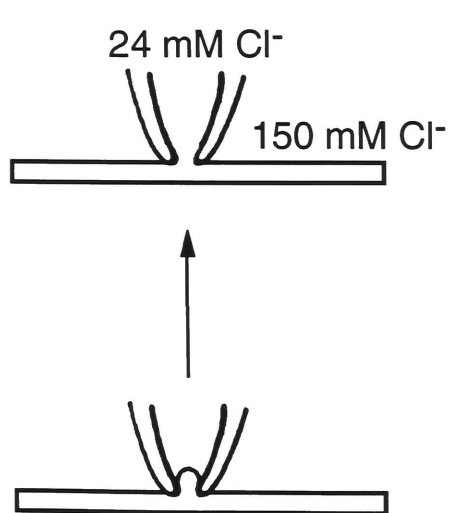
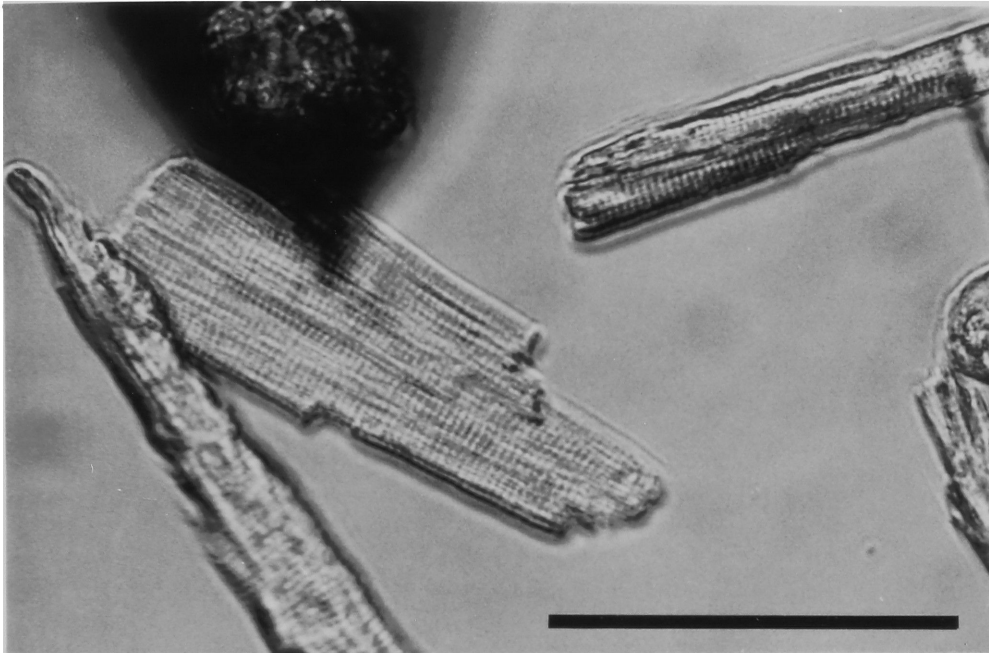
Figure 4 shows a photograph of a typical ventricular myocyte used for a whole-cell experiment, and a cartoon depicting the formation of a gigaseal and rupture of the membrane within the pipette tip to obtain the whole-cell configuration (lower left). Once in the whole-cell-configuration, activation of cardiac CFTR  $\text{Cl}^-$  conductance (here by bath application of 1  $\mu\text{M}$  isoproterenol) results in a  $\sim 200$  pA outward shift in membrane current at the 0 mV holding potential, reflecting the net *inward* movement of  $\text{Cl}^-$  ions through  $\sim 500$  open CFTR  $\text{Cl}^-$  channels (see below).

Whole-cell currents were measured with a custom built amplifier, and the holding current was continuously monitored. Membrane capacitance ( $C_m$ ) and access resistance ( $R_{\text{acc}}$ ) were determined using a 10 mV (dur. 10

**Fig. 4. Whole-cell configuration.** Photograph shows a typical ventricular myocyte used for whole-cell recording. The shadow is cast from the microelectrode glass pipette. Lower left panel depicts the steps in forming the whole-cell configuration. Once a gigaseal is formed between the glass pipette and the cell membrane, the patch of membrane covering the pipette tip is ruptured, allowing control of the intracellular milieu and the monitoring of whole-cell currents. Under the standard recording conditions, activation of whole-cell  $\text{Cl}^-$  conductance by 1  $\mu\text{M}$  Iso typically results in a  $\sim 200$  pA outward shift in the holding current at the 0 mV holding potential, the result of current passing through  $\sim 500$  open CFTR channels (*lower right*; see Chapter 3, III). Bar = 100  $\mu\text{m}$ .



## Whole-cell configuration





ms) hyperpolarization, by fitting the decay time constant  $\tau$  ( $=R_{acc} \cdot C_m$ ) and by integrating the current under the transient phase ( $Q = \int I dt$ ;  $C_m = Q/\Delta V$ ). Voltage errors due to series resistance were ignored: with the largest whole-cell currents observed,  $\sim 1$  nA, and  $R_{acc}$  typically 1-3 M $\Omega$ , maximum expected voltage errors are  $\leq 3$  mV. Whole-cell currents were recorded in response to 80 ms voltage pulses to potentials between -100 and +100 mV, from the 0 mV holding potential, in 20 mV increments. Steady-state current-voltage (I-V) relationships were plotted from the current levels averaged over the final 12.5 ms of each pulse. Current and voltage signals were filtered at 2 kHz, digitized at 8 kHz, stored in an IBM PC computer, and subsequently analyzed with Asyst software (MacMillan Software Co.).

#### **IV. Excised-Patch Recording**

Early cell-attached patch experiments, using standard small pipette electrodes (electrode resistance 3-5 M $\Omega$ ) (Ehara & Ishihara, 1990), indicated a very low CFTR Cl<sup>-</sup> channel density in guinea-pig ventricular myocytes, with channels being detected in  $< 5\%$  of patches. To increase the likelihood of obtaining patches with channels, we used the giant excised-patch technique developed by Hilgemann (Collins, Somlyo & Hilgemann, 1992), on spherical sarcolemmal membrane blebs. These membrane blebs, induced by placing cells in a hypotonic KCl solution (see above), exhibit roughly the same Na<sup>+</sup> channel current (Hilgemann, 1989), Na<sup>+</sup> pump current (Hilgemann, Nagel & Gadsby, 1991), and Na<sup>+</sup>-Ca<sup>2+</sup> exchange current (Hilgemann, 1989) densities inferred from whole-cell measurements. Most important, however, CFTR Cl<sup>-</sup> channel density in excised patches formed from these sarcolemmal blebs is roughly that expected from whole-cell



measurements (Nagel et al., 1992), and their regulation by PKA and nucleoside triphosphates, appears indistinguishable from CFTR Cl<sup>-</sup> channels in whole-cell studies (e.g., Nagel et al., 1992; Hwang, Horie & Gadsby, 1993; Hwang et al., 1994).

Low resistance, wide-tipped (8-20  $\mu$ m inner diameter) recording electrodes were fabricated from borosilicate glass (N51A; i.d. 1.6 mm, o.d. 2.0 mm; Drummond Scientific Co.) using a Narishige PP-83 vertical microelectrode puller and a conventional double-pull technique. Pipette tips were then cut and firepolished using a modified microforge to re-melt and shear the pipette tip to the desired diameter (Hilgemann, 1995). Pipettes were first made hydrophobic at the tips by coating with a hydrocarbon mixture of light and heavy mineral oils and Parafilm (American Can Corp.), to aid in seal formation and to enhance patch stability after excision (Hilgemann, 1995). ~100  $\mu$ l of the solution containing the dispersed cells was placed in a 35x10 mm disposable tissue culture dish containing ~5 ml hypo-osmotic blebbing solution, and placed on the stage of an inverted microscope (TMS; Nikon Inc.). Pipettes were backfilled with standard 160 mM Cl<sup>-</sup> pipette solution and sealed to sarcolemmal blebs with light suction. After a gigaohm seal was established, the patch was excised and placed in a custom-built flow chamber in which solutions can be rapidly changed on the intracellular face of the membrane (within ~1 s). Bath solutions were placed in inverted 60 ml plastic syringes, and forced by positive pressure through thin (i.d. 0.025") silastic tubing to the manifold in the flow chamber. Outflow was controlled by means of electric valves interposed between the syringes and the flow chamber (General Valve Corp.).



Figure 5 shows a typical myocyte and the procedure used for excised-patch experiments. Placed in hypo-osmotic storage solution, the cell membrane has formed two blebs. The procedure for obtaining excised patches is depicted in the lower left panel. Once a gigaseal is formed between the pipette tip and a membrane bleb, the electrode is rapidly pulled away from the cell, leaving a patch of membrane covering the pipette tip. Thereafter, the opening and closing of a channel in the membrane patch is detected as an outward current step, reflecting net flow of  $\text{Cl}^-$  ions *out* of the pipette and into the bath.

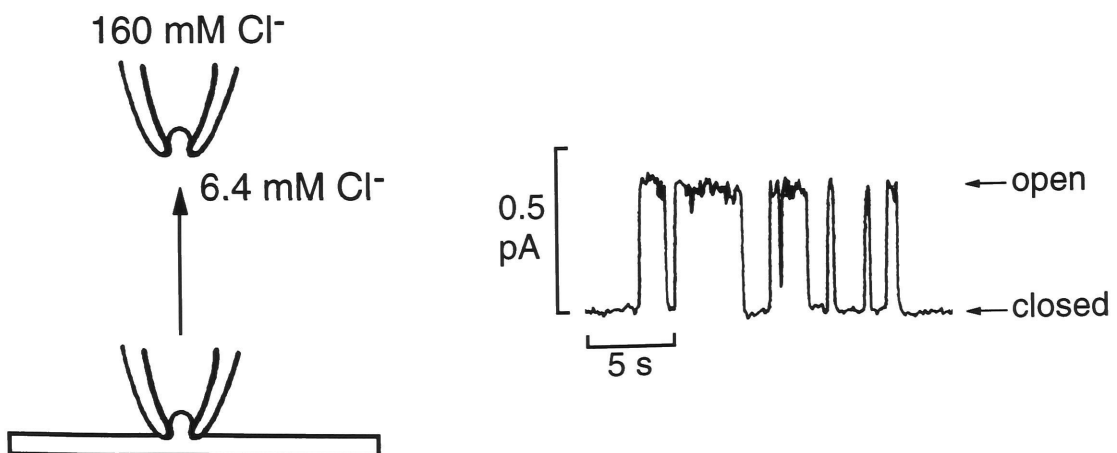
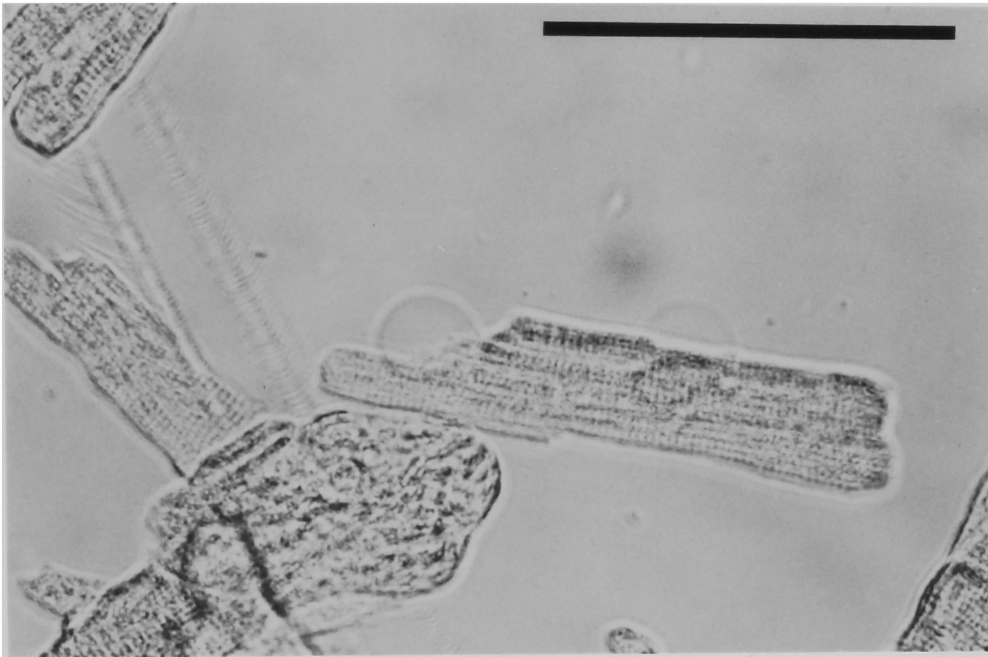
Patch current was recorded with a List EPC-7 amplifier (List Electronics), filtered at 200 Hz, monitored directly on a chart recorder (BD41; Kipp and Zonen), and stored on videotape for later replay and analysis using Asyst software (MacMillan Software Co.). Seal resistance was determined at the outset of each experiment by measuring the current during a 20 mV step hyperpolarization. All experiments were carried out at room temperature (20-22 °C).

Figure 6 plots the number of evident CFTR  $\text{Cl}^-$  channels *versus* the estimated membrane area for the 143 patch experiments in this study. Most patches contained between one and six channels; however, ten patches contained between seven and fifteen channels. 34% of patches contained a single channel. From the mean number of channels elicited in excised patches (2.7), and the estimated mean membrane area of a patch ( $118 \mu\text{m}^2$ ), the channel density in bleb membrane is estimated to be  $0.023 \mu\text{m}^{-2}$ .

**Fig. 5. Inside-out, excised-patch configuration.** Photograph shows a typical cell used for excised patch experiments. Note the two blebs of the cell membrane which were induced by placing the cell in a hypo-osmotic solution. Once a gigaseal is formed between the pipette and the cell membrane, the pipette is abruptly pulled away, retaining a patch of membrane on the tip (*lower left*). Application of the catalytic subunit of PKA and MgATP elicits individual cardiac CFTR channels in the patch (*lower right*). Bar = 100  $\mu\text{m}$ .



## Inside-out, excised-patch configuration





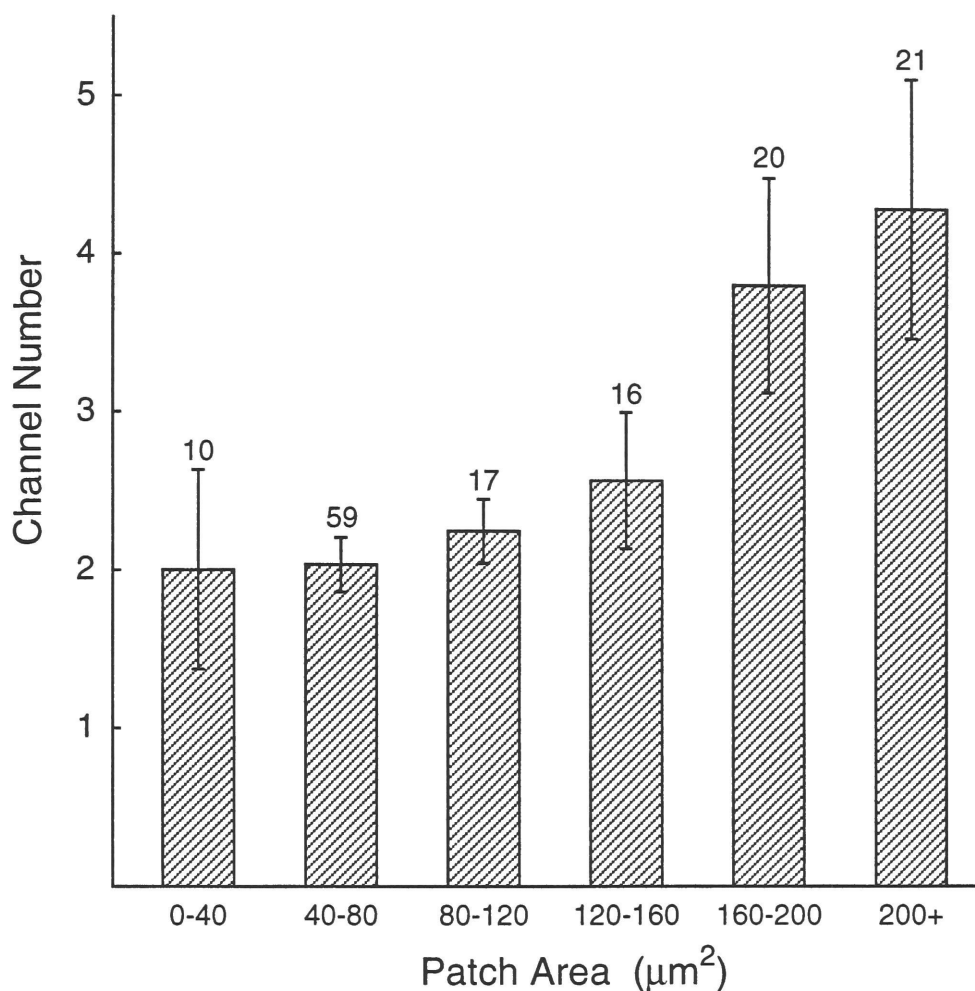


**Fig. 6. Channel density in excised membrane patches.** Summary of number of channels versus patch area in 143 excised membrane patches exhibiting  $\geq 1$  CFTR  $\text{Cl}^-$  channel. For each experiment, microelectrode tip inner diameter ( $d$ ) was measured, from which an estimate of membrane area was calculated, assuming a circular membrane patch of area  $\pi(d/2)^2$ . Experiments were binned based on estimated membrane area, and the number of channels were averaged for each bin. 34% of patches contained a single channel. Mean number of channels in a patch =  $2.7 \pm 0.2$ . Mean patch area =  $118 \pm 6 \mu\text{M}^2$ . Channel density =  $0.023 \mu\text{m}^{-2}$ . Numbers above each bar indicate number of patches comprising each bin.



## V. Channel Density

In the whole-cell configuration, at +10 mV and with 150 mM  $\text{Cl}^-_{\text{out}}$ /24 mM  $\text{Cl}^-_{\text{in}}$ , the activated CFTR  $\text{Cl}^-$  current amplitude averaged  $238 \pm 23$  pA ( $n = 39$ ). The average single-channel current amplitude at +10 mV, with 160 mM  $\text{Cl}^-$  in the pipette and 6.4 mM  $\text{Cl}^-$  in the bath, was  $0.44 \pm 0.02$  (s.d.) pA ( $n = 81$ ; see Chapter 4). This implies that, on average, ~550 open channels contributed to the whole-cell current. If channel  $P_o$  during the whole-cell recordings is ~0.4 (see Chapter 5), then the typical ventricular myocyte contains ~1400 CFTR  $\text{Cl}^-$  channels. Based on the whole-cell measurements, then, for a cell surface area of  $13,000 \mu\text{m}^2$  (assuming a specific membrane capacitance of  $1 \mu\text{Fcm}^{-2}$ , and given a measured cell capacitance of 130 pF), the average channel density is estimated to be  $\sim 0.11 \mu\text{m}^{-2}$ , the same as that reported by Ehara and Ishihara on the basis of recordings in cell-attached patches (1990), but roughly two-fold higher than the estimate of Nagel et al. (1992). For an average excised patch membrane area of  $\sim 120 \mu\text{m}^2$  (Fig. 6), this density of  $0.11 \mu\text{m}^{-2}$  suggests that ~12 channels should be present per patch. But in fact, the mean number of channels in a patch was ~3, implying a roughly four-fold lower density of channels in bleb patch membrane than in intact whole myocyte membrane. If, as has been suggested recently (Prat et al., 1995), the actin cytoskeleton plays a role in the activation of CFTR, then since excised patches obtained from blebs appear free of cytoskeletal elements (Collins, 1992a), it seems possible that some CFTR channels in the patch membrane might be removed from the activatable pool. Another possibility is that bleb membrane may represent "old" sarcolemma diluted by insertion of additional membrane (e.g., from the transverse tubular system; Collins,



1992a), which may not contain  $\text{Cl}^-$  channels, and this might at least partly explain the lower density of channels in patch membrane.

## **VI. Junction Potentials**

To minimize the development of liquid junction potentials during whole-cell experiments, two 3M KCl half cells connected the voltage-clamp amplifier to the pipette interior and to the recording chamber (Barry & Diamond, 1970). With Tyrode solution in the bath, and the pipette backfilled with Tyrode, and before the solution at the pipette electrode tip was replaced with standard pipette solution, the voltage clamp output was set to zero. For the bi-ionic reversal potential experiments, a flowing 3 M KCl bath electrode minimized contamination of the bath electrode tip by the anion change. To detect any time-dependent changes in the holding current, the zero-current potential was determined at the end of the experiment by reperfusion of Tyrode solution in the bath, breaking the seal, and direct measurement. This offset, typically  $< 1.5$  mV over 20-30 min, was left uncorrected.

In the excised patch experiments, an  $\sim 10$  mV junction potential was present between the standard pipette solution ( $\text{NMG}^+/\text{Cl}^-$ ) and the blebbing solution in the bath ( $\text{K}^+/\text{Cl}^-$ ), and was corrected for.

## **VII. Data Analysis**

### **A. Whole-Cell Experiments**

In  $\sim 20\%$  of intact cells, Fsk-activated whole-cell  $\text{Cl}^-$  conductance was either not present, or was small. This seemed correlated with the appearance of the cells after dispersion. When cells appeared healthy, i.e.,





bright and translucent, with clear, straight myofilament striations, and crisp, sharp edges, Cl<sup>-</sup> conductance was typically robust. If the current elicited by maximal concentrations of Iso or Fsk, at 0 mV, was < ~100 pA, cells were not used.

For the experiments on the regulation of adenylyl cyclase, the magnitude of whole-cell CFTR conductance was conveniently assayed as the current elicited at 0 mV. To account for occasional slow small (10-20 pA) drifts of baseline current, evident between exposures to agonists, linear interpolation was used to determine the appropriate magnitude of the drift for subtraction from the measured amplitude of the elicited current. If this drift was > 50 pA, results were not included.

For whole-cell current-voltage relations, currents were recorded in response to 80 ms voltage pulses from the 0 mV holding potential to  $\pm 20$ ,  $\pm 40$ ,  $\pm 60$ ,  $\pm 80$ , and  $\pm 100$  mV. Steady-state I-V relationships were obtained by averaging the current levels over the final 12.5 ms of each pulse, and agonist-activated currents were obtained by appropriate subtraction of currents elicited in the presence and absence of agonist (see Fig. 7).

The reversal potential ( $E_{\text{rev}}$ ) of the activated whole-cell anion conductance was determined by linear interpolation between the smallest inward and outward currents in the steady-state difference I-V relation (see, e.g., Fig. 12B). For all of the determinations of relative anion permeability, steady-state difference I-V relations of the activated conductance were obtained in symmetric 125 mM Cl<sup>-</sup>, both before (1) and after (3) bath replacement of Cl<sup>-</sup> with the test anion (2).  $\Delta E_{\text{rev}}$  was then defined by:

$$\Delta E_{\text{rev}} = E_{\text{rev}}(2) - \left( \frac{E_{\text{rev}}(1) + E_{\text{rev}}(3)}{2} \right) \quad (\text{eqn. 4})$$



$E_{rev}$  measurements were very sensitive to increases in leak current if the currents reversed at either very positive, or negative, potentials (see Fig. 11), or if the I-V relation was flat near  $E_{rev}$  (see Fig. 15C). To minimize the effects of any small increase in leak conductance on  $E_{rev}$  measurements in the former case, for tests of the relative permeability of  $Asp^-$ ,  $Iseth^-$ , and  $HEPES^-$ ,  $E_{rev}$  in the bi-ionic situation was determined by subtracting the average of two control I-V relations, obtained before and after activation of the whole-cell conductance, from the I-V relation obtained in the presence of agonist (see Fig. 11D). For the latter case (viz., the iodide experiments), exposure to the test anion was kept brief, and experiments were not used if the increase in leak was judged significant relative to the magnitude of the currents.

For estimates of the minimum pore diameter of the channel, we used the geometric mean diameter for each anion (Dwyer, Adams & Hille, 1980), using:

$$D_{mean} = \sqrt[3]{L \times W \times H} \quad (\text{eqn. 5})$$

where L, W, and H are the dimensions of the non-hydrated anion calculated using molecular model building software (WindowChem Software Inc.).

## **B. Excised-Patch Experiments**

To calculate the relative channel open probability ( $P_o$ ) as a function of [ATP], relative  $P_o$  was taken as the  $P_o$  during the test [ATP] divided by the average  $P_o$  during the two bracketing exposures to 2 mM ATP. This minimized the effects of channel rundown and/or dephosphorylation on the



measurements. If the patch contained  $< 4$  channels,  $P_o$  was measured directly from the chart paper, by dividing the area under open channel currents by the total possible open area (if all observed channels were open for the whole exposure). If there were  $\geq 4$  open channels in a recording during an exposure to a given [ATP],  $P_o$  during that exposure was estimated by eye as the mean current level, which approximates the total open area, and the  $P_o$  at the lower [ATP] was measured directly as the open area.

To fit latencies to first channel opening, or closing, or open/closed dwell times, individual measurements were ranked in descending order, plotted against rank, and fit to a single exponential. If progress from the initial state (e.g., closed channel) to the final state (open channel) is dominated by a single kinetic process, the dwell times until the event occurs should be exponentially distributed, according to Poisson's Law:

$$P(t) = e^{-bt} \quad (\text{eqn. 6})$$

where  $P(t)$  represents the probability of observing a channel closed (or open) dwell time greater than time  $t$ , and  $b$  is the opening (or closing) rate (see, e.g., Coronado & Miller, 1982);  $1/b$  represents the mean channel closed (or open) time. Once the data are thus fit, the ranks are normalized by the fitted y-intercept to yield the probability distribution function; thus, at time zero, the probability that the channel is closed (or open) is 1.

Because of the typically small number of measurements, this procedure was preferable to the standard practice of binning the dwell times and fitting these to an exponential function. However, in the case of the latencies to channel opening in 1.2 mM  $Mg^{2+}$  (Fig. 25), there were enough individual measurements to do so. Confirming the validity of the



technique, the opening rate ( $0.19 \pm 0.03 \text{ s}^{-1}$ ) calculated with the data so binned and fit to a single exponential was not significantly different from that ( $0.22 \pm 0.01$ ) calculated by fitting the unbinned, individual times ( $P > 0.05$ ).

For determination of mean channel open and closed times, measurements were made directly from the pen chart recorder paper. Tests with rectangular voltage pulses revealed that the amplitude of the recorded signal was reduced to one half (the cut-off for inclusion as an opening or closing) for pulse durations of  $\sim 35$  ms, implying that open times (and closed times) as short as 35 ms would be detected, but briefer events would be missed. The effect of these missed events on the estimations of mean open and mean closed times should be minimal.

## VIII. Statistics

Mean values, unless otherwise specifically stated, are given as standard error of the mean (S.E.M.). All calculations of statistical significance, unless otherwise stated, were calculated using an unpaired two-tailed Student's *t*-test. The level of significance was  $P < 0.05$ .





## Chapter 3

### UPSTREAM REGULATION OF THE CARDIAC CFTR Cl<sup>-</sup> CHANNEL

#### I. Introduction

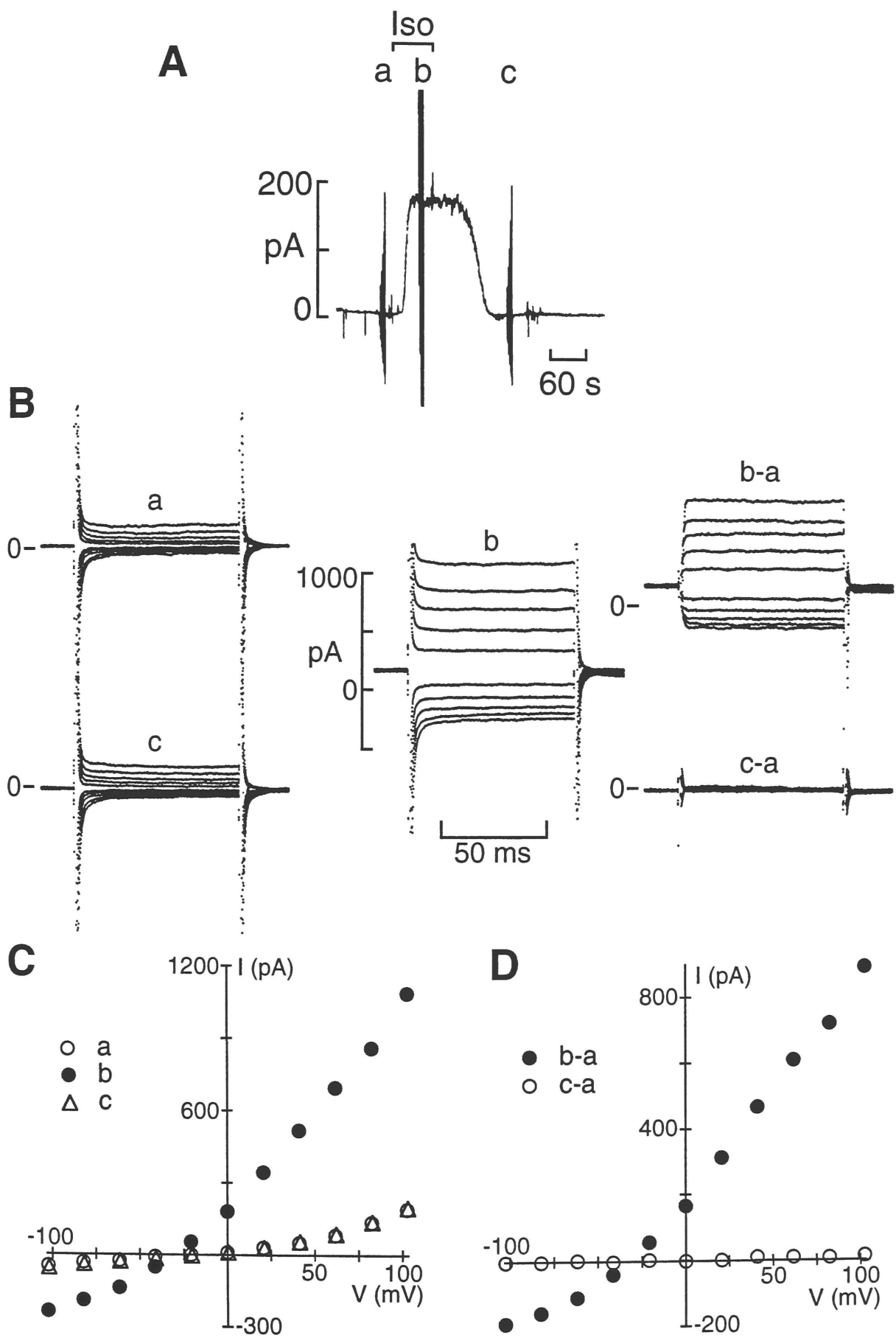
By employing whole-cell cardiac CFTR Cl<sup>-</sup> conductance as an on-line assay of cellular cAMP levels, changes in adenylyl cyclase activity are readily detected. In particular, we can study how modulators of adenylyl cyclase, the key early component of the regulatory pathway of the CFTR Cl<sup>-</sup> conductance, act and interact at the cyclase to alter cAMP levels. In this way, we examined how the physiologic modulators of adenylyl cyclase activity, G<sub>s</sub> (activated by stimulation of  $\beta$ -adrenoceptors), G<sub>i</sub> (activated by stimulation of muscarinic acetylcholine receptors), and the direct adenylyl cyclase activator forskolin (Fsk), interact at the cyclase to modulate its activity. Portions of this work have been presented in abstract (Hwang et al., 1992a).

#### II. Results

Figure 7 shows the activation and deactivation of the whole-cell CFTR Cl<sup>-</sup> conductance, measured in an acutely dissociated guinea-pig ventricular myocyte. Panel A shows whole-cell membrane current from a voltage-clamped myocyte, with a strong Cl<sup>-</sup> gradient across the membrane. For this and all experiments on the modulation of adenylyl cyclase, pipette solution contained 24 mM Cl<sup>-</sup>, bath solution contained 150 mM Cl<sup>-</sup>, and the holding potential was 0 mV. The upper bar marks the period of bath application of 1  $\mu$ M isoproterenol (Iso). Vertical lines (*a*, *b*, *c*) indicate

**Fig. 7. Activation and deactivation of the whole-cell CFTR Cl<sup>-</sup> conductance.**

**A.** Current trace from an experiment showing activation and deactivation of whole-cell Cl<sup>-</sup> conductance. Upper bar marks bath application of 1  $\mu$ M isoproterenol (Iso). Vertical lines (*a*, *b*, *c*) indicate application of 80-ms voltage pulses from the 0 mV holding potential to collect I-V data. Bath solution contains 150 mM Cl<sup>-</sup>, pipette solution 24 mM Cl<sup>-</sup>. **B.** Superimposed records of whole-cell currents elicited by voltage pulses to  $\pm 20$ ,  $\pm 40$ ,  $\pm 60$ ,  $\pm 80$ , and  $\pm 100$  mV, recorded before (*a*), during (*b*), and after (*c*) application of Iso. Iso-activated currents (*b-a*) were obtained by subtracting currents elicited in the absence of Iso from the corresponding currents elicited during exposure to Iso. Subtracting the currents elicited after Iso washout from those before Iso application shows that the membrane leak conductances were unchanged throughout the experiment (*c-a*). **C.** Plot of steady-state currents, obtained by averaging the steady current levels over the final 12.5 ms of each 80 ms pulse, elicited before (*a*,  $\circ$ ), during (*b*,  $\bullet$ ), and after (*c*,  $\Delta$ ) bath application of 1  $\mu$ M Iso. **D.** Steady-state difference I-V relations showing the Iso-activated current (*b-a*,  $\bullet$ ), and the absence of any change in the background conductance (*c-a*,  $\circ$ ). Cell capacitance ( $C_m$ ) = 129 pF; initial pipette resistance ( $R_{pip}$ ) = 0.8 M $\Omega$ ; access resistance ( $R_{acc}$ ) = 3.7 M $\Omega$ . External solution 1, internal solution 1 (E1/I1).





application of 80-ms voltage pulses to collect current-voltage (I-V) data. When 1  $\mu$ M Iso was introduced into the bathing solution, a large,  $\sim$ 200 pA outward shift in holding current developed (stable within  $\sim$ 30 s), reflecting the net influx of  $\text{Cl}^-$  through open channels, which, upon withdrawal of Iso from the bathing solution, returned to control levels within  $\sim$ 90 s. Panel *B* shows superimposed records of the whole-cell currents elicited by 80 ms voltage pulses to  $\pm 20$ ,  $\pm 40$ ,  $\pm 60$ ,  $\pm 80$ , and  $\pm 100$  mV, recorded before (*a*), during (*b*), and after (*c*) exposure to Iso.

The experimental conditions effectively eliminated virtually all time- and voltage-dependent components of membrane current (Fig. 7*B*, *a*, *c*).  $\text{Na}^+$  and  $\text{Ca}^{2+}$  channels were inactivated by the 0 mV holding potential.  $\text{K}^+$  channel currents were minimized by omitting  $\text{K}^+$  from the pipette and bath solutions, and by replacing internal  $\text{K}^+$  with  $\text{Cs}^+$  and  $\text{TEA}^+$ .  $\text{Na}^+/\text{K}^+$  pump currents were eliminated by the lack of intracellular  $\text{Na}^+$  and extracellular  $\text{K}^+$ , and  $\text{Na}^+/\text{Ca}^{2+}$  exchange currents by the lack of intracellular  $\text{Na}^+$  and of both intracellular and extracellular  $\text{Ca}^{2+}$ .  $\text{Cd}^{2+}$  further prevented current flow through  $\text{Ca}^{2+}$  channels.

Subtracting the currents elicited after Iso washout from the corresponding currents elicited before Iso application shows that the residual membrane leak conductance was unchanged throughout the experiment (Fig. 7*B*, *c-a*). Iso-activated currents were therefore obtained by subtracting the currents elicited in the absence of Iso from the corresponding currents elicited during exposure to Iso (e.g., Fig. 7*B*, *b-a*). These currents remained constant for the 80 ms duration of the voltage pulse. Panel *C* shows a plot of the steady-state whole-cell currents, obtained by averaging the steady current levels over the final 12.5 ms (100 points) of each 80 ms pulse, elicited before (*a*,  $\circ$ ), during (*b*,  $\bullet$ ), and after (*c*,  $\Delta$ ) bath



application of 1  $\mu\text{M}$  Iso. Panel *D* shows the steady-state difference I-V relations, representing the Iso-activated currents (*b-a*, ●), and confirming the absence of change in background leak conductance (*c-a*, ○). The Iso-activated currents are carried by  $\text{Cl}^-$ , since there is an outward shift in holding current at 0 mV in asymmetric, high  $[\text{Cl}^-]_o/\text{low}[\text{Cl}^-]_i$  (Fig. 7A), the current exhibits outward rectification in these asymmetric  $[\text{Cl}^-]_s$  (Fig. 7D, *b-a*, ●), and the currents reverse near (but ~15 mV positive to) the calculated  $\text{Cl}^-$  equilibrium potential ( $E_{\text{Cl}}$ , ~ -50 mV under these conditions). In addition, reversal potential shifts upon changes in intracellular and extracellular  $[\text{Cl}^-]$  are consistent with an anion selective conductance (see Chapter 4, Table 3).

To examine the interaction of the GTP-binding proteins  $G_s$  and  $G_i$  at adenylyl cyclase, the dose-response relations to Iso were determined, in the absence, and in the presence, of supramaximal activation of muscarinic receptors by 5  $\mu\text{M}$  carbachol (CCh), a muscarinic cholinergic receptor agonist (Fig. 10A). Figure 8 illustrates a typical experiment used to generate the data in Figure 10A. Figure 8A shows the whole-cell current trace. Upper bars mark the time of bath applications of Iso and CCh at the indicated concentrations. Vertical lines (*a*, *b*, *c*, *d*) indicate the collection of I-V data. 1  $\mu\text{M}$  Iso activated an ~200 pA outward current at 0 mV which was not increased by raising [Iso] to 5  $\mu\text{M}$ , suggesting that adenylyl cyclase was maximally stimulated (but see Chapter 3, Discussion). Even so, 5  $\mu\text{M}$  CCh could still halve the current at 0 mV. The steady-state difference I-V relations in Figure 8B confirm that the  $\text{Cl}^-$  conductances activated by 1  $\mu\text{M}$  and 5  $\mu\text{M}$  Iso are similar (Fig. 8B, *c-b*,  $\Delta$ ), and that despite this apparent maximal cyclase activation by  $G_s$ ,  $\text{Cl}^-$  conductance activated by 5  $\mu\text{M}$  Iso (*c-*





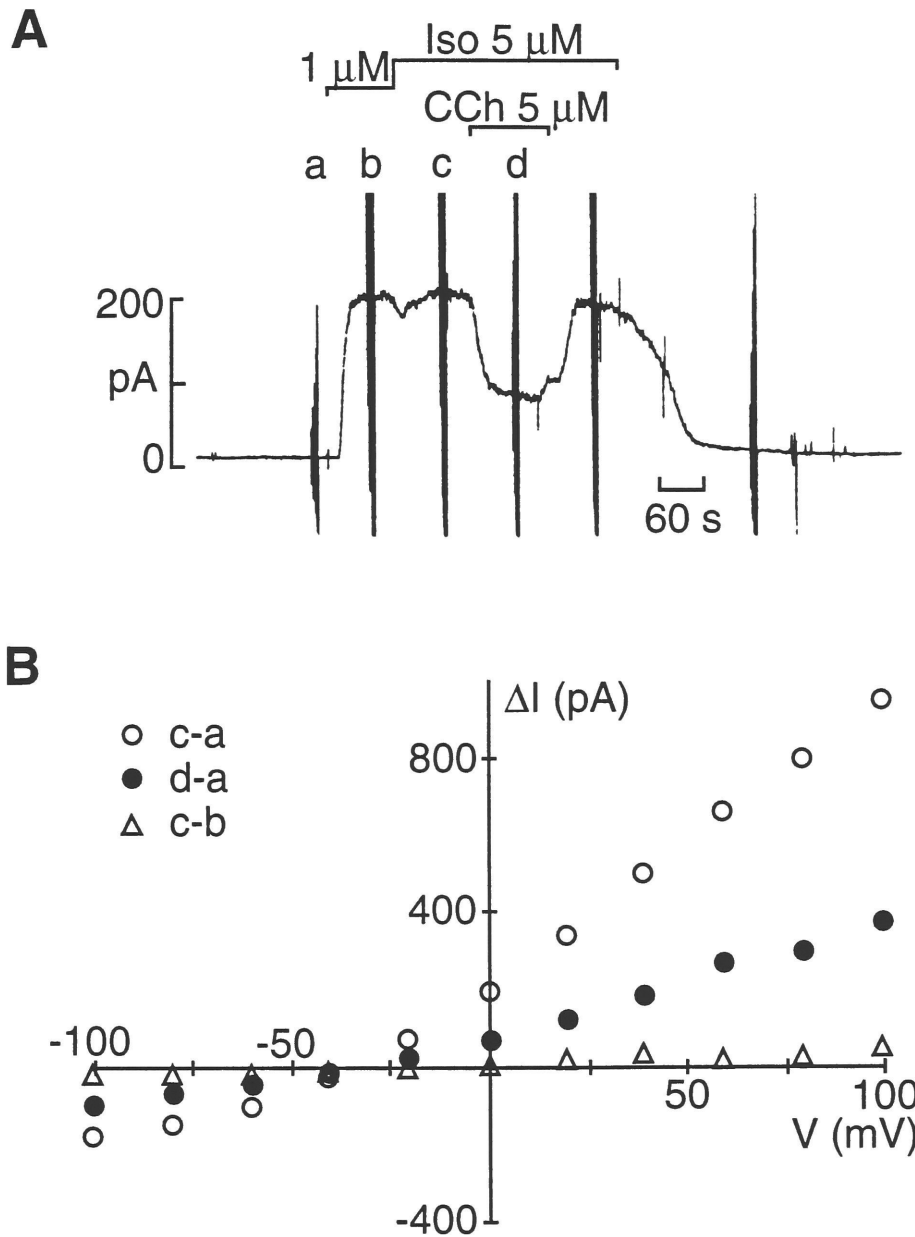


**Fig. 8. Carbachol inhibition of the Iso-activated  $\text{Cl}^-$  conductance cannot be overcome by maximal concentrations of Iso.** **A.** Whole-cell current trace of a typical experiment used to generate the data in Fig. 10A. Upper bars mark time of bath application of indicated agonists. Vertical lines (*a*, *b*, *c*, *d*) indicate application of 80-ms voltage pulses from the 0 mV holding potential to collect I-V data. **B.** Steady-state difference I-V relations obtained by subtractions in A.  $\text{Cl}^-$  current induced by 5  $\mu\text{M}$  Iso (*c-a*, ○) is diminished by 5  $\mu\text{M}$  CCh (*d-a*, ●). Moreover, 1  $\mu\text{M}$  Iso maximally activates  $\text{Cl}^-$  conductance, since currents induced by 1  $\mu\text{M}$  and 5  $\mu\text{M}$  Iso are similar (*c-b*, △).  $C_m = 187$  pF;  $R_{\text{pip}} = 0.6$  M $\Omega$ ;  $R_{\text{acc}} = 2.0$  M $\Omega$ .  $E_{\text{Cl}}/I_{\text{Cl}}$ .

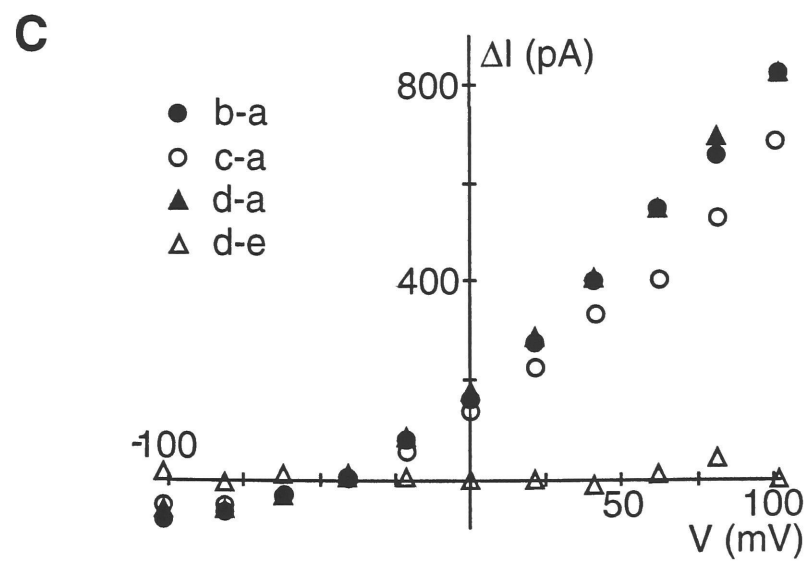
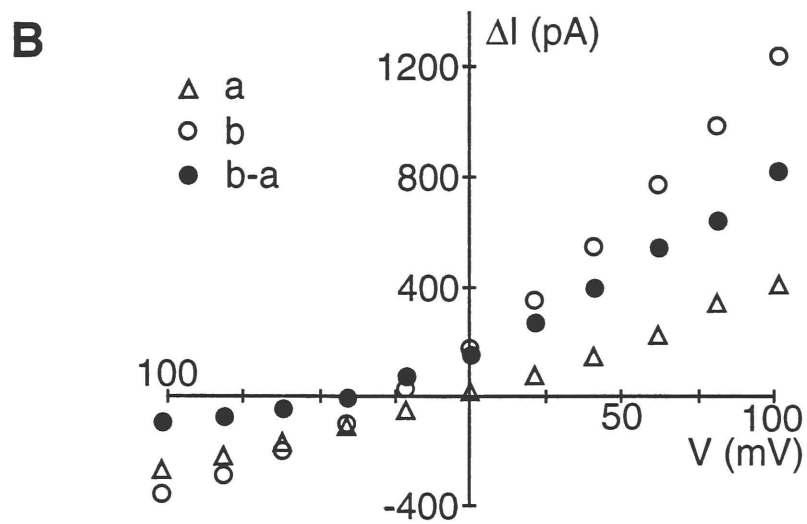
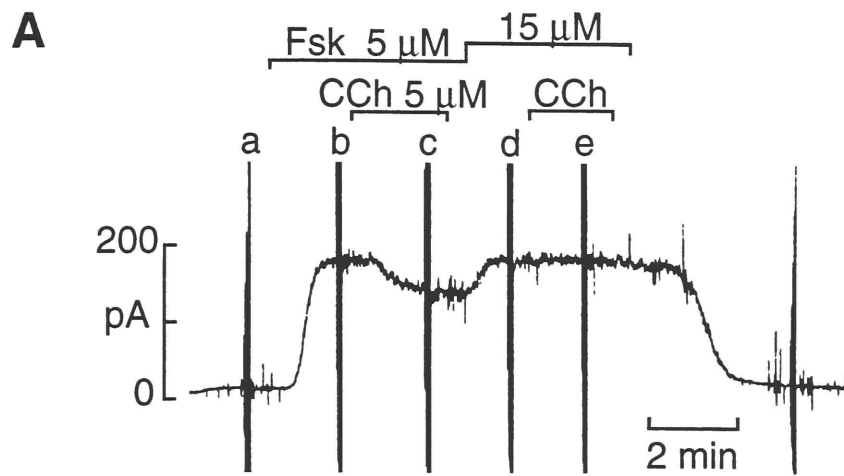


$\alpha$ ,  $\circ$ ) could still be markedly inhibited (by ~60%) by strong stimulation of  $G_i$  with 5  $\mu$ M CCh ( $d$ - $\alpha$ ,  $\bullet$ ).

Similarly, to examine the interaction of the GTP-binding protein  $G_i$  with Fsk at adenylyl cyclase, the dose-response relation to Fsk was determined without and with supramaximal activation of muscarinic receptors, using 5  $\mu$ M CCh (Fig. 10B). Figure 9 illustrates a typical experiment used to generate the data in Figure 10B. Upper bars mark the time of bath applications of the direct cyclase activator Fsk, and of the muscarinic receptor agonist CCh, at the stated concentrations. Vertical lines ( $a$ ,  $b$ ,  $c$ ,  $d$ ,  $e$ ) indicate the collection of I-V data. 5  $\mu$ M Fsk activated a large  $Cl^-$  conductance, resulting in an almost 200 pA outward current at 0 mV, which was weakly inhibited by simultaneous application of 5  $\mu$ M CCh. Raising [Fsk] to 15  $\mu$ M after withdrawing the CCh activated a  $Cl^-$  conductance comparable to that initially elicited by 5  $\mu$ M Fsk, but which was no longer inhibited by 5  $\mu$ M CCh. Figure 9B shows the steady-state currents elicited before ( $a$ ,  $\Delta$ ) and during ( $b$ ,  $\circ$ ) exposure to 5  $\mu$ M Fsk, as well as the steady-state difference I-V relation corresponding to the Fsk-activated current ( $b$ - $a$ ,  $\bullet$ ). Figure 9C shows several other relevant I-V relations.  $Cl^-$  current induced by 5  $\mu$ M Fsk ( $b$ - $a$ ,  $\bullet$ ) was weakly inhibited by 5  $\mu$ M CCh ( $c$ - $a$ ,  $\circ$ ). The similar magnitudes of the conductances activated by 5  $\mu$ M and 15  $\mu$ M Fsk (cf. Fig. 6C,  $b$ - $a$ ,  $\bullet$ ;  $d$ - $a$ ,  $\blacktriangle$ ) implies that adenylyl cyclase is maximally activated by 15  $\mu$ M Fsk. And, with the cyclase thus maximally activated, maximal stimulation of  $G_i$  by 5  $\mu$ M CCh cannot diminish the  $Cl^-$  current ( $d$ - $e$ ,  $\Delta$ ).

Figure 10 summarizes the stimulatory effects of Iso and Fsk, and the inhibitory effects of CCh. For the Iso dose-response relation (Fig. 8A,  $\bullet$ ), each point represents the mean of 3-8 measurements, at all concentrations

**Fig. 9. Carbachol inhibition of the Fsk-activated Cl<sup>-</sup> conductance can be overcome by maximal concentrations of Fsk.** **A.** Whole-cell current trace of a typical experiment used to generate the data in Fig. 10B. Upper bars mark time of bath application of indicated agonists. Vertical lines (*a*, *b*, *c*, *d*, *e*) indicate application of 80-ms voltage pulses from the 0 mV holding potential to collect I-V data. **B.** Steady-state currents elicited before (*a*,  $\Delta$ ) and after (*b*,  $\circ$ ) bath application of 5  $\mu$ M Fsk, and the steady-state difference I-V relation (*b-a*,  $\bullet$ ). **C.** Difference I-V relations showing that Cl<sup>-</sup> current induced by 5  $\mu$ M Fsk (*b-a*,  $\bullet$ ) is mildly inhibited by 5  $\mu$ M CCh (*c-a*,  $\circ$ ), but Cl<sup>-</sup> current induced by 15  $\mu$ M Fsk (*d-a*,  $\blacktriangle$ ) is not (*d-e*,  $\Delta$ ).  $C_m = 173$  pF;  $R_{pip} = 0.8$  M $\Omega$ ;  $R_{acc} = 2.9$  M $\Omega$  (E1/I1).





except at the lowest (0.01  $\mu\text{M}$ ;  $n = 1$ ), of the magnitude of the current elicited at 0 mV at each concentration, normalized to that elicited by 1  $\mu\text{M}$  Iso. The smooth curve shows the non-linear least-squares fit to the data of the Hill equation:

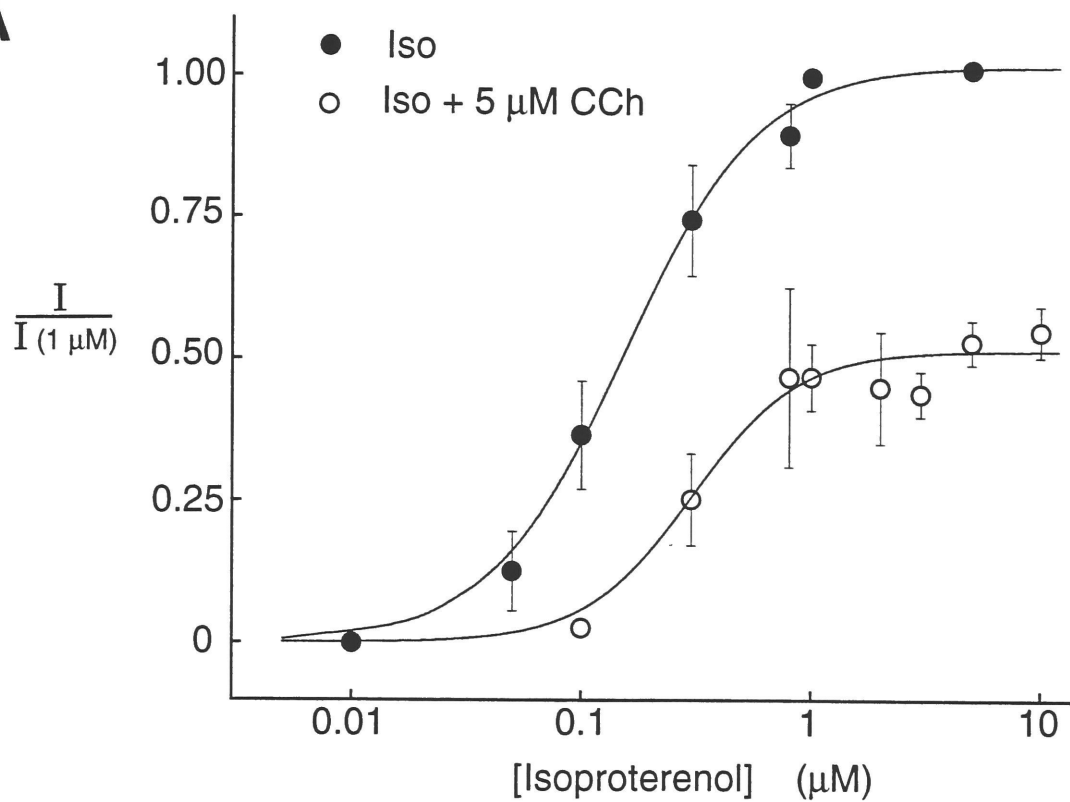
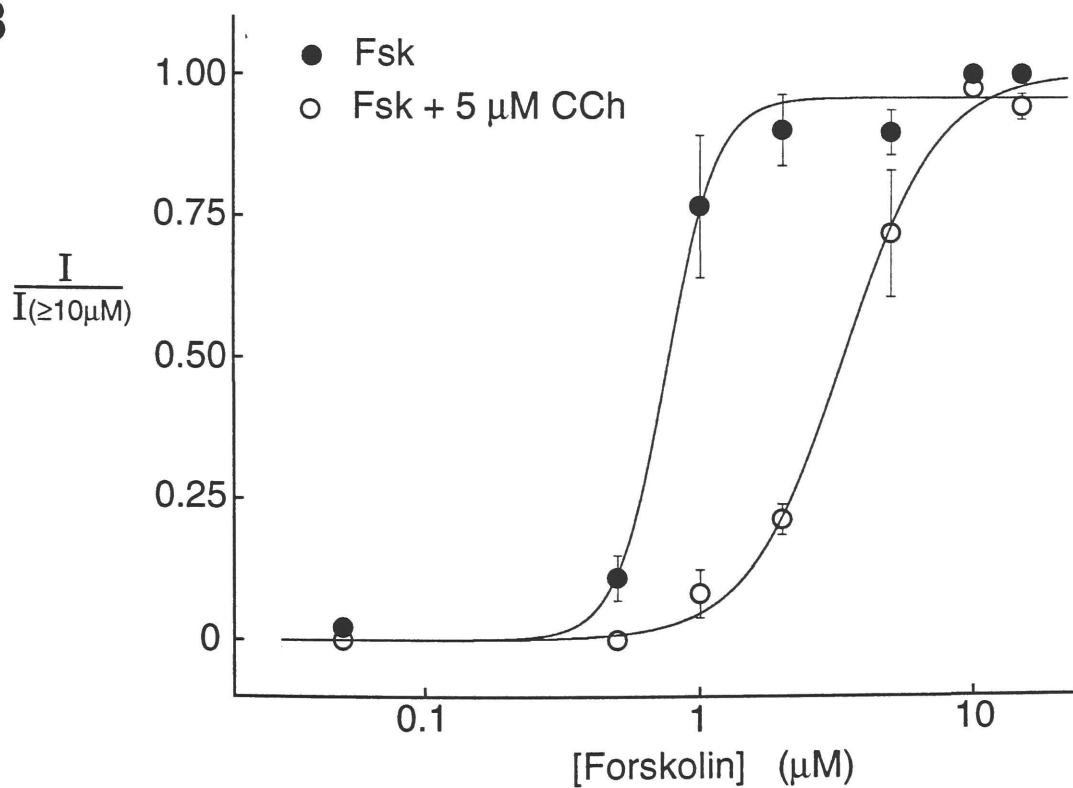
$$\frac{I}{I_{(1\mu\text{M})}} = \frac{I_{\text{max}}}{1 + \left( \frac{K_{0.5}}{[\text{Iso}]} \right)^n} \quad (\text{eqn. 7})$$

giving  $I_{\text{max}} = 1.03 \pm 0.08$ ,  $n = 1.5 \pm 0.4$ , and  $K_{0.5} = 0.15 \pm 0.03 \mu\text{M}$ . Likewise plotted is the dose-response relation of Iso in the presence of 5  $\mu\text{M}$  CCh ( $\circ$ ), where each point represents 4-9 measurements at each [Iso], except for the lowest concentration (0.1  $\mu\text{M}$  Iso;  $n = 1$ ). The current at each concentration was normalized to the current elicited by 1  $\mu\text{M}$  alone in that cell. The smooth curve shows the fitted Hill equation, with  $I_{\text{max}} = 0.52 \pm 0.04$ ,  $n = 1.9 \pm 1.0$ , and  $K_{0.5} = 0.31 \pm 0.10 \mu\text{M}$ . Clearly, under the conditions of these experiments, inhibition of adenylyl cyclase by CCh (via  $G_i$ ) cannot be overcome by increasing the stimulatory drive of Iso (via  $G_s$ ). Thus, carbachol seems to decrease the apparent efficacy with which Iso activates adenylyl cyclase, with little effect on its apparent potency, which suggests a non-competitive, allosteric type of inhibition.

Each point in the dose-response relation for Fsk (Fig. 10B,  $\bullet$ ) represents the mean of 3-7 measurements, and gives elicited currents at 0 mV normalized to the maximum current elicited by either 10  $\mu\text{M}$  or 15  $\mu\text{M}$  Fsk. The fit to the Hill equation yielded  $I_{\text{max}} = 0.96 \pm 0.02$ ,  $n = 4.8 \pm 0.9$ , and  $K_{0.5} = 0.76 \pm 0.05 \mu\text{M}$ . For inhibition by 5  $\mu\text{M}$  CCh ( $\circ$ ), the elicited current was normalized to the maximal current elicited in that cell by 10  $\mu\text{M}$  or 15  $\mu\text{M}$  Fsk; each point represents 4-5 measurements, except at the lowest concentrations ( $\leq 1 \mu\text{M}$  Fsk;  $n = 1-2$ ). The fit to the Hill equation yielded

**Fig. 10. Dose-response relations for Iso- and Fsk-activated currents in the absence and presence of CCh.** **A.** Dose-response relationships of the Iso-activated current (●), and of the Iso-activated current in the presence of 5  $\mu\text{M}$  CCh (○). The smooth curves were both generated by least-squares fits of the Hill equation (eqn. 7), yielding, for the Iso dose-response relation,  $n$  (the Hill coefficient) =  $1.5 \pm 0.4$ ,  $K_{0.5} = 0.15 \pm 0.03 \mu\text{M}$ , and  $I_{\text{max}} = 1.03 \pm 0.08$ , and for the Iso dose-response relation in the presence of 5  $\mu\text{M}$  CCh,  $n = 1.9 \pm 1.0$ ,  $K_{0.5} = 0.31 \pm 0.1 \mu\text{M}$ , and  $I_{\text{max}} = 0.52 \pm 0.04$ . **B.** Dose-response relationships of the current activated by Fsk alone (●), and by Fsk in the presence of 5  $\mu\text{M}$  CCh (○). The smooth curves are least-squares fits to the data of equation 7. For the Fsk dose-response relation,  $n = 4.8 \pm 0.9$ ,  $K_{0.5} = 0.76 \pm 0.05 \mu\text{M}$ , and  $I_{\text{max}} = 0.96 \pm 0.02$ , and for the dose-response relation in the presence of 5  $\mu\text{M}$  CCh,  $n = 2.5 \pm 0.5$ ,  $K_{0.5} = 3.7 \pm 0.3 \mu\text{M}$ , and  $I_{\text{max}} = 1.00 \pm 0.05$ .



**A****B**



$I_{\max} = 1.00 \pm 0.05$ ,  $n = 2.5 \pm 0.5$ , and  $K_{0.5} = 3.7 \pm 0.3 \mu\text{M}$ . In contrast to CCh inhibition of the cyclase stimulation by Iso, these results show that inhibition of adenylyl cyclase by  $G_i$  can be overcome by increasing concentrations of forskolin.  $G_i$  thus acts like a competitive inhibitor of forskolin's stimulatory action on adenylyl cyclase, decreasing the apparent potency but not the apparent efficacy of forskolin.

### III. Discussion

#### A. $\text{Cl}^-$ Conductance Provides a Convenient Monitor of Adenylyl Cyclase Activity

For functional studies on the *in situ* regulation of adenylyl cyclase, a membrane conductance that is modulated by PKA provides a simple method for investigating the interactions among modulators of adenylyl cyclase. Although dihydropyridine-sensitive  $\text{Ca}^{2+}$  conductance has previously been used for this purpose (e.g., Fischmeister & Shrier, 1989; Parsons et al., 1991), cardiac CFTR  $\text{Cl}^-$  conductance offers several advantages. First, whole-cell cardiac CFTR  $\text{Cl}^-$  conductance is time- (Fig. 7B) and voltage- (Fig. 11D, ○) independent, implying that the  $\text{Cl}^-$  current at a fixed membrane voltage monitors simply and accurately the time course of conductance changes. Second, whereas  $\text{Ca}^{2+}$  channel activity is probably merely modulated by phosphorylation by PKA (Herzig et al., 1993; Ono & Fozzard, 1993), CFTR  $\text{Cl}^-$  channels absolutely require phosphorylation before they can open. Third, because whole-cell  $\text{Cl}^-$  conductance is far less subject to rundown (Horie et al., 1992) than is  $\text{Ca}^{2+}$  conductance (Belles et al., 1988), low resistance, wide-tipped pipettes can be used to modify and control the intracellular environment.



## **B. Is Cardiac CFTR Cl<sup>-</sup> Conductance Activated Without Hormone Stimulation?**

Is there basal activation of the cardiac CFTR Cl<sup>-</sup> conductance in the resting state without receptor-driven stimulation of adenylyl cyclase? This would require that both adenylyl cyclase and/or PKA are basally active. Under our usual recording conditions (with wide-tipped pipettes), without a stimulus for PKA activation there is negligible Cl<sup>-</sup> conductance, since there is little change in the holding current after Cl<sup>-</sup> substitutions in the pipette (see Fig. 11, and Bahinski et al., 1989a) or in the bath (Figs. 11, 12). Also, pipette application of the specific, peptide PKA inhibitor, PKI, abolishes precisely that component of Cl<sup>-</sup> conductance activated by Iso, Fsk, or pipette cAMP (Bahinski et al., 1989a; Hwang et al., 1993), no more and no less. Moreover, PKI alone does not alter basal whole-cell Cl<sup>-</sup> conductance (Hwang et al., 1992c).

Since phosphorylation is required for CFTR channels to open, the finding that basal Cl<sup>-</sup> conductance is negligible means that there must be a low basal phosphorylation rate by PKA and/or a high basal level of phosphatase activity. If high basal phosphatase activity were counteracting significant basal PKA activity, then inhibition of the relevant phosphatase(s) would be expected to lead to activation of Cl<sup>-</sup> conductance. However, neither okadaic acid nor microcystin, both specific inhibitors of phosphatases 1 and 2A (Takai et al., 1987; Honkanen, 1990), elicited measurable Cl<sup>-</sup> conductance when applied alone at high concentration, without PKA stimulation (Hwang et al., 1993). This makes it unlikely that high phosphatase activity keeps the Cl<sup>-</sup> channels inactive. In contrast, these phosphatase inhibitors both enhanced PKA-activated Cl<sup>-</sup> conductance and slowed its deactivation, suggesting that phosphatase 1 and/or 2A are



important in dephosphorylating cardiac CFTR Cl<sup>-</sup> channels. The simplest interpretation, then, is that low basal CFTR Cl<sup>-</sup> channel activity is likely due to a low rate of PKA phosphorylation.

It is possible, however, that in the whole-cell configuration, using wide-tipped pipettes, we lower resting intracellular cAMP levels substantially by allowing its diffusion into the pipette and, hence, that we mask basal activity of the cyclase. We might thus prevent *in vitro* basal phosphorylation of CFTR Cl<sup>-</sup> channels which might otherwise occur in resting cells *in vivo*. This is suggested by excised patch experiments in which, upon excision, the patch was exposed immediately to just MgATP, without any prior exposure to the catalytic subunit of PKA. In 3 of 10 such cases, channels could be activated, which suggests that cardiac CFTR channels might be phosphorylated in the basal state in non-dialyzed cells.

### **C. Do G<sub>s</sub>, and G<sub>i</sub>, and Forskolin Bind to Independent Sites on Adenylyl Cyclase?**

Muscarinic agonists, under our recording conditions, affect only the Cl<sup>-</sup> conductance, since the reversal potential and macroscopic voltage dependence of the current inhibited is identical to that of the induced Cl<sup>-</sup> current (Figs. 8C, 9B). It is likely that muscarinic stimulation leads to inhibition of adenylyl cyclase via the direct action of a G<sub>i</sub>-type GTP-binding protein, since CCh or ACh inhibit Cl<sup>-</sup> current activated by Iso and by Fsk, but not by pipette cAMP, and this inhibition is abolished by a high (1 μM) pipette concentration GDPβS, or by treating the cells with PTX, or by depleting cells of GTP (Horie et al., 1992; Hwang et al., 1992c). Although it might be possible to explain the inhibition of Iso-activated current by CCh by a hypothetical complexation of α<sub>s</sub> by βγ subunits released upon G<sub>i</sub>





activation, muscarinic inhibition of currents activated by Fsk cannot be explained by such a mechanism because Fsk acts independently of GTP-binding proteins.  $G_i$  therefore most likely acts via direct inhibition by its  $\alpha$  subunit.

Our experiments demonstrate that, with GTP in the pipette, the ability of  $G_i$  to inhibit adenylyl cyclase depends on whether the cyclase is stimulated by  $G_s$  or forskolin. That raising the [Fsk] can overcome inhibition of Fsk-induced  $Cl^-$  currents mediated by maximal muscarinic stimulation agrees with result of Tareen et al. (1991), who showed a similar shift of the Fsk dose-response relation to higher concentrations upon maximal stimulation of muscarinic receptors with 5.5  $\mu M$  ACh. This effect is also similar to the effect of muscarinic inhibition of  $Ca^{2+}$  currents caused by 10  $\mu M$  ACh in frog myocytes (Fischmeister & Shrier, 1989). A similar rightward shift of the Fsk dose-response relation, without a reduction in the maximum current elicited, was observed when the non-hydrolyzable GTP analog, GTP $\gamma$ S, was introduced into the pipette solution in the absence of autonomic receptor agonists (Hwang et al., 1992a; Hwang et al., 1992c). Since this effect mimicked that observed with muscarinic agonists, GTP $\gamma$ S was concluded to preferentially activate  $G_i$ , presumably reflecting a higher basal turnover rate of  $G_i$  than of  $G_s$ .

Our finding of a reduction of the maximal current response to Iso by CCh is in agreement with a study of muscarinic inhibition, using 10  $\mu M$  ACh, of Iso-stimulated cardiac  $Ca^{2+}$  current in frog (Fischmeister & Shrier, 1989), but contrasts with other studies in guinea-pig ventricular myocytes, both of PKA-activated  $Cl^-$  conductance (Tareen et al., 1991), and of  $Ca^{2+}$  current (Hescheler et al., 1986). In those studies, ACh was found to simply shift the dose-response relation for Iso to higher doses, as for Fsk.



However, in both of those studies the free  $[Mg^{2+}]$  in the pipette solution was  $\sim 20 \mu M$ , whereas in ours it was  $\sim 1 mM$ . If the low free  $[Mg^{2+}]$  in their solutions were to have slowed down GTP hydrolysis, then it would be expected that their results would more closely approximate the results observed by Hwang et al. (1992a) with  $GTP\gamma S$  in the pipette. In those experiments, a brief exposure to Iso caused persistent activation of CFTR which could not be diminished by ACh, but which was abolished by PKI. The implication is that fully activated  $G_s$  can overwhelm the inhibitory influence of fully activated  $G_i$  and, hence, that  $G_s$  never attains full activation in the presence of GTP. Presumably, at high (e.g.,  $1 mM$ ) free  $Mg^{2+}$ , a relatively high rate of GTP hydrolysis prevents simultaneous activation of the entire population of  $G_s$  proteins, but at  $\mu M$  levels of free  $Mg^{2+}$ , GTP hydrolysis is slowed (cf. Chapter 5, below), permitting activation of a larger fraction of  $G_s$  and so yielding responses more comparable to those seen with  $GTP\gamma S$ . In support of this interpretation, in the study of the inhibition of  $Ca^{2+}$  current in frog ventricle (Fischmeister & Shrier, 1989), in which a decrease in the apparent efficacy of Iso was also observed upon muscarinic stimulation, the free  $[Mg^{2+}]$  was also  $\sim 1 mM$ , as in the present experiments.

We found a small, but insignificant, increase in the estimated Hill coefficient for the Iso dose-response relation in the presence of CCh (from 1.5 to 1.9;  $P > 0.05$ ), similar to the small increase (from 1.9 to 2.2) observed by Tareen et al. (1991) who used ACh to inhibit Iso-activated currents. The large errors in our estimates of Hill coefficients ( $\pm 1$ , S.E.M.) preclude any further analysis. Likewise, we also observed an apparent decrease, from 4.8 to 2.5, in the Hill coefficient for the Fsk dose-response relation in the presence of CCh, whereas Tareen et. al. (1991) reported a small increase,



from 3 to 4.3. Additional measurements to better define the dose-response relation of Fsk at low concentrations, e.g., at  $\sim 0.25$  and  $0.75 \mu\text{M}$ , would be needed for a proper evaluation of these differences.

These results do not allow us to specify whether there are three separate binding sites on adenylyl cyclase, one for Fsk, another for  $G_{\alpha_s}$ , and a third for  $G_{\alpha_i}$ . The finding that muscarinic activation simply shifts the Fsk dose-response relation in a competitive manner, suggests that there could indeed be two stimulatory sites, one for Fsk and one for  $G_{\alpha_s}$ , and that  $G_{\alpha_i}$  can compete at both of them. There could even be a single stimulatory binding site on adenylyl cyclase, where either Fsk or  $G_{\alpha_s}$  can bind, and  $G_{\alpha_i}$  can compete with either.

These possibilities will be difficult to distinguish in native systems, not least because CFTR channel conductance might not accurately monitor adenylyl cyclase activity during strong stimulation. It is possible that maximal activation of CFTR conductance is limited by later steps in the activation pathway; e.g., PKA could be maximally stimulated by cAMP, or the CFTR channels could become maximally phosphorylated. The latter is unlikely, however, since pipette application of the phosphatase inhibitors microcystin or okadaic acid were found to enhance steady-state  $\text{Cl}^-$  conductance in response to Fsk, suggesting that even with strong stimulation by Fsk CFTR channels are submaximally phosphorylated (Hwang et al., 1993).



## **Chapter 4**

### **PERMEATION THROUGH THE CARDIAC CFTR Cl<sup>-</sup> CHANNEL PORE**

#### **I. Introduction**

The aim of this portion of the study is to characterize the permeation pathway of the channel which underlies the PKA-activated Cl<sup>-</sup> conductance in guinea-pig ventricular myocytes. In particular, what is the relative and absolute ease with which it passes different anions? How well does the channel discriminate amongst anions, and between anions and cations? Determining which anions are prevented altogether from permeating the pore will allow for an estimate of the minimum effective pore diameter. These measurements then will be used to make inferences about the selectivity filter within the pore of the channel, and to make predictions about energy barriers/wells for permeating ions. Portions of this work have been presented in abstract (Dousmanis & Gadsby, 1994; Hwang et al., 1992a).

#### **II. Results**

##### **A. Cl<sup>-</sup> Accumulation/Depletion**

The simplest method, in principle, for determining the relative permeabilities of anions through the CFTR channel is to measure the reversal potential ( $E_{rev}$ ) for channel currents under bi-ionic conditions, that is, with a single species of anion in the solution bathing each face of the membrane. This requires control over the composition of the solutions

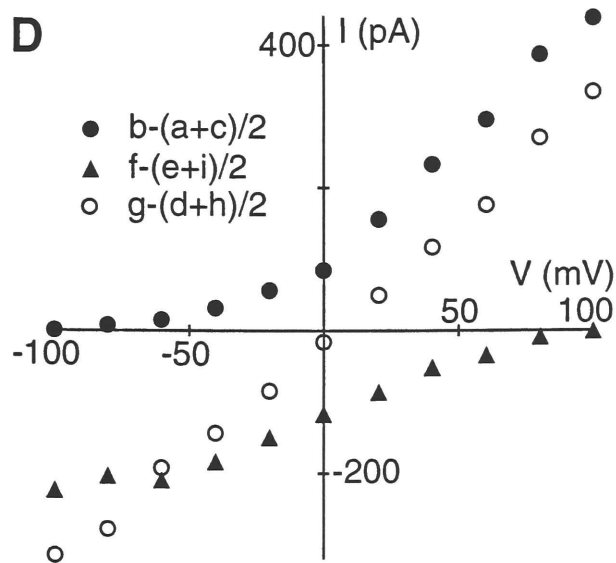
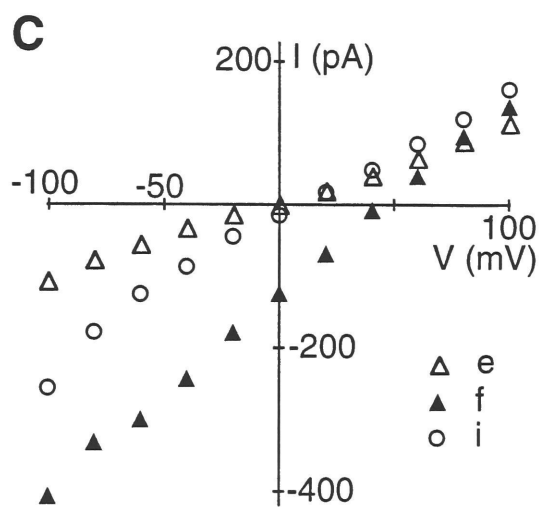
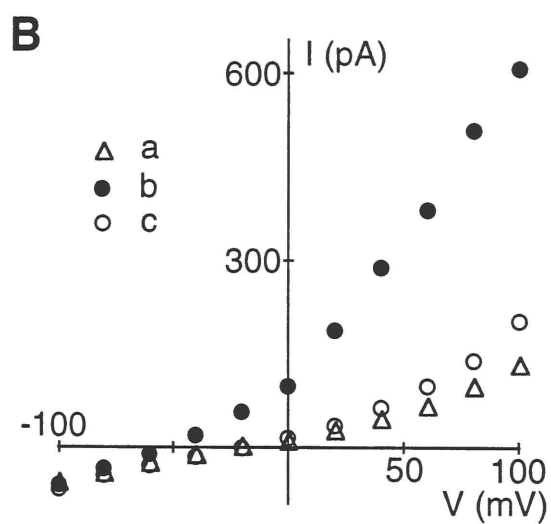
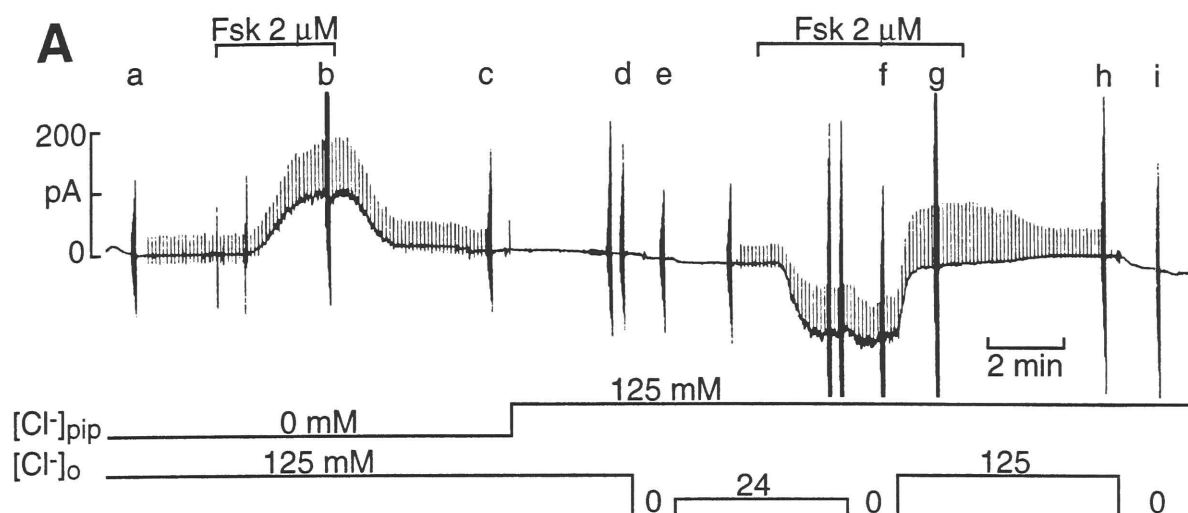




bathing the intracellular and extracellular faces of the membrane. In whole-cell experiments, it is particularly important to control the intracellular milieu, e.g., to prevent a build-up of  $\text{Cl}^-$  at the inner face of the membrane near the channels, during periods of high net  $\text{Cl}^-$  influx. Such intracellular  $\text{Cl}^-$  accumulation would shift  $E_{\text{Cl}}$ , and hence  $E_{\text{rev}}$ , in the positive direction, and might account for the positive deviation of  $E_{\text{rev}}$  from estimated  $E_{\text{Cl}}$  in low  $[\text{Cl}^-]_i$ /high  $[\text{Cl}^-]_o$  solutions (Hwang et al., 1992b). Similarly,  $\text{Cl}^-$  might be depleted from the immediate vicinity outside  $\text{Cl}^-$  channels, so decreasing the local  $\text{Cl}^-$  concentration, as could occur if the channels were clustered on membrane infoldings of the T-tubular system, or in calveolae at the cell surface. To test these possibilities, and hence the degree of control of the ionic composition of the solutions bathing each face of the membrane, experiments were carried out with either all intracellular  $\text{Cl}^-$ , or all extracellular  $\text{Cl}^-$ , replaced by impermeant anions.

Figure 11A shows a chart recording of whole-cell current, at 0 mV, from an experiment testing the influence on  $E_{\text{rev}}$  measurements of  $\text{Cl}^-$  accumulation and depletion. Upper bars mark applications of 2  $\mu\text{M}$  Fsk, and vertical lines show periods of I-V data acquisition. Lower lines mark changes in pipette  $[\text{Cl}^-]$  ( $[\text{Cl}^-]_{\text{pip}}$ ) and bath  $[\text{Cl}^-]$  ( $[\text{Cl}^-]_o$ ). The first exposure to Fsk was with 0 mM  $\text{Cl}^-$  in the pipette, replaced by 85 mM aspartate and 20 mM methanesulfonate ( $\text{MeSO}_3$ ), and it elicited an  $\sim 100$  pA outward shift in holding current, which reversed within  $\sim 90$  s upon Fsk withdrawal. Holding current was little affected by subsequently raising pipette  $[\text{Cl}^-]$  to 125 mM. During the second exposure to Fsk, I-V relations were obtained either with 125 mM  $\text{Cl}^-$  in the bath, or after complete replacement of bath  $\text{Cl}^-$  by isethionate. Figure 11B shows the steady-state currents elicited before ( $\alpha$ ,  $\Delta$ ), during ( $b$ ,  $\bullet$ ), and after ( $c$ ,  $\circ$ ) exposure to Fsk, with 125 mM

**Fig. 11. Effects of Cl<sup>-</sup> accumulation and Cl<sup>-</sup> depletion on reversal potential ( $E_{rev}$ ) measurements.** **A.** Chart record of the whole-cell current trace, at 0 mV, from an experiment testing effects on  $E_{rev}$  measurements of Cl<sup>-</sup> accumulation and depletion. Upper bars mark periods of bath application of 2  $\mu$ M Fsk, and vertical lines periods of I-V data acquisition. Lower bars indicate pipette [Cl<sup>-</sup>] ([Cl<sup>-</sup>]<sub>pip</sub>) and bath [Cl<sup>-</sup>] ([Cl<sup>-</sup>]<sub>o</sub>). Small upward deflections represent 80 ms voltage steps to +20 mV, every 6 s, to monitor current activation. **B.** Steady-state currents elicited before (*a*,  $\Delta$ ), during (*b*,  $\bullet$ ), and after (*c*,  $\circ$ ) first bath application of 2  $\mu$ M Fsk. 0 mM [Cl<sup>-</sup>]<sub>pip</sub>, 125 mM [Cl<sup>-</sup>]<sub>o</sub> (E2/I2). **C.** Steady-state currents elicited before (*a*,  $\Delta$ ), during (*b*,  $\blacktriangle$ ), and after (*c*,  $\circ$ ) second bath application of 2  $\mu$ M Fsk. 125 mM [Cl<sup>-</sup>]<sub>pip</sub>, 0 mM [Cl<sup>-</sup>]<sub>o</sub> (E2,3,4/I3). **D.** Steady-state difference I-V relations for the experiment shown above, obtained by subtraction of the average of the control I-V relations, obtained before and after Fsk application, from the I-V relation obtained during Fsk application, in which all pipette Cl<sup>-</sup> is replaced by aspartate and MeSO<sub>3</sub> {*b*-(*a*+*c*)/2,  $\bullet$ }, in symmetric 125 mM Cl<sup>-</sup> {*g*-(*d*+*h*)/2,  $\circ$ }, and with all bath Cl<sup>-</sup> replaced by isethionate {*f*-(*e*+*i*)/2,  $\blacktriangle$ }.  $C_m = 97$  pF;  $R_{pip} = 0.9$  M $\Omega$ ;  $R_{acc} = 4.7$  M $\Omega$ .





$[\text{Cl}^-]_o$  and 0 mM  $[\text{Cl}^-]_{\text{pip}}$ . Figure 11C shows corresponding currents before (e,  $\Delta$ ) during (f,  $\blacktriangle$ ), and after (i,  $\circ$ ) activation of  $\text{Cl}^-$  conductance with 125 mM  $[\text{Cl}^-]_o$  and 0 mM  $[\text{Cl}^-]_o$ . Figure 11D summarizes the difference I-V relations for the Fsk-activated conductance with all pipette  $\text{Cl}^-$  replaced by aspartate and  $\text{MeSO}_3$   $\{b-(a+c)/2, \bullet\}$ , in symmetric 125 mM  $\text{Cl}^-$   $\{g-(d+h)/2, \circ\}$ , and with all bath  $\text{Cl}^-$  replaced by isethionate  $\{f-(e+i)/2, \blacktriangle\}$ . In symmetric 125 mM  $\text{Cl}^-$ , the activated current reversed at +6.1 mV. With no  $\text{Cl}^-$  in the pipette, even at -100 mV, there was no inward current, implying that intracellular  $\text{Cl}^-$  accumulation, if it occurs, raises  $[\text{Cl}]_i$  by little more than 5 mM (if  $\text{Cl}^-$  were the only permeant anion, for  $\Delta E_{\text{rev}} = -100$  mV, estimated  $[\text{Cl}]_i = 3$  mM). Likewise, with 0  $\text{Cl}^-$  in the bath, any outward current was unmeasurably small, even at +100 mV. These results strongly suggest that neither intracellular nor extracellular  $\text{Cl}^-$  accumulation (or, by corollary, depletion) causes deviations from the experimental  $[\text{Cl}^-]$  larger than a few mM, and, hence, that reasonable control of ionic compositions is achieved under these whole-cell current-recording conditions.

## B. Anion Selectivity of the Cardiac CFTR Channel

Under the standard recording conditions, with 24 mM  $\text{Cl}^-$  in the recording pipette and 150 mM  $\text{Cl}^-$  in the bath, the measured reversal potential of the PKA-activated  $\text{Cl}^-$  conductance is 10-15 mV more positive than calculated  $E_{\text{Cl}}$  (Matsuoka, Ehara & Noma, 1990; Hwang et al., 1992b). One possible explanation for this deviation is that the channel could be slightly permeable to other ions in the pipette and/or bathing solution. As a first step towards resolving this issue,  $\text{Cl}^-$  selectivity was examined by measuring the shift in  $E_{\text{rev}}$  as the  $[\text{Cl}^-]$  gradient was altered.



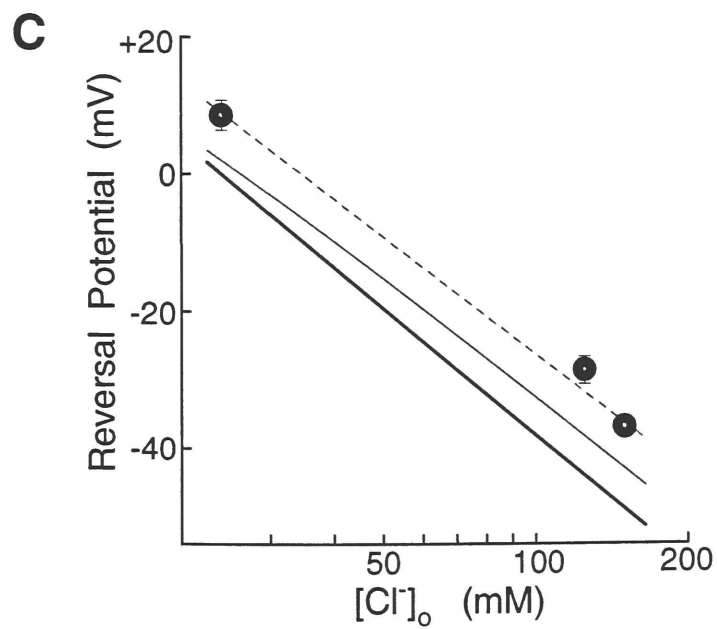
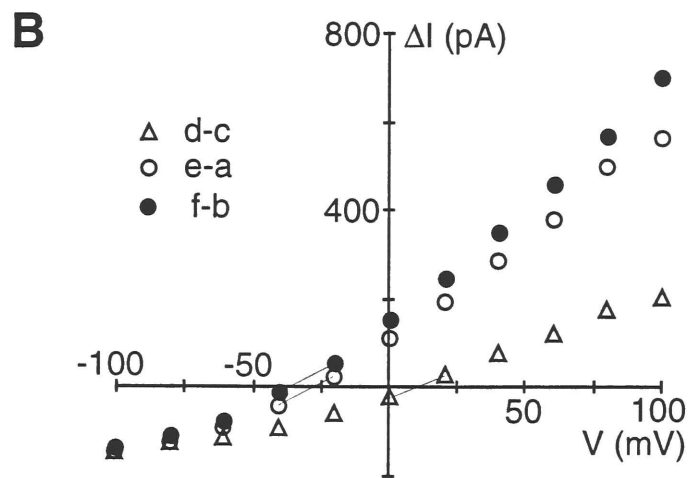
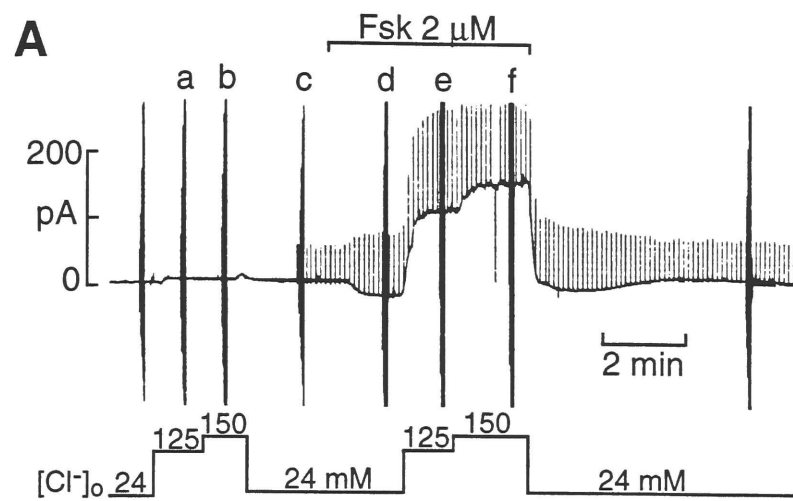
Figures 12A, B illustrate a typical experiment in which the bath  $[Cl^-]$  gradient was varied, by substitution with isethionate. Figure 12A shows whole-cell current at 0 mV. Pipette  $[Cl^-]$  was fixed at 24 mM, and the lower line indicates changes in bath  $Cl^-$  concentration. In symmetric 24 mM  $Cl^-$ , activation of whole-cell  $Cl^-$  conductance by Fsk was detected as an increase in the current responses to the +20 mV test pulses, in parallel with a small, ~20 pA, inward shift of holding current. Raising bath  $[Cl^-]$  to 125 mM, and then 150 mM, then caused outward shifts of holding current, to ~130 pA, and then to ~180 pA. Figure 12B shows the corresponding steady-state difference I-V relations for 24 mM  $[Cl^-]_o$  (*d-c*,  $\Delta$ ), 125 mM  $[Cl^-]_o$  (*e-a*,  $\circ$ ), and 150 mM  $[Cl^-]_o$  (*f-b*,  $\bullet$ ). Faint straight line segments show interpolations reversal potentials for the activated currents. In this experiment,  $E_{rev}$  was +9.0 mV at 24 mM  $Cl^-_o$ , -27.8 mV at 125 mM  $Cl^-_o$ , and -36.8 mV at 150 mM  $Cl^-_o$ .

Figure 12C plots average reversal potentials against  $\log [Cl^-]_o$ , for the Iso- or Fsk-activated conductance, from 4, 5, and 23 cells, at 24, 125, and 150 mM  $Cl^-_o$ , respectively.  $[Cl^-]_{pip} = 24$  mM. The dashed line represents a linear least squares fit to the data, and has a slope of  $-56.9 \pm 2.6$  mV per 10-fold change in  $[Cl^-]_o$ . The heavy straight line shows  $E_{Cl}$  at 37 °C, calculated from the Nernst equation, assuming that the  $Cl^-$  concentrations in the pipette and inside the cell are the same, and that the  $Cl^-$  activity coefficient in the cell equals that in the bath; its slope is -61.5 mV/decade. The smooth curve (middle) represents predicted reversal potentials if finite, but small, permeabilities to isethionate and aspartate are included (see Chapter 4, Discussion).

Measurements of  $E_{rev}$ , with various  $Cl^-$  gradients, are summarized in Table 3. With  $[Cl^-]$  lower inside than outside the cell,  $E_{rev}$  is more positive

**Fig. 12. Anion selectivity of the cardiac CFTR channel.** **A.** Whole-cell current trace, at 0 mV, from a typical experiment testing Cl<sup>-</sup> selectivity of the cardiac CFTR Cl<sup>-</sup> channel, as measured by shifts in reversal potential ( $E_{rev}$ ) as the Cl<sup>-</sup> gradient is varied, by alteration of the bath [Cl<sup>-</sup>] ( $[Cl^-]_o$ ). The upper bar marks bath Fsk application, the lower lines indicate bath Cl<sup>-</sup> concentration, with Cl<sup>-</sup> replaced by isethionate, as required. Pipette solution contained 24 mM Cl<sup>-</sup>. **B.** Steady-state difference I-V relations obtained by subtraction in A, showing the Fsk-activated current with 24 mM  $[Cl^-]_o$  (*d-c*,  $\Delta$ ), with 125 mM  $[Cl^-]_o$  (*e-a*,  $\circ$ ), and with 150 mM  $[Cl^-]_o$  (*f-b*,  $\bullet$ ). Straight lines show interpolated reversal potentials for the activated currents.  $E_{rev}$  of the difference current shifts to more negative potentials as bath [Cl<sup>-</sup>] is raised.  $C_m = 123$  pF;  $R_{pip} = 0.6$  M $\Omega$ ;  $R_{acc} = 3.5$  M $\Omega$  (E1,2,3/I1). **C.** Chloride selectivity of the whole-cell Fsk- or Iso-activated conductance. Plot of reversal potential against  $\log [Cl^-]_o$ , from 23, 5, and 4 cells, at 150, 125, and 24 mM  $[Cl^-]_o$ , respectively.  $[Cl^-]_i = 24$  mM. The dashed straight line represents the least squares best fit to the data, of:  $E_{rev} = m \cdot \log([Cl^-]_o/[Cl^-]_i) + b$ , where  $m$  (the slope) =  $-56.9 \pm 2.6$  mV and  $b = 9.0$  mV. Assuming Cl<sup>-</sup> is the only permeant ion, the Nernst equation predicts a slope of -61.5 mV, at 37 °C (*straight line*; see Chapter 4, Discussion).







**Table 3. Anion Selectivity of the Cardiac CFTR Channel**

$[\text{Cl}]_i/[\text{Cl}]_o^*$ (mM)	$E_{\text{rev}}$ (mV)	SEM (mV)	n	estimated $E_{\text{Cl}}$ (mV) <sup>†</sup>	$E_{\text{rev}}-E_{\text{Cl}}$ (mV)
24/150	-36.9	0.7	23	- 49.0	+ 12.1
24/125	- 28.6	2.0	5	- 44.1	+ 15.5
24/24 <sup>#</sup>	+ 8.6	2.2	4	0	+ 8.6
125/125	+ 5.8	0.2	51	0	+ 5.8
160/160 <sup>@</sup>	- 4.3	2.3	3	0	- 4.3
125/24	+ 39.6	1.9	10	+ 44.1	- 5.0

\* Aspartate was substituted for pipette  $\text{Cl}^-$  in low  $[\text{Cl}]_i$  experiments;  
isethionate was substituted for bath  $\text{Cl}^-$  in low  $[\text{Cl}]_o$  experiments

<sup>†</sup> Estimated  $E_{\text{Cl}}$  was determined using the Nernst equation and assuming  $\text{Cl}^-$  the only permeant ion, where, at 37 °C,  $E_{\text{Cl}} = -26.73 \cdot \ln\{[\text{Cl}]_o/[\text{Cl}]_i\}$

<sup>#</sup> Two of the four experiments were with 25 mM  $\text{Cl}^-$  in pipette and bath

<sup>@</sup> From giant patch experiments, with channel(s) locked open with a mixture of 0.5 mM AMP-PNP plus 0.5 mM ATP.  $E_{\text{rev}}$  corrected for a junctional potential of  $+11.2 \pm 0.6$  mV, measured between the pipette solution and the initial bath solution.



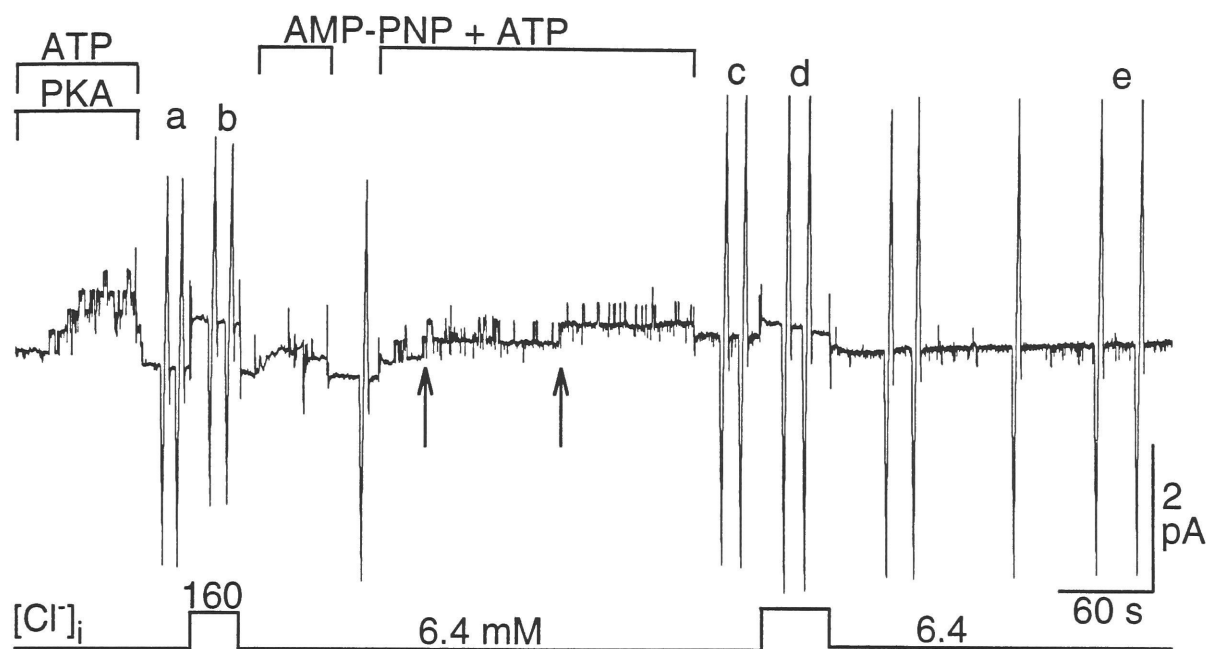
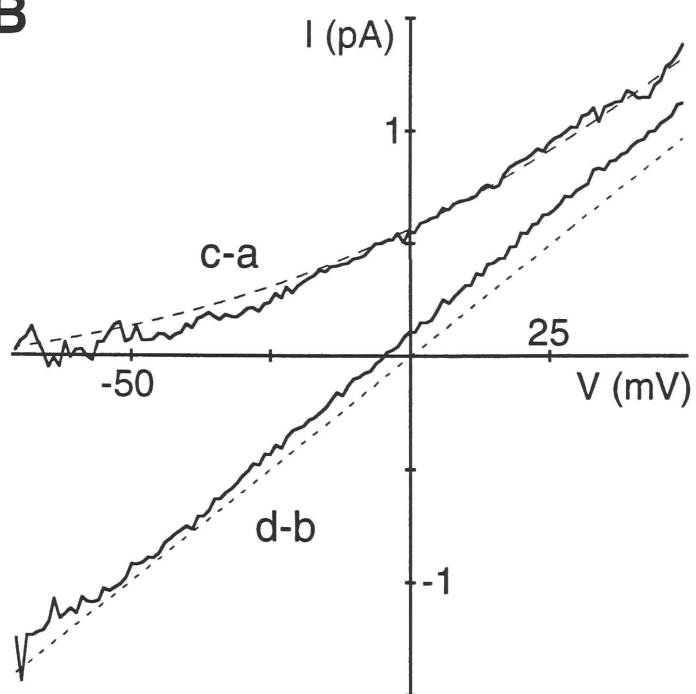
than  $E_{Cl}$ , but with  $[Cl^-]$  higher on the outside,  $E_{rev}$  is more negative than  $E_{Cl}$ . In symmetric 125 mM  $Cl^-$  solutions,  $E_{rev}$  is +6 mV, significantly more positive than  $E_{Cl}$ , 0 mV ( $P < 0.05$ );  $E_{rev}$  of single channel currents in excised patches exposed to symmetric 160 mM NMGCl solutions, however, is not significantly different from 0 mV ( $P > 0.05$ ; e.g., see Fig. 13B, below).

### C. Single-Channel $Cl^-$ Conductance and Permeability Coefficient

Voltage ramps ( $\pm 60$  mV, 40 mV/s) were used to measure the single-channel CFTR  $Cl^-$  conductance in excised patches. I-V relationships were obtained before and after locking the channels open using an equal mixture of ATP and AMP-PNP (see Chapter 5, IID, below). Figure 13 shows a current recording, at -10 mV, from a patch in which four channels were activated by bath (cytoplasmic surface) application of 1 mM ATP plus ~100 nM PKA, and then closed by withdrawal of ATP. Upon subsequent application of 0.5 mM ATP plus 0.5 mM AMP-PNP first one, and then a second, channel became locked open (*arrows*) and remained so for the duration of the experiment. Pipette  $[Cl^-]$  was kept at 160 mM, and bath  $[Cl^-]$  was switched between 6.4 and 160 mM. I-V data were collected at the two bath  $[Cl^-]$ s, with the channels closed, and again once the channels were locked open.

Figure 13B shows the difference currents, representing the current through the two locked open CFTR channels. The two channel conductance, determined from a least squares fit to the data in symmetric 160 mM  $Cl^-$  (*d-b*), was  $20.73 \pm 0.08$  pS, implying a single-channel conductance of 10.4 pS. The mean single-channel conductance, determined in a similar fashion from five patches containing 1-3 channels, was  $10.3 \pm 0.4$  pS.

**Fig. 13. Single channel conductance and permeability coefficient of the locked open cardiac CFTR Cl<sup>-</sup> channel.** **A.** Current trace from an excised patch experiment in which two channels were locked open with AMP-PNP.  $V_h = -10$  mV. Upper bars mark bath (intracellular surface) application of ~100 nM PKA, 1 mM ATP, and 0.5 mM ATP + 0.5 mM AMP-PNP. Lower bar indicates bath [Cl<sup>-</sup>]; pipette [Cl<sup>-</sup>] fixed at 160 mM (E1/I1,18). Vertical current deflections indicate periods of I-V data acquisition (*a,b,c,d,e*) using voltage ramps ( $\pm 60$  mV, 40 mV/s). Initial seal resistance ( $R_s$ ) = 32 G $\Omega$ . **B.** Currents through two locked open CFTR channels in symmetric 160 mM Cl<sup>-</sup> (*d-b*), and with intracellular [Cl<sup>-</sup>] lowered to 6.4 mM (*c-a*). Dashed lines represent the least squares fits of the data to the GHK current equation (eqn. 8). From this experiment,  $P_{abs}$  for Cl<sup>-</sup> through a single CFTR channel is  $\sim 2 \times 10^{-17}$  cm<sup>3</sup>s<sup>-1</sup>. Straight line fit to *d-b* yields the two channel conductance,  $20.73 \pm 0.08$  pS, implying a single channel conductance ( $\gamma$ ) of 10.4 pA.  $E_{rev} = -5.1$  mV.

**A****B**





The permeability coefficient,  $P_{Cl}$ , of a single cardiac CFTR  $Cl^-$  channel can be estimated by fitting the two I-V relations to the Goldman equation (*dashed lines*),

$$I = P_{Cl} \frac{VF^2}{RT} \left( \frac{[Cl^-]_i - [Cl^-]_o e^{\left(\frac{VF}{RT}\right)}}{1 - e^{\left(\frac{VF}{RT}\right)}} \right) \quad (\text{eqn. 8})$$

yielding a value of  $3.3 \times 10^{-17} \pm 3 \times 10^{-19} \text{ cm}^3 \text{ s}^{-1}$  for 160 mM  $Cl^-_i$ , and  $3.9 \times 10^{-17} \pm 4 \times 10^{-19} \text{ cm}^3 \text{ s}^{-1}$  for 6.4 mM  $Cl^-_i$ . Averaging the two values and dividing by two implies that  $P_{Cl}$  for a single CFTR channel was  $1.8 \times 10^{-17} \text{ cm}^3 \text{ s}^{-1}$ . From similar measurements from two additional experiments, one a single-channel patch and the other a patch with three channels,  $P_{Cl}$  was  $2 \times 10^{-17} \pm 9 \times 10^{-19} \text{ cm}^3 \text{ s}^{-1}$  ( $n = 3$ ).

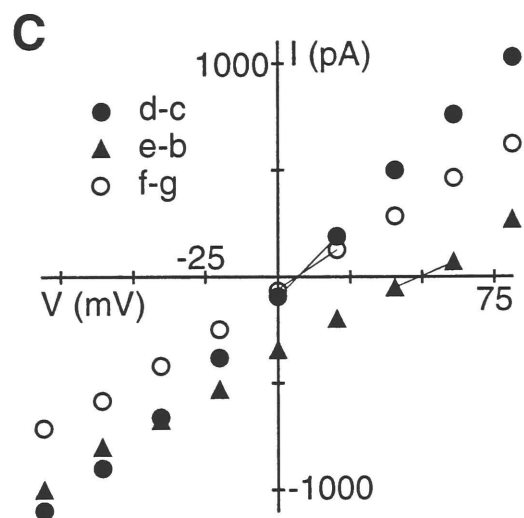
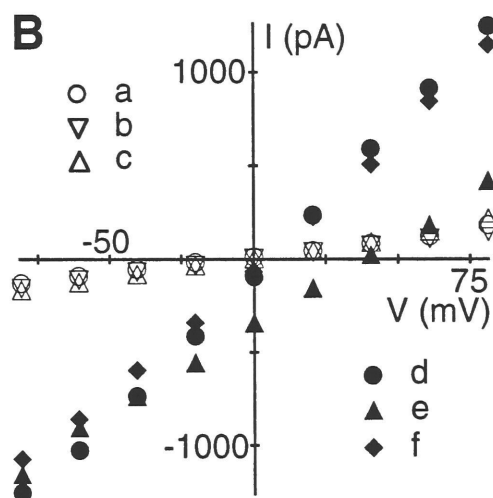
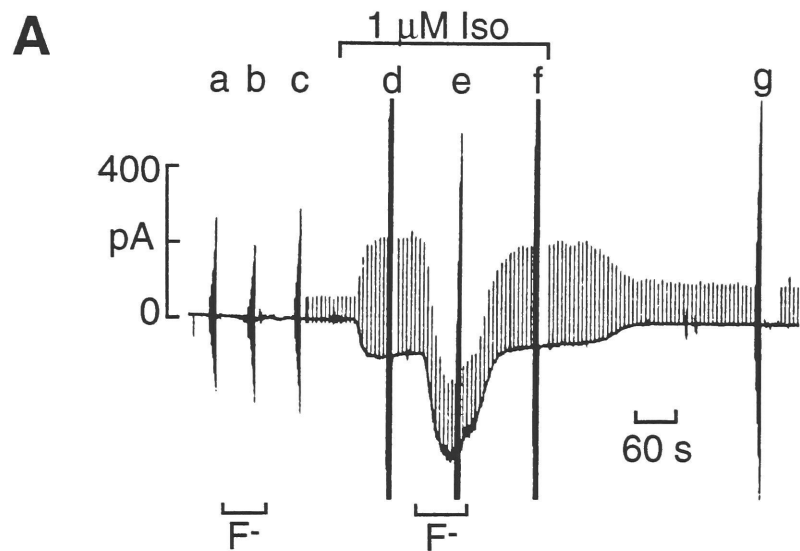
#### **D. Relative Anion Permeability Determined by Shifts in Whole-Cell Bi-Ionic Reversal Potentials**

Relative permeabilities,  $P_X/P_{Cl}$ , of cardiac CFTR channels to various anions ( $X^-$ ), were determined from measured reversal potential shifts,  $\Delta E_{rev} = E_{rev}(X^-_o) - E_{rev}(Cl^-_o)$  (eqn. 4), upon equimolar replacement of extracellular  $Cl^-$  with each test anion, using:

$$\Delta E_{rev} = \frac{RT}{zF} \ln \left( \frac{P_A}{P_B} \right)$$

Figure 14 illustrates the protocol, here determining the relative permeability of the halide  $F^-$  to  $Cl^-$ . In a myocyte initially exposed to 125 mM extracellular  $Cl^-$  and dialyzed via a wide-tipped pipette containing 125 mM  $Cl^-$ , steady-state whole-cell I-V relationships were determined before, during, and after brief ( $\sim 30$  s) periods of equimolar substitution of 125 mM

**Fig. 14. Relative anion permeability determined by the shift in bi-ionic reversal potential of the Iso- or Fsk-activated Cl<sup>-</sup> conductance.** **A.** Current trace, at 0 mV, of an experiment testing the relative permeability of F<sup>-</sup> to Cl<sup>-</sup>. Upper bar marks time period of bath application of 1  $\mu$ M Iso, vertical lines periods of I-V data acquisition. Lower bars mark periods of equimolar substitution of bath 125 mM Cl<sup>-</sup> with F<sup>-</sup>. Pipette solution contains 125 mM Cl<sup>-</sup>. Small upward deflections represent 80 ms voltage steps to +20 mV, every 6 s, to monitor current activation. With Cl<sup>-</sup> conductance activated, replacement of bath F<sup>-</sup> for Cl<sup>-</sup> results in an inward shift in holding current, indicating F<sup>-</sup> is less permeant than Cl<sup>-</sup>. **B.** Steady-state current levels in response to voltage pulses to  $\pm 20$ ,  $\pm 40$ ,  $\pm 60$ , and  $\pm 80$  mV obtained before (*a, b, c*), during (*d, e, f*) and after (*g*) bath application of 1  $\mu$ M Iso. **C.** Steady-state difference I-V relationships, obtained by subtraction. Straight lines indicate interpolated reversal potentials of the activated conductance. 1  $\mu$ M Iso activates a large, ohmic conductance in symmetric 125 mM Cl<sup>-</sup> (*d-c*, ●).  $E_{rev} = +7.5$  mV. Upon equimolar substitution of extracellular F<sup>-</sup> for Cl<sup>-</sup>,  $E_{rev}$  of the activated current shifts inward (*e-b*, ▲).  $E_{rev} = +49.1$  mV. Activated conductance in symmetric Cl<sup>-</sup>, after resuperfusion of bath Cl<sup>-</sup>, brackets test anion (*f-g*, ○).  $E_{rev} = +7.1$  mV. The relative permeability,  $P_F/P_{Cl}$ , is then calculated from the measured shifts of reversal potential,  $\Delta E_{rev} = E_{rev}(X^-_o) - E_{rev}(Cl^-_o)$  [ $49.1 - (7.1 + 7.5)/2 = +41.8$ ] using equation 4.  $P_F/P_{Cl} = 0.21$ .  $C_m = 140$  pF;  $R_{pip} = 0.8$  M $\Omega$ ;  $R_{acc} = 1.4$  M $\Omega$  ( $E_{2,6/13}$ ).





F<sup>-</sup> for bath Cl<sup>-</sup>. And this whole procedure was carried out twice, once in the absence, and once in the presence, of activated CFTR Cl<sup>-</sup> conductance (by 2  $\mu$ M Fsk or 1  $\mu$ M Iso; Fig. 14A). In both of those conditions, I-V relationships were obtained immediately before, during, and after brief (~30 s) equimolar substitutions of the test anions for extracellular Cl<sup>-</sup>. The brief exposures to the test anion minimized contamination of the intracellular milieu resulting from net influx. Steady-state difference I-V relationships were then obtained by appropriate subtraction (Fig. 14C). The fine lines indicate the interpolated reversal potentials of the activated current in the two different bath solutions. 1  $\mu$ M Iso activated a large, ohmic conductance in symmetric 125 mM Cl<sup>-</sup> (*d-c*, ●), with E<sub>rev</sub> at +7.5 mV. Upon equimolar substitution of extracellular F<sup>-</sup> for Cl<sup>-</sup>, the activated current shifted inward at all voltages (*e-b*, ▲), and E<sub>rev</sub> became +49.1 mV. After removing bath F<sup>-</sup> and restoring symmetric Cl<sup>-</sup> (*f-g*, ○), E<sub>rev</sub> shifted back to +7.1 mV. A relative permeability, P<sub>F</sub>/P<sub>Cl</sub>, was then determined from these measured shifts of reversal potential;  $\Delta E_{rev} = E_{rev}(F^-_o) - E_{rev}(Cl^-_o) = 49.1 - (7.1 + 7.5)/2 = +41.8$  mV. P<sub>F</sub>/P<sub>Cl</sub> = 0.21.

The permeabilities of NO<sub>3</sub><sup>-</sup>, Br<sup>-</sup>, I<sup>-</sup>, aspartate, isethionate, and HEPES, relative to that of Cl<sup>-</sup>, were similarly determined from the shifts of the bi-ionic reversal potential on replacing extracellular Cl<sup>-</sup> with the test anion. Figure 15 summarizes the results of six such experiments, each testing the relative permeability of a single anion. Only the steady-state Iso- or Fsk-activated I-V relationships are shown, and these were obtained both before (●) and after (○) replacing Cl<sup>-</sup> with the test anion (▲). Pipette [Cl<sup>-</sup>] was fixed at 125 mM. Straight lines show interpolations used to estimate the reversal potentials of the activated currents, from which the relative permeabilities, P<sub>X</sub>/P<sub>Cl</sub>, were calculated. Replacing bath Cl<sup>-</sup> with nitrate

**Fig. 15. Relative permeability of six anions through the cardiac CFTR channel.** **A-F.** Each panel shows the results of an experiment testing the relative permeability of a single anion, as in Fig. P5. In each case, only the steady-state difference I-V relationships are shown. Pipette  $[Cl^-] = 125$  mM. For each experiment, the I-V relation of the conductance activated by either 2  $\mu$ M Fsk (C, D, F) or 1  $\mu$ M Iso (A, B, E) in symmetric 125 mM  $Cl^-$  was obtained, both before ( $\bullet$ ) and after ( $\circ$ ) replacement of the  $Cl^-$  in the external solution with the test anion ( $\blacktriangle$ ). Straight lines represent interpolated reversal potentials of the activated conductance. Relative permeability of the test anion,  $P_X/P_{Cl}$ , was calculated from the measured shifts of reversal potential (eqn. 3). **A.** Nitrate is more permeant than  $Cl^-$ .  $\Delta E_{rev} = -17$  mV.  $P_{NO_3}/P_{Cl} = 1.89$ . **B.** Bromide is more permeant than  $Cl^-$ .  $\Delta E_{rev} = -13.5$  mV.  $P_{Br}/P_{Cl} = 1.66$ . **C.** Iodide is more permeant than  $Cl^-$ .  $\Delta E_{rev} = -4.1$  mV.  $P_I/P_{Cl} = 1.17$ . **D.** Fluoride is less permeant than  $Cl^-$ .  $\Delta E_{rev} = 39.4$  mV.  $P_F/P_{Cl} = 0.23$ . **E.** Aspartate is less permeant than  $Cl^-$ .  $\Delta E_{rev} = 69.8$  mV.  $P_{Asp}/P_{Cl} = 0.07$ . **F.** HEPES is impermeant through the CFTR  $Cl^-$  channel.  $\Delta E_{rev} > 100$  mV.  $P_{HEPES}/P_{Cl} \leq 0.03$ . For experiments depicted in panels C and D, AMP-PNP was included in the pipette solution to lock channels open, to increase current magnitudes and decrease rundown (see Chapter 4, below).

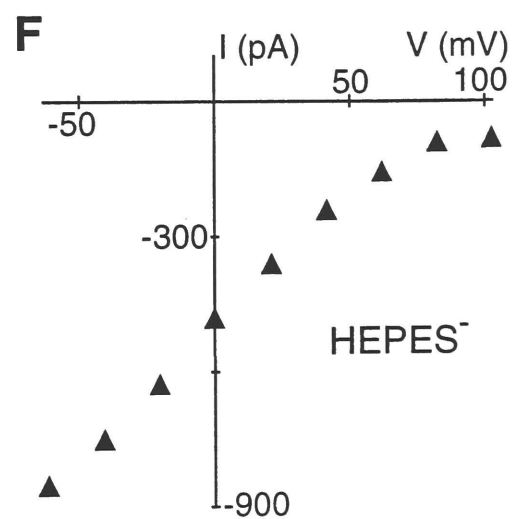
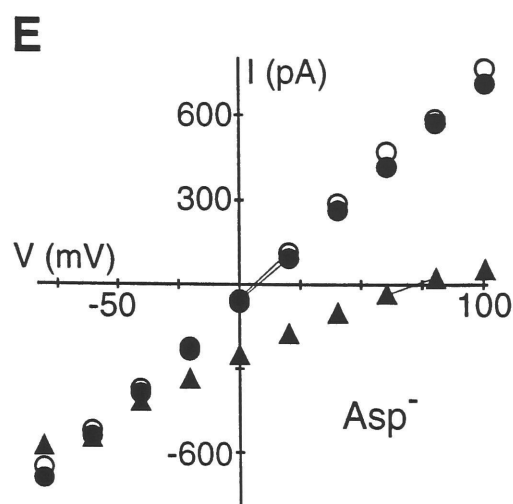
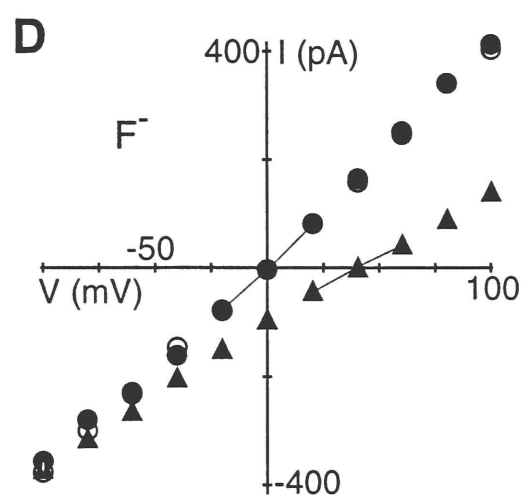
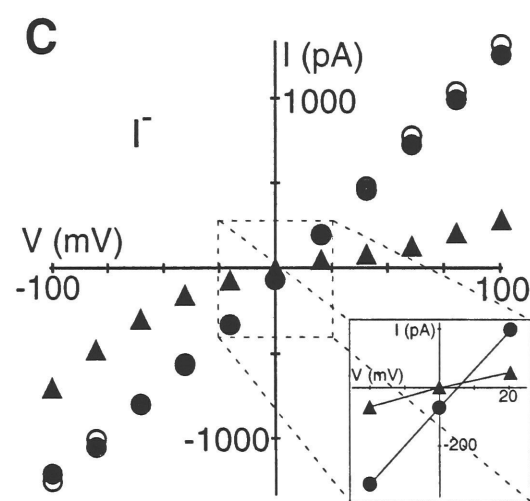
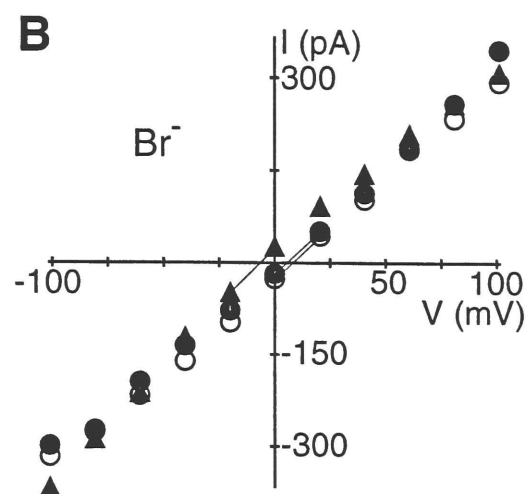
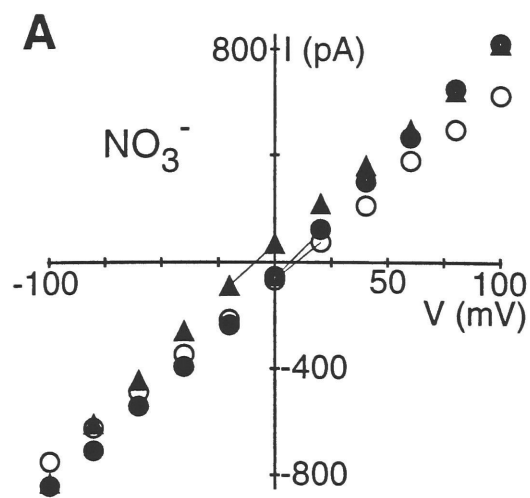






(Fig. 15A) or bromide (Fig. 15B) caused negative shifts of  $E_{rev}$ , indicating that both ions are more permeant than  $Cl^-$ ;  $\Delta E_{rev}$  was -17 mV for  $NO_3^-$ , and -13.5 mV for  $Br^-$ , yielding  $P_{NO_3}/P_{Cl} = 1.89$ , and  $P_{Br}/P_{Cl} = 1.66$ . Replacing  $Cl^-$  with fluoride (Fig. 15D) or aspartate (Fig. 15E) markedly diminished outward currents, shifting  $E_{rev}$  positive by 39.4 mV, and 69.8 mV, respectively, reflecting low relative permeabilities;  $P_F/P_{Cl} = 0.23$ , and  $P_{Asp}/P_{Cl} = 0.07$ . HEPES, a large monovalent anion (~40% anionic at pH 7.4), is completely impermeant through the CFTR  $Cl^-$  channel (Fig. 15F). Inward currents (representing  $Cl^-$  efflux) remain robust, but even at very positive potentials, HEPES carries no measurable current, so that  $\Delta E_{rev} > 100$  mV.  $P_{HEPES}/P_{Cl} \leq 0.03$ .

Iodide has complex effects on CFTR channel permeation (Fig. 15C), diminishing both outward current at positive potentials (reflecting net influx of  $I^-$  ions), and inward current at negative potentials (reflecting net efflux of  $Cl^-$  ions). Because both effects occurred within seconds of switching to  $I^-$ , they suggest that iodide may bind in the pore and inhibit chloride efflux. Nevertheless,  $I^-$  caused a small negative shift of  $E_{rev}$ ;  $\Delta E_{rev} = -4.1$  mV, indicating that  $I^-$  ions are more permeant than  $Cl^-$  ions, with  $P_I/P_{Cl} = 1.17$ .

## E. Gating and Regulatory Effects on Relative Permeability Measurements

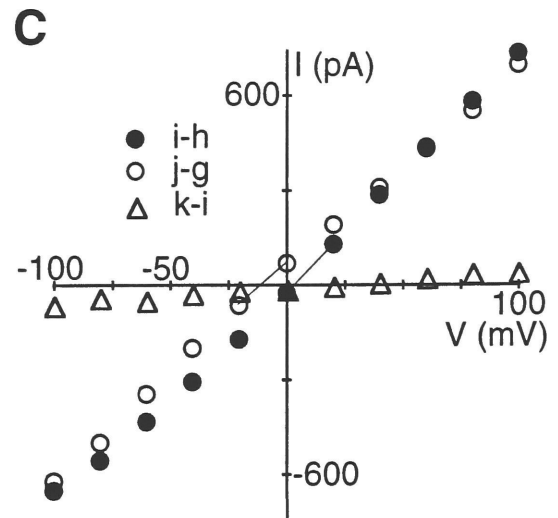
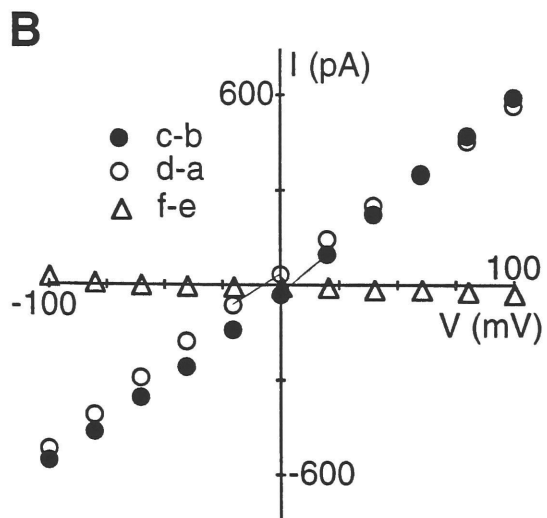
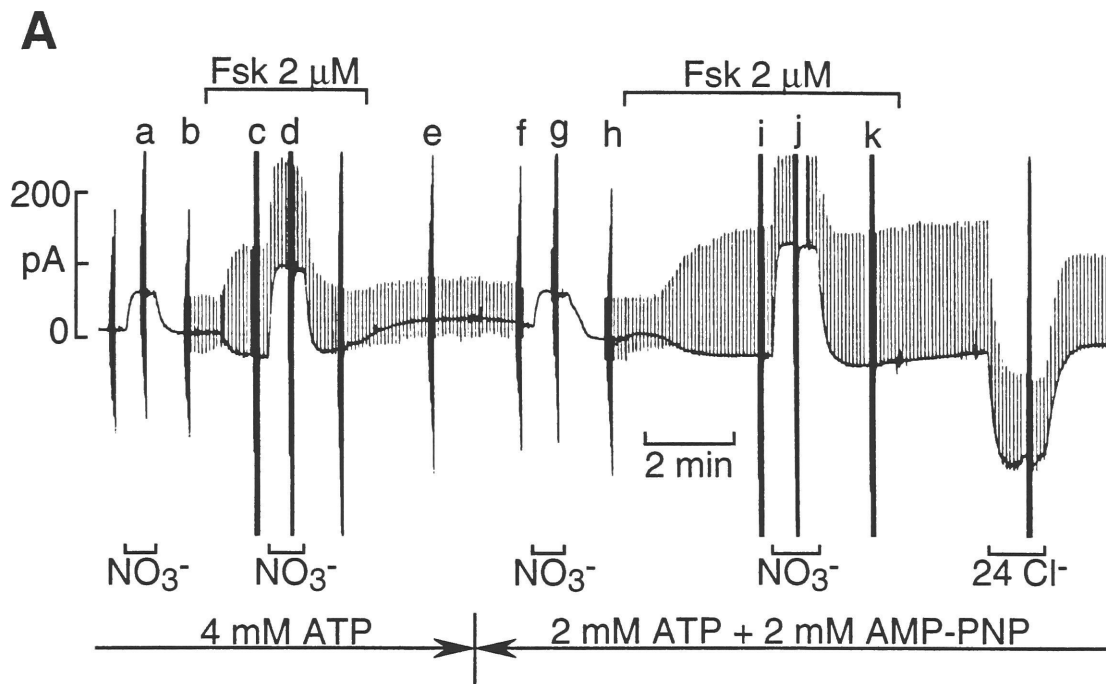
PKA-phosphorylated CFTR  $Cl^-$  channels continuously open and close in guinea-pig ventricular myocytes dialyzed with ATP-containing solutions, but become locked open for minutes at a time when pipette solutions also contain the non-hydrolyzable ATP analog AMP-PNP (Hwang et al., 1994). Because iodide diminishes whole-cell currents at both positive and negative membrane potentials (Fig. 15C), a possible interpretation



would be that iodide alters the gating characteristics of individual channels (e.g., by decreasing the channel open probability). Additionally, it is possible that iodide ions, or other replacement anions, influence regulation of the channels by kinases/phosphatases, independent of the anion's ability to permeate the CFTR channels (e.g., Walsh & Long, 1992). Such effects might confound interpretation of the I-V relationships and introduce error into the reversal potential measurements. To avoid this, a mixture of ATP and AMP-PNP was included in the pipette solution, so that relative permeabilities could be determined with the channels locked open. As usual, exposures to the test anions were kept brief, to minimize compromise of the bi-ionic assumption by entry of the test anion into the cell, as well as to minimize possible intracellular effects of the anions on background conductances and on CFTR channel regulation.

In whole-cell experiments with 2 mM ATP and 2 mM AMP-PNP in the pipette, the magnitudes of the currents elicited on first exposure to agonist are up to two times larger than with ATP alone, there is less low-frequency whole-cell current noise with large driving forces, and the current activates and deactivates more slowly (Figs. 16, 17, and Hwang et al., 1994). Figure 16 illustrates an experiment in which the relative permeability of nitrate was tested, both in the presence of 4 mM pipette ATP, and after switching to a pipette solution containing 2 mM ATP and 2 mM AMP-PNP (lower, arrowed lines). Upper bars mark applications of 2  $\mu$ M Fsk, and lower bars mark periods of equimolar bath substitution of  $\text{NO}_3^-$  for  $\text{Cl}^-$ , and of superfusion of a 24 mM  $\text{Cl}^-$  solution. The outward shift in holding current upon replacing bath  $\text{Cl}^-$  with  $\text{NO}_3^-$  indicates that  $\text{NO}_3^-$  is more permeant than  $\text{Cl}^-$  through the background leak conductance pathway. Comparing the difference in holding current before and after activation of CFTR

**Fig. 16. Nitrate permeability is unaffected by locking open the cardiac CFTR channel.** **A.** Chart record of the whole-cell current trace, at 0 mV, from a single cell. Upper bars mark bath applications of 2  $\mu$ M forskolin. Smallcase letters mark periods of current-voltage (I-V) data acquisition. Lower bars mark periods of equimolar bath substitution of  $\text{NO}_3^-$  for  $\text{Cl}^-$ , and superfusion of a 24 mM  $\text{Cl}^-$  solution. Arrowed lines represent pipette solution changes. Small upward deflections represent 80 ms voltage steps to +20 mV, every 6 s, to monitor current activation. **B.** Steady-state difference I-V relationships obtained in the presence of 4 mM pipette ATP. Activation of whole-cell  $\text{Cl}^-$  conductance in symmetric 125 mM  $\text{Cl}^-$  induces an ohmic conductance which reverses at +6.6 mV (*c-b*, ●). With extracellular  $\text{Cl}^-$  replaced by  $\text{NO}_3^-$ ,  $E_{\text{rev}}$  of the activated conductance shifts to more negative voltages (*d-a*, ○).  $E_{\text{rev}} = -7.0$  mV.  $\Delta E_{\text{rev}} = -13.6$  mV.  $P_{\text{NO}_3}/P_{\text{Cl}} = 1.66$ . Also shown is the difference I-V relation before and after pipette substitution of 2 mM AMP-PNP for ATP (*f-e*,  $\Delta$ ), indicating that pipette AMP-PNP does not activate a conductance in the absence of activators of the CFTR  $\text{Cl}^-$  channel stimulatory pathway. **C.** Steady-state difference I-V relationships obtained with 2 mM ATP and 2 mM AMP-PNP in the pipette solution, in symmetric 125 mM  $\text{Cl}^-$  (*i-h*, ●), and with extracellular  $\text{Cl}^-$  replaced by  $\text{NO}_3^-$  (*j-g*, ○). The shift in  $E_{\text{rev}}$  is similar to that in the presence of pipette ATP alone.  $\Delta E_{\text{rev}} = -14.2$  mV.  $P_{\text{NO}_3}/P_{\text{Cl}} = 1.70$ ). The difference I-V relation in symmetric 125 mM  $\text{Cl}^-$ , obtained before and after  $\text{NO}_3^-$  substitution, indicates that there is little increase in leak current over this time (*k-i*,  $\Delta$ ).  $C_m = 101$  pF;  $R_{\text{pip}} = 1.0$  M $\Omega$ ;  $R_{\text{acc}} = 7.3$  M $\Omega$  (E2,3,6/I4,5).





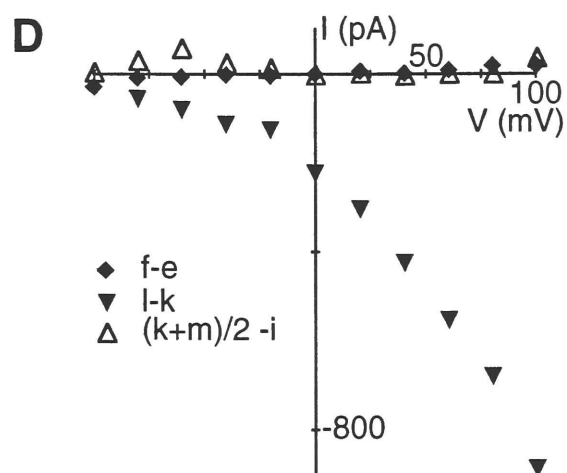
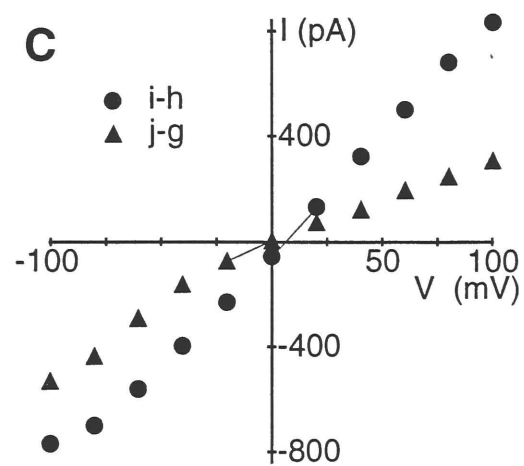
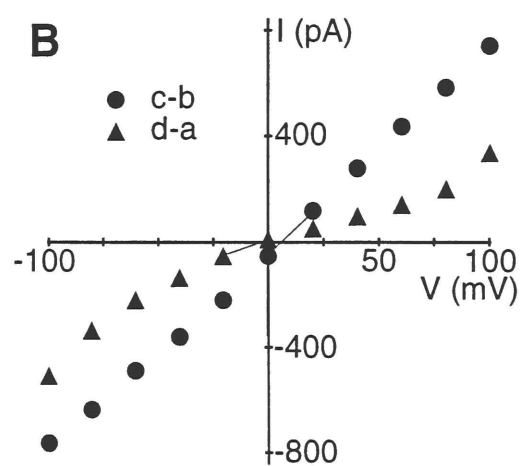
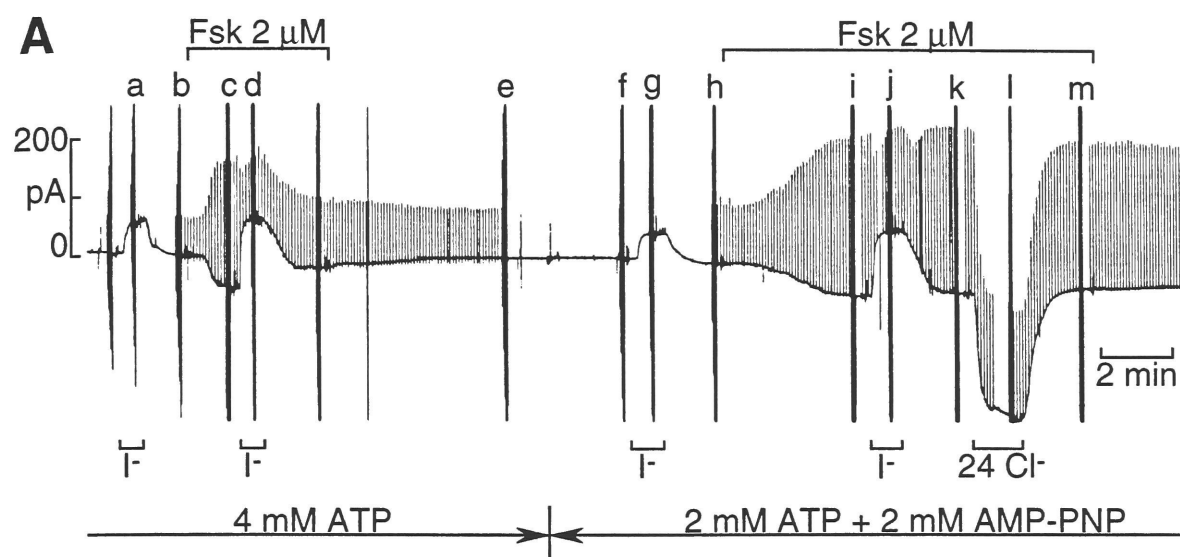
conductance by Fsk, with either  $\text{Cl}^-$  or  $\text{NO}_3^-$  in the bath, it is clear that, at 0 mV, the difference current in symmetric  $\text{Cl}^-$  is slightly inward but is slightly outward with  $\text{NO}_3^-$  in the bath. This was observed with both pipette solutions and reflects the enhanced permeability of CFTR channels for  $\text{NO}_3^-$  than for  $\text{Cl}^-$  ions. Figure 16B and 16C show the steady-state difference CFTR I-V relationships, in the presence of 4 mM pipette ATP, or upon switching to 2 mM ATP plus 2 mM AMP-PNP. In both cases, when extracellular  $\text{Cl}^-$  was replaced by  $\text{NO}_3^-$ ,  $E_{\text{rev}}$  of the activated conductance shifted to a more negative voltage, and  $\Delta E_{\text{rev}}$  was -13.1 mV, yielding  $P_{\text{NO}_3}/P_{\text{Cl}} = 1.66$  with ATP in the pipette, and  $\Delta E_{\text{rev}}$  was -14.2 mV, giving  $P_{\text{NO}_3}/P_{\text{Cl}} = 1.70$  with ATP plus AMP-PNP in the pipette.

Figure 17A depicts a similar experiment in which iodide permeability was measured, both with ATP in the pipette, and again with ATP plus AMP-PNP in the pipette. As found with  $\text{NO}_3^-$ , the outward shift in background holding current upon switching bath anion from  $\text{Cl}^-$  to  $\text{I}^-$  indicates that  $\text{I}^-$  is more permeant than  $\text{Cl}^-$  through the residual conductance pathways. Activation of CFTR conductance by Fsk is signaled by the small inward shift in holding current and the ~2-fold increase in current in response to the +20 mV test pulses. The current at 0 mV during the brief exposures to  $\text{I}^-$ , however, was practically unaltered by activation of CFTR conductance, either with ATP alone in the pipette, or after the pipette solution had been changed for the one containing ATP plus AMP-PNP.

Again, the slower activation of the conductance by Fsk, the relative lack of inactivation of the conductance upon Fsk withdrawal, and the lack of significant current noise in the holding current after lowering extracellular  $\text{Cl}^-$  to 24 mM, all reflect the action of AMP-PNP to cause prolonged channel openings. Figures 17B and 17C show that the steady-

**Fig. 17. Iodide permeability is unaffected by locking open the cardiac CFTR channel.** **A.** Chart record of whole-cell current, at 0 mV, from a single cell. Upper bars mark bath Fsk application, lower bars indicate bath anion substitutions, both of I<sup>-</sup> for Cl<sup>-</sup>, and of a low Cl<sup>-</sup> solution, and pipette solution changes (*arrowed lines*). **B.** Steady-state difference I-V relationships obtained from cell in A, with 4 mM ATP in the pipette. Activation of whole-cell Cl<sup>-</sup> conductance in symmetric 125 mM Cl<sup>-</sup> induces an ohmic conductance which reverses at +7.0 mV (*c-b*, ●). With extracellular Cl<sup>-</sup> replaced by I<sup>-</sup>, E<sub>rev</sub> of the activated conductance shifts to more negative voltages (*d-a*, ▲). E<sub>rev</sub> = -2.6 mV. ΔE<sub>rev</sub> = -9.6 mV. P<sub>I</sub>/P<sub>Cl</sub> = 1.43. **C.** Steady-state difference I-V relationships obtained with 2 mM ATP and 2 mM AMP-PNP in the pipette solution, in symmetric 125 mM Cl<sup>-</sup> (*i-h*, ●), and with extracellular Cl<sup>-</sup> replaced by I<sup>-</sup> (*j-g*, ▲). Shifts in E<sub>rev</sub> are similar to those in the presence of pipette ATP alone. ΔE<sub>rev</sub> = -6.8 mV. P<sub>I</sub>/P<sub>Cl</sub> = 1.29. **D.** The steady-state difference I-V relation, obtained before and after pipette substitution of 2 mM AMP-PNP for ATP, shows that pipette AMP-PNP does not activate a conductance in the absence of activators of the CFTR Cl<sup>-</sup> channel stimulatory pathway (*f-e*, ◆). The steady-state difference I-V relation in symmetric 125 mM Cl<sup>-</sup>, obtained before and after I<sup>-</sup> substitution, indicates that there is little increase in leak currents over this time [(*k+m*)/2 - *i*, Δ]. Lowering external [Cl<sup>-</sup>] to 24 mM reveals the Cl<sup>-</sup> sensitive nature of the activated current (*l-k*, ▼). C<sub>m</sub> = 101 pF; R<sub>pip</sub> = 0.6 MΩ; R<sub>acc</sub> = 8.0 MΩ (E2,3,6/I4,5).







state bi-ionic I-V relationships ( $I_o/Cl_i$ ) are similar whether or not CFTR channels are held open by AMP-PNP; in either case, outward currents at positive potentials (reflecting  $I^-$  influx) and inward currents at negative potentials (reflecting  $Cl^-$  efflux) are diminished. Despite these reduced currents, the bi-ionic reversal potentials were a few mV more negative than those with symmetric 125 mM  $Cl^-$ . The shifts in  $E_{rev}$  were -9.6 mV in the presence of pipette ATP alone, and -6.8 mV with ATP plus AMP-PNP, with  $P_I/P_{Cl}$  estimates of 1.43 and 1.29, respectively. Together, these results suggest that although iodide ions have a higher permeability than  $Cl^-$  ions (reflecting a lower peak barrier to ion flow), they have a lower dissociation rate than  $Cl^-$  ions from the anion binding site(s) within the pore. Thus, iodide ions act as permeant blockers of the CFTR channel.

The relative permeabilities ( $P_X/P_{Cl}$ ) of all anions tested in these experiments are summarized in Table 4. Ranked from most permeant to least, they are:  $NO_3^-$  (1.74) >  $Br^-$  (1.51) >  $I^-$  (1.30) >  $Cl^-$  (1) >  $F^-$  (0.25) >  $Asp^-$  (0.07) >>  $Iseth^-$ ,  $HEPES^-$  ( $\leq 0.05$ ).

## F. Sizing the Pore

From the relative permeability measurements, it is evident that the CFTR channel pore is freely permeable to anions as large as  $NO_3^-$  and  $I^-$  (mean diameters  $\sim 4.4$  Å) but can pass aspartate poorly (mean diameter 6.7 Å), and isethionate (mean diameter 6.9 Å) barely, if at all. By relating the calculated size of a three-dimensional model of each anion to that ion's relative permeability, an estimate of the minimum cross-sectional dimensions of the narrowest region pore can be made. Pore diameters have been estimated for both cation (Dwyer, Adams & Hille, 1980; Cohen et al.,



**Table 4. Permeability Ratios of Anions in the Cardiac CFTR Channel**

Anion	n	AMP-PNP*	$\Delta E_{rev}$ (mV) <sup>†</sup>	$P_X/P_{Cl}^{\#}$	Mean Dia. <sup>§</sup> (Å)
<b>NO<sub>3</sub><sup>-</sup></b>	13	-/+	<b>-14.8 ± 0.6</b>	<b>1.74 ± 0.04</b>	4.36
	8	-	-14.0 ± 0.5	1.69 ± 0.03	
	5	+	-16.0 ± 1.0	1.82 ± 0.07	
<b>Br<sup>-</sup></b>	7	-	<b>-10.9 ± 1.0</b>	<b>1.51 ± 0.06</b>	3.92
<b>I<sup>-</sup></b>	12	-/+	<b>-6.7 ± 1.3</b>	<b>1.30 ± 0.07</b>	4.40
	7	-	-6.3 ± 2.2	1.29 ± 0.11	
	5	+	-7.2 ± 1.0	1.32 ± 0.05	
<b>Cl<sup>-</sup></b>	41	-	0 <sup>‡</sup>	<b>1</b>	3.62
	16	+	0 <sup>‡</sup>	<b>1</b>	
<b>F<sup>-</sup></b>	7	-/+	<b>38.9 ± 4.1</b>	<b>0.25 ± 0.03</b>	2.66
	4	-	44.2 ± 5.3	0.20 ± 0.04	
	3	+	31.9 ± 4.1	0.31 ± 0.05	
<b>Asp<sup>-</sup></b>	6	-	<b>72.1 ± 3.4</b>	<b>0.07 ± 0.01</b>	6.67
<b>Iseth<sup>-@</sup></b>	4	-	<b>84.2 ± 7.3</b>	<b>≤0.05 ± 0.02</b>	6.87
<b>HEPES<sup>-@</sup></b>	4	-	<b>91.2 ± 2.1</b>	<b>≤0.03 ± 0.003</b>	9.37

\* Reversal potential measurements and permeability ratios were calculated from experiments with either 4-10 mM pipette ATP (-), or with 2 mM ATP and 2 mM AMP-PNP in the pipette (+). For NO<sub>3</sub><sup>-</sup>, I<sup>-</sup>, and F<sup>-</sup>, the permeability ratios from experiments with ATP in the pipette were not significantly different than those from experiments with ATP and AMP-PNP in the pipette solution ( $P > 0.05$ ); the two groups of measurements are thus pooled (+/-).

<sup>†</sup>  $\Delta E_{rev}$  was defined as the difference in reversal potential, of the conductance elicited by 2  $\mu$ M forskolin or 1  $\mu$ M isoproterenol, in the presence of 125 mM bath and pipette Cl<sup>-</sup> (taken as the average of the bracketing  $E_{rev}$



measurements, i.e., before and after anion substitution), and after equimolar substitution of bath  $\text{Cl}^-$  with the test anion  $\text{X}^-$ .

$$\Delta E_{\text{rev}} = E_{\text{rev}}(\text{X}^-_o) - E_{\text{rev}}(\text{Cl}^-_o).$$

#  $P_{\text{X}}/P_{\text{Cl}}$  was calculated using:  $\Delta E_{\text{rev}} = RT/zF \cdot \ln(P_{\text{X}}/P_{\text{Cl}})$ .

§ Mean diameter taken as the geometric mean of the dimensions of the anion, calculated with a model building program (Molecular Modeling Pro; WindowChem Software)

‡ With 125 mM  $\text{Cl}^-$  in the pipette and bath, the reversal potential of the activated conductance was  $+6.0 \pm 0.3$  mV, with 4-10 mM ATP in the pipette (-), and  $+5.1 \pm 0.5$  mV, with 2 mM ATP and 2 mM AMP-PNP in the pipette (+).

@ For both isethionate and HEPES,  $E_{\text{rev}}$  in 2 of the 4 experiments was  $>100$  mV. To calculate a lower limit for  $\Delta E_{\text{rev}}$ , and an upper limit for  $P_{\text{X}}/P_{\text{Cl}}$ , in these cases,  $E_{\text{rev}}$  was taken to be 100 mV. In all other measurements in this series of experiments, measured  $E_{\text{rev}}$  was between  $\pm 100$  mV.





1992), and anion (Bormann, Hamill & Sakmann, 1987) channels by modeling the pore as a cylinder permeated by spherical ions.

For a circular cylinder of fixed diameter  $d$ , and a permeating ion of diameter  $a$ ; the area available for diffusion becomes smaller as  $a$  increases, and is proportional to  $[1-(a/d)]^2$ , reflecting the excluded volume effect (Dwyer et al., 1980). Since an ion's permeability may also be decreased by frictional forces as  $a$  increases (Dwyer et al., 1980), relative permeabilities can be related to pore diameter by:

$$\frac{P_X}{P_{Cl}} = \frac{k}{a} \left(1 - \frac{a}{d}\right)^2 \quad (\text{eqn. 9})$$

where  $k$  (Å) is a proportionality constant,  $a$  (Å) is the mean diameter of anion  $X^-$  (eqn. 5), and  $d$  (Å) is the estimated minimum pore diameter. Figure 18 shows plot of mean ionic diameter versus the log of the relative permeability for each anion tested. The smooth curve is a fit (by eye) of eqn. 9, scaled arbitrarily so that it passes through  $P_{NO_3}/P_{Cl} = 1.74$ , at  $4.36$  Å, for a circular pore diameter of  $7$  Å;  $k = 53.3$  Å. The implication is that the narrowest region of the pore has a diameter of  $\sim 7$  Å.

### III. Discussion

#### A. $E_{rev}$ Deviation from $E_{Cl}$

##### i. Ion Accumulation/Depletion

One possible explanation for the positive deviation of measured  $E_{rev}$  from the estimated  $E_{Cl}$ , in high  $Cl^-_{out}$ /low  $Cl^-_{in}$  solutions (Table 3) is  $Cl^-$  ion accumulation near the intracellular face of the membrane during periods of net  $Cl^-$  influx (Hwang et al., 1992b), so that the  $[Cl^-]_i$  assumed in the calculation of  $E_{Cl}$  is in error. Figure 11 shows that with all pipette  $Cl^-$



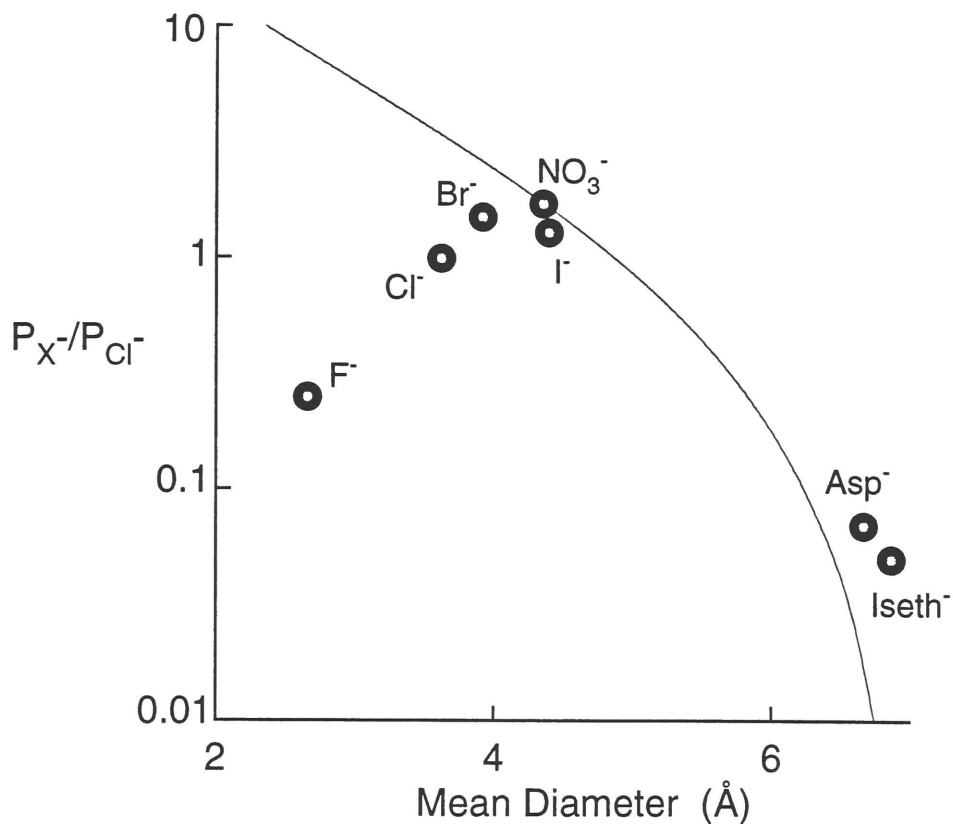


**Fig. 18. Dependence of relative ion permeability on mean ion diameter.**

Mean ion diameter (calculated as the geometric mean; see Methods) *versus* the log of the relative permeability for each anion. Smooth curve represents equation 9, where  $a$  is the mean diameter of the test anion  $X^-$ ,  $d$  is the estimated minimum pore diameter (7 Å), and  $k$  a proportionality constant (53.3).



replaced by 85 mM aspartate and 20 mM MeSO<sub>3</sub><sup>-</sup>, the reversal potential of the activated current was < -100 mV. An E<sub>rev</sub> of -100 mV, assuming that Cl<sup>-</sup> were the only permeant ion, would require an intracellular Cl<sup>-</sup> accumulation of ~3 mM. The same accumulation with 24 mM Cl<sup>-</sup> pipette solutions would result in an ~+4 mV shift in E<sub>Cl</sub>, accounting for at most one-third of the +12 to +15 mV deviation of E<sub>rev</sub> observed.

Two simple calculations confirm that this is probably an upper limit to the extent of Cl<sup>-</sup> accumulation that occurs. An outward Cl<sup>-</sup> current of 100 pA flowing for 100 s would be expected to raise intracellular [Cl<sup>-</sup>] of a cell of 10 pl volume by 10 mM. This assumes no Cl<sup>-</sup> dissipation into the pipette. Assuming that equilibration between pipette ([Cl<sup>-</sup>]<sub>pip</sub>) and the cell interior ([Cl<sup>-</sup>]<sub>i</sub>) is characterized by a time constant (τ<sub>pip</sub>) of ~50 s (Nakao & Gadsby, 1989), the 100 pA Cl<sup>-</sup> current (I<sub>Cl</sub>) would be expected to establish a concentration difference across the pipette of:

$$[Cl]_{pip} - [Cl]_i = \frac{\tau_{pip} * I_{Cl}}{vol * F} \cong 5mM. \text{ Moreover, aspartate seems measurably}$$

permeant when applied in the bath (upper limit of relative aspartate permeability ~0.07; see below), and any aspartate permeability would tend to shift E<sub>rev</sub> to the right. On this basis, cellular Cl<sup>-</sup> accumulation seems likely to make only a minor contribution to the positive deviation of E<sub>rev</sub> from E<sub>Cl</sub> observed in some conditions. Far more likely is that aspartate is somewhat permeant and that there is little internal Cl<sup>-</sup> accumulation.

Figure 9 also suggests that extracellular Cl<sup>-</sup> accumulation contributes little to the negative deviation of E<sub>rev</sub> from estimated E<sub>Cl</sub> in the high [Cl<sup>-</sup>]<sub>i</sub>/low [Cl<sup>-</sup>]<sub>o</sub> condition. When all extracellular Cl<sup>-</sup> was replaced with isethionate, E<sub>rev</sub> is ~84.2 ± 7.3 mV (Table 4; comparable to the worst case in Fig. 11C, *f-e*). If we assume, on the one hand, that isethionate is impermeant and that E<sub>rev</sub> = E<sub>Cl</sub>, we can calculate a maximum



extracellular  $\text{Cl}^-$  accumulation of  $\sim 5$  mM. If that extent of  $\text{Cl}^-$  accumulation also occurred when 24 mM  $\text{Cl}^-$  was in the bath, true  $E_{\text{Cl}}$  would be +39 mV, close to the average measured  $E_{\text{rev}}$  of +39.6 mV under those conditions (Table 3). If, on the other hand, isethionate permeability is assumed solely responsible for any outward current at +100 mV (Table 4; cf. Fig. 11C), then its relative permeability would have to be 0.02. In that case, factoring in this isethionate permeability, the expected  $E_{\text{rev}}$  for the case of 125 mM  $\text{Cl}^-_{\text{i}}$ , 24 mM  $\text{Cl}^-_{\text{o}}$  (plus 130 mM iseth $^-_{\text{o}}$ ) is +41.0 mV, also close to the value measured. So, although we cannot rule out a small contribution from  $\text{Cl}^-$  accumulation in the extracellular space to the negative deviation in  $E_{\text{rev}}$  measured in high  $[\text{Cl}^-]_{\text{i}}$ /low  $[\text{Cl}^-]_{\text{o}}$  experiments, it seems more likely that external  $\text{Cl}^-$  accumulation is negligible and that isethionate is slightly permeant.

## ii. Chloride Selectivity

The reversal potential of the activated whole-cell  $\text{Cl}^-$  conductance varied roughly linearly with  $\log [\text{Cl}^-]_{\text{o}}$ , with a slope of  $-57 \pm 3$  mV, not far from the Nernst prediction, at 37 °C, of 61.5 mV (Fig. 12C), a finding in reasonable agreement with others for the PKA-activated conductance in guinea-pig ventricular myocytes;  $\sim 60$  mV (Matsuoka et al., 1990), and  $\sim 53$  mV (Harvey, Clark & Hume, 1990). The large magnitude of the measured slope implies that cardiac CFTR channels are relatively impermeable to the other anion in the bath (isethionate) and to the cations in the pipette ( $\text{Cs}^+$  and  $\text{TEA}^+$ ), since substantial permeability to any of these would decrease the slope. Other measurements, however, suggest that aspartate and isethionate are somewhat permeant, with relative permeabilities (upper limits) of  $\leq 0.07$  for aspartate, and  $\leq 0.05$  for isethionate. The smooth curve





in Figure 12C (middle) represents  $E_{rev}$  predicted on the basis of these additional permeabilities, using the Goldman-Hodgkin-Katz voltage equation:

$$E_{rev} = \frac{RT}{zF} \ln \left( \frac{[Cl^-]_o + \frac{P_{Iseth}}{P_{Cl}} [Iseth^-]_o}{[Cl^-]_i + \frac{P_{Asp}}{P_{Cl}} [Asp^-]_i} \right) \quad (\text{eqn. 10})$$

These additional permeabilities can account for some of the systematic positive offset of  $E_{rev}$  from the Nernst prediction in Figure 12C, but they do not completely account for it. One possibility is that there is a small, selective permeability to  $Na^+$  (relative to  $Cs^+$ ), since all the bath solutions contain 150 mM  $Na^+$ . If a relative permeability to  $Na^+$  of 0.05 is assumed, along with the measured isethionate and aspartate permeabilities, the predicted  $E_{rev}$  would be very close to that observed:  $E_{rev}$  would be within a few mV of those observed as  $[Cl^-]_o$  is raised from 24 to 150 mM; in particular, it would be within 0.5 mV of that observed in 150 mM  $Cl^-_o/24$  mM  $Cl^-_i$  solution, *and* within 0.5 mV of that observed in 24 mM  $Cl^-_o/125$  mM  $Cl^-_i$  solution. The relative permeabilities of CFTR channels to  $Na^+$  and  $Cs^+$  have not been examined, although the similar amplitude of single CFTR channel currents in  $Cl^-$ -containing solutions with either  $Na^+$  or  $NMG^+$  as the principal cation had been interpreted as demonstrating a rather small relative permeability to cations (Nagel et al., 1992).

Could a liquid junction potential cause such a systematic positive deviation? Since our initial pipette solution is the same as that in the bath (normal Tyrode's), there should be no liquid junction potential when the amplifier is zeroed. However, it is probable that on membrane rupture, a Donnan equilibrium liquid junction potential arises between the pipette



solution and the cell interior, due to the excess of relatively immobile anions in the cell, which makes the cell interior a few mV more negative than the pipette (i.e., clamp) potential, and which is maximal upon breakthrough (Barry & Lynch, 1991; Marty & Neher, 1995). This potential should diminish over minutes, however, as the cell interior and the pipette solution equilibrate, but could result in a systematic positive offset for *all*  $E_{revs}$  measured with a fixed pipette solution. However, its sign would not be expected change on altering pipette  $[Cl^-]$  from 24 mM to 125 mM, yet we observe a *negative* offset in 125 mM  $Cl^-_i$ /24 mM  $Cl^-_o$  solutions (Table 3). Nor does a lower intracellular, than extracellular, activity coefficient seem a likely explanation for the deviation in Fig. 12C, since the ionic strengths are expected to be, if anything, higher in the pipette solutions (tending to lower activity coefficients) whereas the observed deviations would require higher internal activity coefficients. A final explanation for Figure 12C could be an asymmetric channel structure. For example, fixed negative surface charges on the channel exterior could impair  $Cl^-$  influx, although this would lead to a systematic positive offset and could not account for the negative offset from  $E_{Cl}$  in 125 mM  $Cl^-_i$  /24 mM  $Cl^-_o$  solutions (Table 3).

## B. Inferences About the Anion Binding Site in the Pore

The sequence of relative permeabilities was:

$$\begin{array}{ccccccc} NO_3^- & > & Br^- & > & I^- & > & Cl^- & > & F^- & > & Asp & >> & Iseth^-, & HEPES \\ 1.7 & & 1.5 & & 1.3 & (1) & 0.25 & 0.07 & 0.05 & & 0.03 \end{array}$$

This sequence differs slightly from that of another study of anion permeability of CFTR conductance in guinea-pig cardiac myocytes (Overholt & Harvey, 1992), in which the sequence of relative permeabilities



was:  $\text{NO}_3^-$  2.1 >  $\text{Br}^-$  1.3  $\geq$   $\text{Cl}^-$  1  $\geq$   $\text{I}^-$  0.88 > Iseth<sup>-</sup> 0.1  $\geq$  Glutamate 0.03. The major difference is the estimated relative permeability to  $\text{I}^-$  (1.3 *versus* 0.9). One other study examined the relative permeability of  $\text{I}^-$  but no other anions in guinea-pig ventricular myocytes and found  $P_{\text{I}}/P_{\text{Cl}} = 1.3$ , in agreement with our estimate (Walsh & Long, 1992).

Relative permeability measurements for epithelial CFTR channels have produced a less clear picture, although the sequence  $\text{Br}^- > \text{Cl}^- > \text{F}^-$  is a consistent feature (e.g., Cliff & Frizzell, 1990; Anderson et al., 1991). In most studies, iodide seems less permeant than  $\text{Cl}^-$  (~0.6; e.g., Cliff & Frizzell, 1990; Anderson et al., 1991; Haws et al., 1992), although it has been estimated to be ~1 (Gray et al., 1990; Kartner et al., 1991), and even as high as 1.7 (Tabcharani et al., 1992). Independent of its importance in understanding the selectivity filter/binding site interactions within the pore, the issue of iodide permeability is significant since a low iodide permeability has been (and still is) considered a distinguishing feature of epithelial CFTR  $\text{Cl}^-$  channels (Quinton & Reddy, 1989; Cliff & Frizzell, 1990; Anderson et al., 1991; Reddy, Bell & Quinton, 1991; Welsh et al., 1992).

Importantly, the series of bi-ionic reversal potential measurements with cardiac CFTR channels locked in the open state rule out any indirect effects the substituent anions might have on regulation of CFTR channels. Since the calculated permeability ratios are closely similar regardless of whether the channels are gating normally, or whether they are locked open by AMP-PNP, the implication is that the ionic substitutions do not affect gating of the channel. We thus conclude that iodide is indeed more permeant than  $\text{Cl}^-$  through the cardiac CFTR  $\text{Cl}^-$  channel. Furthermore, we conclude that iodide reduces currents both at positive potentials and negative potentials by direct effects on the permeation pathway, not by



altering the gating or by other indirect regulatory mechanisms, as suggested by Walsh & Long (1992).

The small discrepancy between the results of the iodide relative permeability measurements shown here (1.3) and the work of Overholt et al. (~0.9; 1992) is likely explained by the extreme sensitivity of the reversal potential measurements in the I<sup>-</sup>/Cl<sup>-</sup> bi-ionic condition to changes in membrane leak, since iodide markedly diminishes both inward and outward currents so that the slope of the I-V relation near  $E_{rev}$  is thus quite small (see Figs. 15C, 17). This problem is confounded by the observation that iodide solutions increased membrane leak rapidly and substantially, and so we were careful to expose cells to iodide only for brief, ~30 s, intervals. Any unnoticed increase in leak would lead to an underestimation of the relative permeability by drawing  $E_{rev}$  closer to that of the leak currents (~0 mV). Since Overholt et al. (1992) reported no effort to keep anion exposures brief (and no time courses of experiments are shown), this might account for their measured relative permeability for I<sup>-</sup> being close to 1. Interestingly, their estimates of relative permeabilities for Br<sup>-</sup> (1.3) and for Iseth<sup>-</sup> (0.1) are also both closer to 0 than in this study. Ultimately, prolonged exposures to any of the test anions must be expected to compromise the assumed bi-ionic condition.

In addition to the factors listed above, the systematic low relative iodide permeability reported in many of the studies on epithelial CFTR could be due to voltage errors resulting from liquid junction potentials, or a possible influence of iodide on the activation pathway (cf. Walsh & Long, 1992). Finally, minute differences in amino acid sequences resulting in slight alterations in the selectivity filter cannot presently be ruled out. The





identification of residues that line the pore of the CFTR channel is still controversial.

According to Eisenman's equilibrium theory of ionic selectivity, selectivity depends on the difference between the energy lost in dehydration of an ion and the energy gained by its interaction with the binding site (Wright & Diamond, 1977; Eisenman & Horn, 1983). For anion binding to a very weak site, selectivity is expected to be determined solely by the relative hydration energies, and the selectivity sequence should parallel the free solution mobilities of the anions (Diamond & Wright, 1969; Wright & Diamond, 1977); viz.,  $I^- > NO_3^- > Br^- > Cl^- > F^-$  (Eisenman sequence I). At the strongest anion site, selectivity is expected to be determined by the ability of the anion to approach and interact with the binding site. Thus, the ion with the smallest non-hydrated radius will be preferred and the selectivity sequence becomes the inverse sequence of the anionic radius (Wright & Diamond, 1977); viz.,  $F^- > Cl^- > Br^- > NO_3^- > I^-$  (Eisenman sequence VII). In between these extremes are five transitional sequences, reflecting the predicted selectivity as the binding site progresses from weak to strong.

The relative permeability sequence found here for CFTR channels,  $NO_3^- > Br^- > I^- > Cl^- > F^-$ , corresponds to Eisenman's sequence II, suggesting that the binding site in the channel is relatively weak. In contrast, based on their measurements of relative permeability of epithelial CFTR native in T84 cells, or exogenously expressed in NIH 3T3 or HeLa cells, Anderson et al. (1991b) concluded that the selectivity suggested a moderately high affinity binding site for anions. Tabcharani and Hanrahan (1993a), on the other hand, determined that expressed CFTR channels contained a weak field strength site, but their measurements were made by cytoplasmic, rather than extracellular, anion substitution.



Direct comparison of the latter data with others requires the assumption that the pore barriers are symmetric, an assumption that might not be warranted.

### C. Estimate of Minimum Pore Diameter

Our estimate of a minimum pore diameter for CFTR is  $\sim 7$  Å. This must be taken as an upper estimate, since we have used upper estimates for the relative permeabilities of isethionate and HEPES. We have plotted the geometric mean diameter of each anion, which corresponds to the mean of the three dimensions of the smallest rectangular box containing a Corey-Pauling-Koltum space-filling model of the anion (Hille, 1975; Dwyer et al., 1980). Apparent ionic diameters are often calculated using the Stokes-Einstein relationship (Robinson & Stokes, 1965) for estimation of the minimum pore diameter (e.g., Bormann et al., 1987). However, since this relation is based on the assumption of a homogeneous fluid environment for the derivation of friction (which is unreasonable because the size of the ion is comparable to the size of H<sub>2</sub>O molecules), and a constant bulk viscosity (which is inappropriate since the movement of the ion through the water perturbs the local water structure and results in a non-constant viscosity), the Stokes diameter is considered a poor estimate of true molecular size (Hille, 1975).

For the fit, we have included both an excluded volume term, since the area available for diffusion should decrease with increasing ion diameter  $a$  as  $1-(a/d)^2$ , and a drag term ( $1/a$ ), since friction should vary directly as a function of  $a$  (Dwyer et al., 1980). The curve has been scaled arbitrarily to pass through NO<sub>3</sub><sup>-</sup> ( $P_{\text{NO}_3}/P_{\text{Cl}} = 1.74$ ), at a diameter of 4.4 Å, and was fitted by eye, yielding a pore diameter of  $\sim 7$  Å. Although this approach is



certainly simplistic, since assumptions about hydrodynamic flow likely break down at the dimensions under study (see, e.g., Bean, 1972), the fit suggests that, at least to a rough approximation, pore size and frictional drag felt by the ion can account for the relative permeabilities of the larger permeant anions through this channel.

Anion channels typically discriminate poorly among anions, which suggests that they have a wide pore (Hille, 1992). Our estimate of a minimum pore size of  $\sim 7$  Å is comparable to the estimate for the epithelial CFTR channel by Tabcharani and Hanrahan (1993), who suggest a pore diameter of  $\sim 5.5$  Å. The GABA and glycine receptor anion channels have estimated pore diameters of 5.6 and 5.2 Å, respectively (Bormann et al., 1987). The minimum pore diameter estimate of the voltage-dependent,  $\sim 40$  pS  $\text{Cl}^-$  channel in T84 epithelial cell is  $\sim 5.5$  Å (Halm & Frizzell, 1992), and of a voltage-dependent,  $\sim 30$  pS  $\text{Cl}^-$  channel in rat hippocampal neurons,  $\sim 5.5$  Å (minimum cross section  $5.5 \times 6.5$  Å; Franciolini & Nonner, 1987). For the volume-regulated  $\text{Cl}^-$  channels of rat parotid acinar cells, it is 5.8-6.4 Å (Arreola, Melvin & Begenisich, 1995).

#### **D. Single Channel $\text{Cl}^-$ Conductance and Permeability Coefficient**

The single channel conductance of the cardiac CFTR  $\text{Cl}^-$  channel, measured with voltage ramps in channels exposed to symmetric 125 mM  $\text{Cl}^-$  and locked in the open state by AMP-PNP, is  $10.3 \pm 0.4$  pS ( $n = 5$ ) at 22 °C. This is close to the limiting slope conductance at positive potentials measured at 36 °C by Ehara and Ishihara (1990) in cell-attached patches on guinea-pig ventricular myocytes (13 pS), and to the slope conductance in excised inside-out patches in roughly symmetric 150 mM  $\text{Cl}^-$  determined at 22 °C using voltage steps (12 pS; Nagel et al., 1992). It also is similar to the



single channel conductance of native epithelial CFTR in T84 cells (9 pS; Tabcharani et al., 1990), and of epithelial CFTR expressed in a range of cell types, and to the limiting slope conductance of epithelial CFTR reconstituted in lipid bilayers (11 pS; Bear et al., 1992).

A fit to the Goldman equation of the current-voltage relation obtained with channels locked open with AMP-PNP both at 160 mM  $\text{Cl}^-_o$ /6.4 mM  $\text{Cl}^-_i$ , and with symmetric 160 mM  $\text{Cl}^-$ , yielded a single-channel permeability coefficient for the CFTR channel to  $\text{Cl}^-$  ions of  $2 \times 10^{-17} \pm 9 \times 10^{-19} \text{ cm}^3 \text{ s}^{-1}$  ( $n = 3$ ). The relatively good fit of the data under the two conditions (see Fig. 13B) suggests that the Goldman model, although simple, can account for the behavior of  $\text{Cl}^-$  ions in the CFTR channel. In particular, it suggests that saturation of the pore is not important at these concentrations, and that there are no ion-ion interactions. At roughly physiological  $\text{Cl}^-$  concentrations ( $\sim 150 \text{ mM } \text{Cl}^-_o$ /24 mM  $\text{Cl}^-_i$ ), the magnitude of the current through a single open CFTR channel, at 0 mV, say, during the prolonged plateau phase of the cardiac ventricular action potential, is  $\sim 0.4 \text{ pA}$ . This corresponds to the passing of  $\sim 2.5$  million  $\text{Cl}^-$  ions per second.





## **Chapter 5**

### **ROLE OF THE NUCLEOTIDE BINDING DOMAINS IN CFTR CHANNEL REGULATION**

#### **I. Introduction**

This series of experiments was conducted to examine the role of nucleoside triphosphate in the opening and closing of CFTR Cl<sup>-</sup> channels. In particular, does channel opening require ATP hydrolysis or simply ATP binding? Does ATP hydrolysis govern channel closure? Can we infer which of CFTR's two nucleotide binding folds is involved in each of those functions? Finally, how does the level of channel phosphorylation control the access to each binding fold? Portions of this work have appeared in abstract form (Dousmanis & Gadsby, 1996).

#### **II. Results**

##### **A. [ATP] Dependence of Channel $P_o$**

Once CFTR Cl<sup>-</sup> channels have been phosphorylated on the R domain, by PKA, they require nucleoside triphosphate to open and close, presumably acting at one or both of the nucleotide binding domains (NBDs). To begin to characterize the means by which the NBDs control channel opening and closing, the [ATP] dependence of the open probability of individual PKA-phosphorylated CFTR Cl<sup>-</sup> channels was examined in inside-out patches excised from guinea-pig ventricular myocytes. Usually, a strong pipette-to-bath Cl<sup>-</sup> gradient was employed, such that channel opening was detected as an outward current jump. Thus, while typically holding the membrane



potential between  $\pm 10$  mV, with high  $\text{Cl}^-$  ( $\sim 160$  mM) at the extracellular surface (in the pipette), and low  $\text{Cl}^-$  ( $\sim 5$  mM) at the cytoplasmic surface (in the bath), the resulting large electrochemical gradient drives net  $\text{Cl}^-$  flux from the extracellular to the intracellular side through the open channels, and channel openings generated outward current steps of 0.3-0.4 pA. Rapid solution changes (within  $\sim 1$  s) at the intracellular side of the patch were made, by switching the continuously flowing solution, allowing rapid modulation of R domain and NBD function.

To determine the [ATP] dependence of channel open probability ( $P_o$ ), at a fixed free  $[\text{Mg}^{2+}]$  of 1.2 mM, channels were first phosphorylated by bath application of  $\sim 100$  nM PKA catalytic subunit (plus 1-2 mM ATP), and patches were then exposed to 2 mM ATP without PKA, then to concentrations of ATP ranging from 1  $\mu\text{M}$  to 2 mM, and then re-exposed to the standard ATP concentration, 2 mM. Patches were exposed to each [ATP] for  $\geq 1$  min, to ensure that a representative sample of channel behavior was recorded. Bracketing the test [ATP] with standard 2 mM ATP applications helped minimize errors resulting from systematic changes in channel  $P_o$  (e.g., due to changes in phosphorylation status) over the course of an experiment (see Fig. 31, and below). To inhibit channel depohosphorylation by any membrane-bound phosphatase 2A, microcystin (0.4-0.5  $\mu\text{M}$ ) was added to all bath solutions in these, and all, excised-patch experiments (see Methods and Chapter 5, Discussion). Relative  $P_o$  was calculated as the ratio of the  $P_o$  in the test [ATP] to the average of the  $P_o$  levels during the two bracketing applications of 2 mM ATP. Figure 19 shows representative recordings from four different patches, and illustrates channel behavior over a range of ATP concentrations. In each case, PKA had been applied prior to, but within 10 min of, the intervals

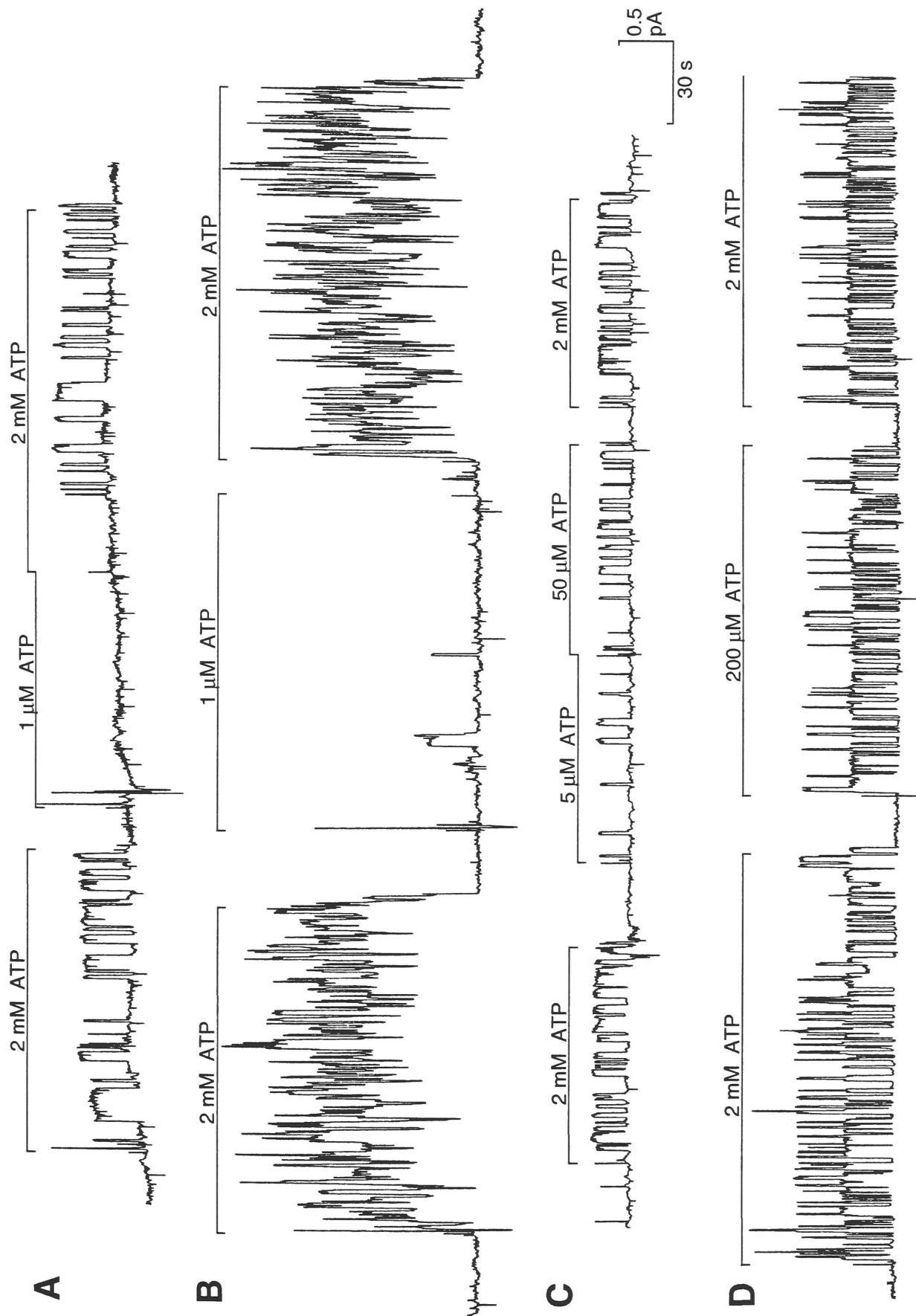


shown. And, most importantly, all four recordings confirm that all CFTR channels were closed within seconds of withdrawal of ATP.

Figure 19A shows a current trace from a patch with a single evident channel. An ~1.5 min exposure to 1  $\mu$ M ATP (*center*) failed to elicit any channel openings, yet during both 2 mM ATP bracketing applications, the channel opened and closed frequently. This yielded a relative  $P_o$  value of  $P_o(1 \mu\text{M ATP})/P_o(2 \text{ mM ATP}) = 0/0.5 = 0$ . To enhance the likelihood of observing rare channel openings at very low [ATP]s, and hence to reliably measure channel  $P_o$  when the frequency of channel opening was low, attempts were made to obtain patches containing several channels. Figure 19B shows membrane currents from a patch containing 4 or 5 channels, in which channel  $P_o$  at 1  $\mu$ M ATP was again tested. During the ~2 min exposure to 1  $\mu$ M ATP, only two channel openings were observed, and the relative  $P_o$  was calculated to be 0.02. In the single-channel patch shown in panel C, channel  $P_o$  at both 5  $\mu$ M and 50  $\mu$ M ATP was measured; relative  $P_o$  was 0.27 at 5  $\mu$ M ATP, and 0.54 at 50  $\mu$ M ATP. Figure 19D shows a test of channel  $P_o$  at 200  $\mu$ M ATP in a patch with three evident channels, and it illustrates that at 200  $\mu$ M ATP, channel  $P_o$  is close to maximal (relative  $P_o = 0.86$ ).

Figure 20 summarizes the experiments on the [ATP] dependence of channel open probability, comprising 5-20 individual measurements at each [ATP]. For each measurement, the  $P_o$  at a given [ATP] was normalized to the average  $P_o$  of the two 2 mM ATP exposures.  $P_o/P_o(2 \text{ mM ATP})$  was plotted as a function of [ATP], and a fit of the Hill equation was performed:

**Fig. 19. [ATP] dependence of relative channel open probability. A-D.** Chart records of unitary channel currents from four different patches. Upward step current deflections reflect net outward current due to efflux of Cl<sup>-</sup> ions from pipette through individual open channels. Application of ~100 nM PKA, to enhance channel phosphorylation, occurred prior to time intervals depicted. Upper bars mark the time period of bath application of ATP at the indicated concentration. Free [Mg<sup>2+</sup>] is fixed at 1.2 mM. Membrane holding potential ( $V_h$ ) = +10 mV in experiments depicted in panels A, B, and D, -10 mV for experiment depicted in panel C. **A.** Membrane currents from a patch containing a single CFTR Cl<sup>-</sup> channel. Channel fails to open during ~1.5 min exposure to 1  $\mu$ M ATP, yet opens frequently when bath contains 2 mM ATP. Relative  $P_o = P_o(1\mu\text{M ATP})/P_o(2\text{ mM ATP})=0/0.5=0.00$  (E1/I1,2,7). **B.** Currents from a patch containing 4-5 channels. 1  $\mu$ M ATP elicits only 2 channel openings over ~2 min. Relative  $P_o(1\text{ }\mu\text{M ATP}) = 0.02$  (E1/I1,2,7). **C.** Membrane currents from a patch containing a single channel. Relative  $P_o(5\text{ }\mu\text{M ATP}) = 0.27$ . Relative  $P_o(50\text{ }\mu\text{M ATP}) = 0.54$  (E1/I1,3,4,7). **D.** Channel  $P_o$  in 200  $\mu$ M ATP is almost equal to  $P_o$  in 2 mM ATP; relative  $P_o(200\text{ }\mu\text{M ATP}) = 0.86$  (E1/I1,5,7).







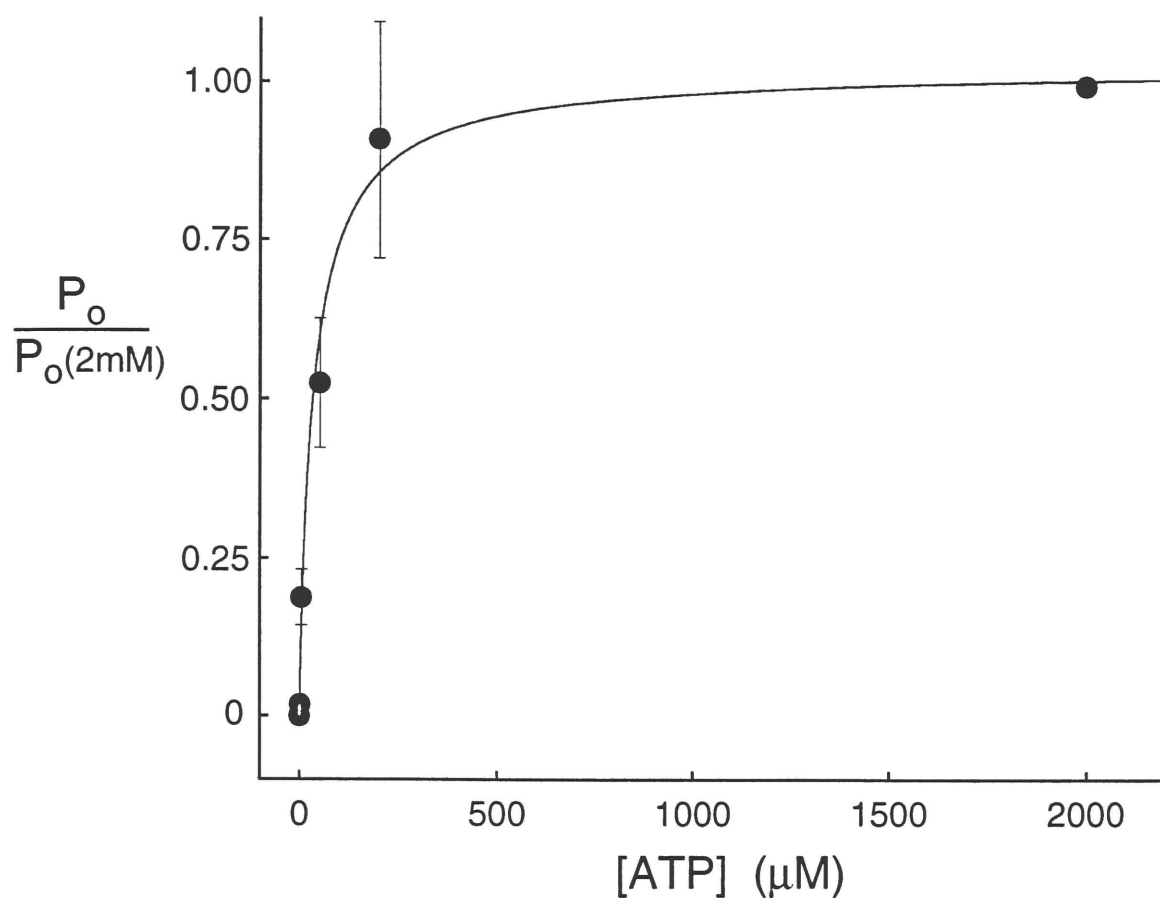


**Fig. 20. Summary of [ATP] dependence of relative channel open probability.** Summary of data depicting relative  $P_o$  in 0, 1, 5, 50, and 200  $\mu M$  ATP, normalized to the average  $P_o$  of the 2 mM ATP bracket intervals. The smooth curve represents the least squares fit of the data to equation 11, where  $n = 0.9 \pm 0.2$ ,  $K_{0.5} = 35 \pm 11 \mu M$ , and  $P_{o\max} = 1.04 \pm 0.06$ .



$$\frac{P_o}{P_o(2\text{mM})} = \frac{P_o(\text{max})}{1 + \left( \frac{K_{0.5}}{[\text{ATP}]} \right)^n} \quad (\text{eqn. 11})$$

The fit shows that channel open probability increased approximately hyperbolically with [ATP], with a half maximal [ATP] ( $K_{0.5}$ ) of  $35 \pm 11 \mu\text{M}$ ;  $P_{o\text{max}} = 1.04 \pm 0.06$ ,  $n = 0.9 \pm 0.2$ . In 15 of the 20 patches in this series of experiments, an absolute  $P_o$  could be determined, since these patches contained either a single channel ( $n = 11$ ), or 2-3 channels ( $n = 4$ ). From these experiments, the absolute  $P_o$  in 2 mM ATP, within 10 min of phosphorylation by PKA, averaged  $0.41 \pm 0.04$  ( $n = 15$ ).

To determine whether the increase in  $P_o$  as [ATP] was raised was due to an increase in channel open time, a decrease in channel closed time, or to a combination of the two factors, mean channel open times and mean channel closed times were measured, for [ATP] levels ranging from 1  $\mu\text{M}$  to 2 mM. Figure 21A summarizes mean channel open time measurements from 22 patches; each point represents the mean channel open time at a given [ATP], after channel phosphorylation by bath application of ~100 nM PKA catalytic subunit which was then withdrawn, during a single experiment. 17 patches contained only a single evident CFTR channel. Data from 5 patches were included in which 2 or 3 channels were observed, but only to obtain mean open time measurements in 1 or 5  $\mu\text{M}$  ATP when two channels were never open at the same time. The filled circle ( $\bullet$ ) represents the mean channel open time at 2 mM ATP in these experiments, which was  $1.55 \pm 0.24$  s ( $n = 22$ ). Figure 21B illustrates mean channel closed times from the 17 single-channel patches, each point representing the mean closed time at a given [ATP] in one patch. The hollow circle ( $\circ$ ) represents the mean channel closed time in 2 mM ATP



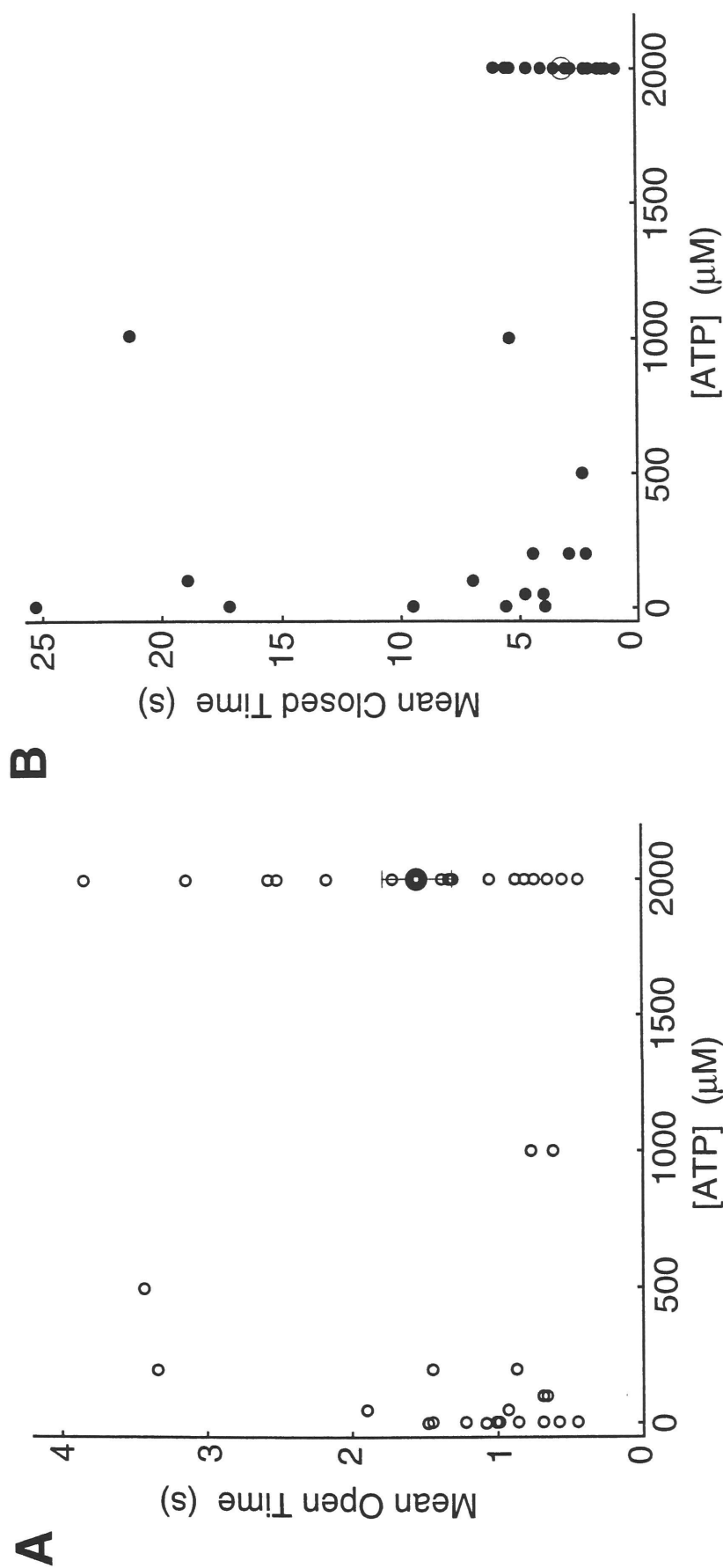


**Fig. 21. Increase in  $P_o$  as  $[\text{ATP}]$  is raised reflects a decrease in channel closed time. A.** Summary of mean open times from 22 membrane patches, which contained either a single channel (17), or contained 2 or 3 channels (5); open times from the latter were used only for low  $[\text{ATP}]$ 's (1 or 5  $\mu\text{M}$ ), and only if there were no overlaps in channel openings. Mean channel open time is largely unaffected by  $[\text{ATP}]$  and, at 2 mM  $\text{ATP} = 1.55 \pm 0.24$  s ( $\bullet$ ;  $n=17$ ). **B.** Summary of mean closed times from 17 patches, all of which contained a single evident  $\text{Cl}^-$  channel. Mean channel closed time decreases as  $[\text{ATP}]$  is increased and, in 2 mM  $\text{ATP} = 3.10 \pm 0.40$  s ( $\circ$ ).



( $3.10 \pm 0.40$  s;  $n = 17$ ). There was substantial patch-to-patch variation in both the mean open and mean closed times at maximally effective, 2 mM ATP, presumably reflecting differences in the level of channel phosphorylation (see, e.g., Figs. 19, 24, 31). To minimize the influence of this variability, the mean open time of a given channel at low  $P_o$ , i.e., at low [ATP]s between 1  $\mu$ M and 50  $\mu$ M, was compared to the mean open time at high  $P_o$ , i.e., at 2 mM ATP. Similar ratios were calculated for the mean channel closed time for each channel. The average ratio of mean open times at low  $P_o$  to mean open times at high  $P_o$  was  $0.94 \pm 0.08$  ( $n = 12$ ), indicating that channel open time remains approximately constant over a range of [ATP] from 1  $\mu$ M to 2 mM. For the mean closed times, however, the corresponding ratio averaged  $6.45 \pm 2.03$  ( $n = 7$ ). We conclude that the increase in channel  $P_o$ , as [ATP] is raised, largely reflects a decrease in closed times or, in other words, an increase in channel opening rate, while the channel open times, reflecting the channel closing rate, remain largely unaffected.

## **B. [Mg<sup>2+</sup>] Dependence of Channel Opening Rate**

If energy liberated by the hydrolysis of ATP is required to open PKA-phosphorylated CFTR Cl<sup>-</sup> channels, then, like all other ATPases, which require Mg<sup>2+</sup> ions to catalyze the hydrolysis of ATP, opening of CFTR channels by ATP should be absolutely dependent on the presence of Mg<sup>2+</sup>. Indeed, channel openings were abolished by complete removal of Mg<sup>2+</sup> ions from the solution bathing the cytoplasmic face of the membrane, using the divalent cation chelator CDTA (2 mM; trans-1,2-diaminocyclohexane-N,N,N',N'- tetraacetic acid), which binds Mg<sup>2+</sup> almost 3 orders of





magnitude more tightly than EDTA does. Figure 22 shows the current trace from one such experiment. PKA was applied to phosphorylate channels, and then removed 10 min before the start of the record, in which 50  $\mu\text{M}$ , 200  $\mu\text{M}$ , or 2 mM ATP, in the presence of high, 1.2 mM free  $\text{Mg}^{2+}$ , elicited normal channel openings and closings. However, after chelation of all bath  $\text{Mg}^{2+}$ , application of even 2 mM ATP for  $\sim 2$  min failed to elicit a single channel opening. Similar results were observed in all six patches so tested. Thus, in the total absence of  $\text{Mg}^{2+}$  ions, channel openings are completely abolished despite the presence of a supramaximal concentration of ATP.

If free  $\text{Mg}^{2+}$  ions catalyze the hydrolysis of ATP, and if nucleotide hydrolysis energizes the conformational change required to open the channel (and to close it; see below), then at a free  $[\text{Mg}^{2+}]$  sufficiently low to slow the rate of ATP hydrolysis, channel opening (and channel closing) ought to be slowed. Figure 23 shows that, when free  $[\text{Mg}^{2+}]$  is lowered to  $\leq 5$   $\mu\text{M}$ , using 10 mM EGTA as the divalent chelator, channels do indeed open and close at a lower than normal rate. In this patch, application of  $\sim 100$  nM PKA, in the presence of 2 mM ATP activated 8 channels, at least 5 of which remained active upon withdrawal of PKA. At high, 1.2 mM free  $\text{Mg}^{2+}$ , all 5 channels closed promptly, and reopened promptly (within  $\sim 10$  s), on withdrawal and reapplication of ATP. But, on suddenly lowering the free  $[\text{Mg}^{2+}]$  to  $\leq 5$   $\mu\text{M}$ , in the presence of 2 mM ATP, channels became stabilized in the open conformation, and after washout of ATP, channel closing was markedly delayed, the last channel closing  $\geq 1$  min later. Furthermore, with the free  $[\text{Mg}^{2+}]$  still at  $\leq 5$   $\mu\text{M}$ , readdition of 2 mM ATP resulted in channel openings which were both markedly delayed and prolonged. The three channels which opened when ATP was withdrawn



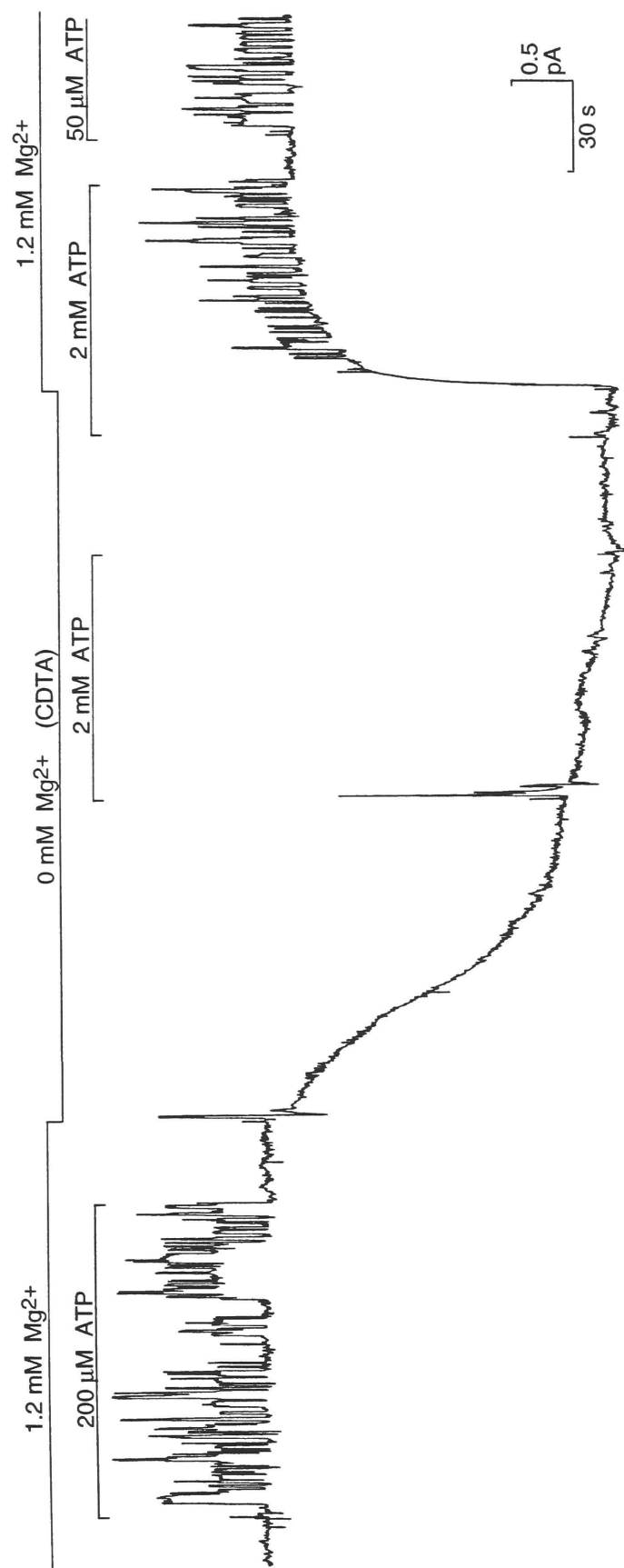


**Fig. 22. Complete removal of bath Mg<sup>2+</sup> prevents channel opening.** Membrane current in a patch containing three channels. 100 nM PKA was applied for 1 min, ~10 min before ATP application at left. The free [Mg<sup>2+</sup>] was set at either 0 or 1.2 mM with 2 mM CDTA (trans-1,2-diaminocyclohexane-N,N',N'-tetraacetic acid). Upper bars mark free [Mg<sup>2+</sup>] and periods of ATP application.  $V = +10$  mV. In 1.2 mM Mg<sup>2+</sup>, channels open and close normally in only 50  $\mu$ M ATP, yet, in the absence of Mg<sup>2+</sup>, even 2 mM ATP applied for ~2 min fails to elicit a single channel opening. During the second exposure to 2 mM ATP, no channel opening occurred until Mg<sup>2+</sup> ions were reintroduced, as signalled by the current drift reflecting restoration of the original seal resistance (57 G $\Omega$ ) (E1/11,4,5,7,8,9).



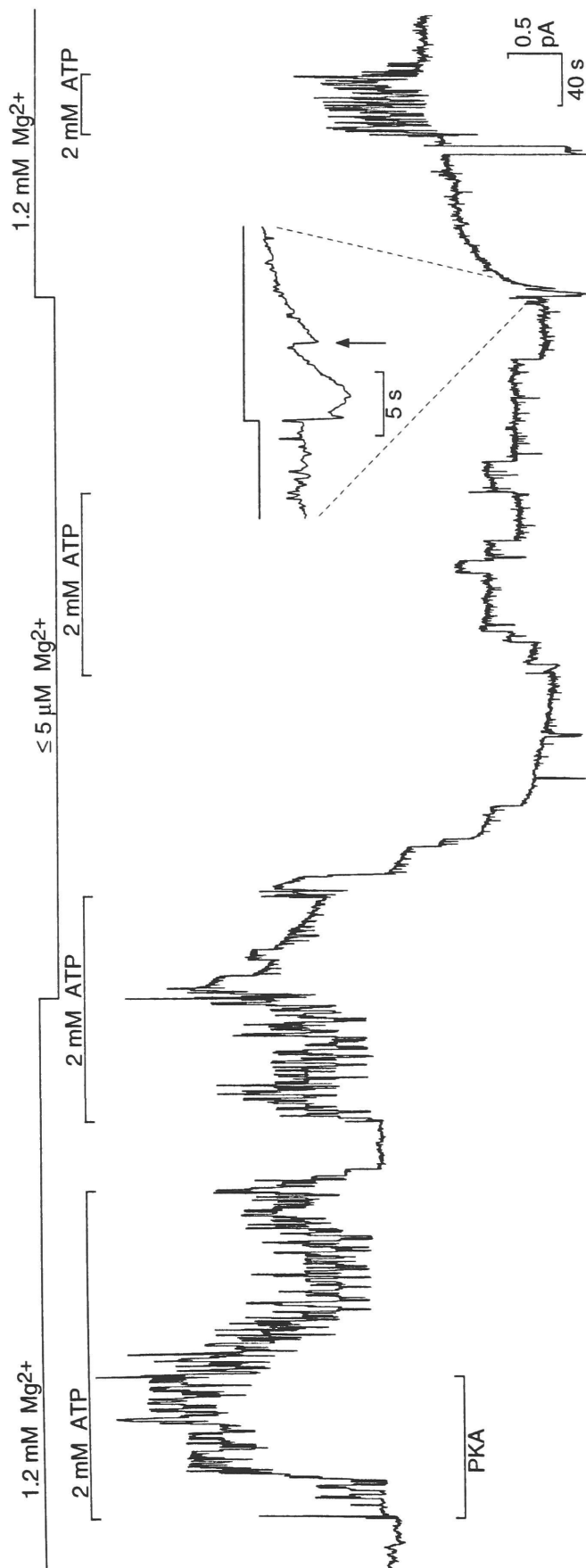


**Fig. 23. Channel opening and closing rates both depend on  $[Mg^{2+}]$ .** Current from a patch containing eight channels. Upper bars show free  $[Mg^{2+}]$  and periods of 2 mM ATP application.  $V_h = -10$  mV. In 1.2 mM  $Mg^{2+}$ , withdrawal of ATP closes channels, and reapplication of ATP opens channels, within  $\sim 10$  s, yet, after lowering  $[Mg^{2+}]$  to  $\leq 5$   $\mu$ M (middle), channel closing and opening, upon withdrawal and reapplication of ATP, respectively, are markedly delayed. When ATP is withdrawn, in low  $[Mg^{2+}]$ , two channels close very slowly, after 25 and 100 s, and third remains open until  $[Mg^{2+}]$  is raised to 1.2 mM, at which time it promptly closes (*inset, arrow*).  $R_s$ , measured at the outset (not shown) and 1.5 min before the end of the experiment, was  $\sim 20$  G $\Omega$  (E1/I10,11,12,13).



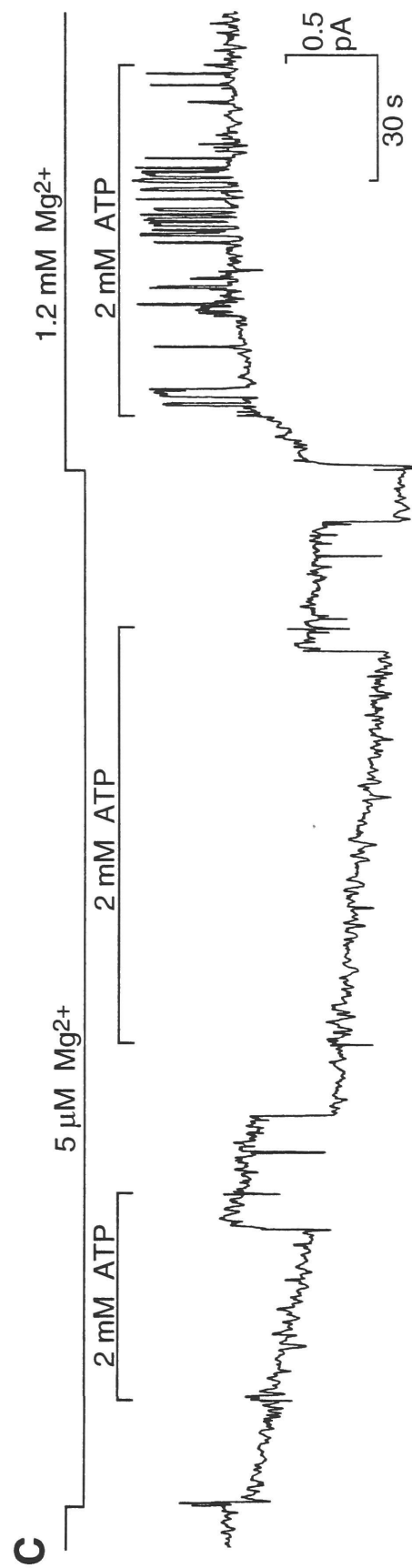
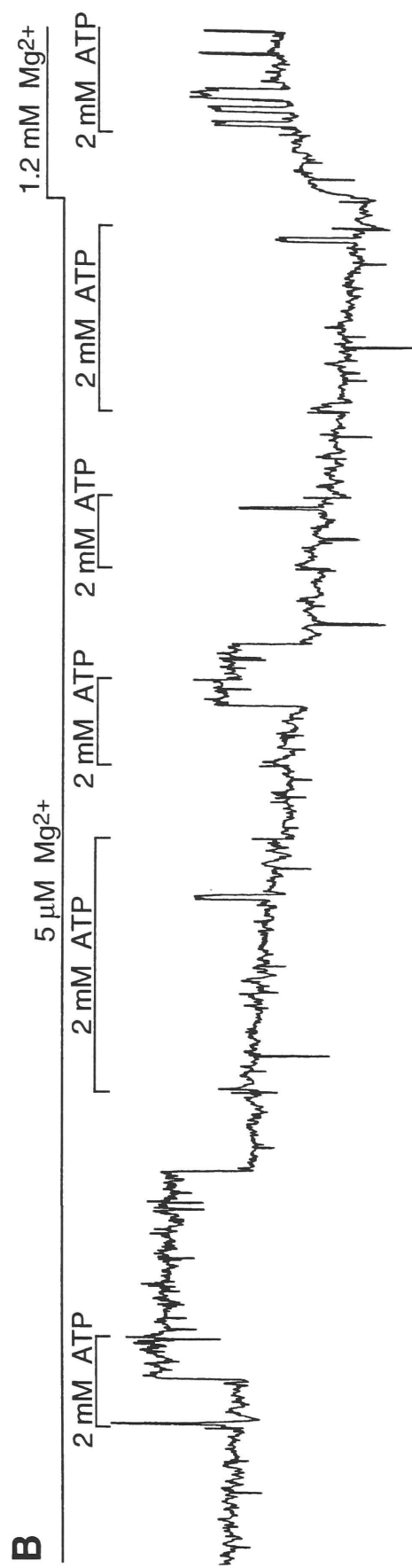
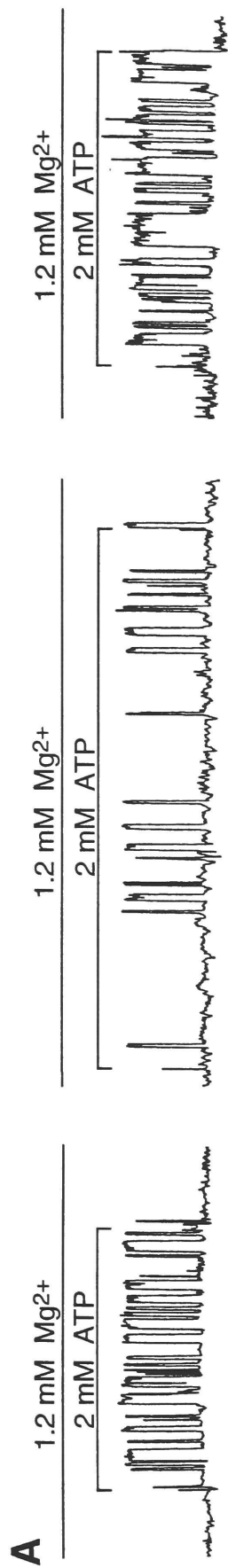
all closed very slowly; one closed ~25 s after ATP withdrawal, one after ~100 s, and one remained open for ~150 s, but closed promptly when free  $[Mg^{2+}]$  was raised to 1.2 mM (*inset, arrow*). And at 1.2 mM free  $[Mg^{2+}]$  at least three channels opened within seconds of adding 2 mM ATP and closed normally after its withdrawal. These results suggest that ATP hydrolysis, catalyzed by  $Mg^{2+}$ , limits the rate of both channel opening and channel closing.

To quantify the effect of  $[Mg^{2+}]$  on the channel opening rate, patches were obtained in which a single CFTR  $Cl^-$  channel was activated by PKA catalytic subunit. Then, starting with the channel closed, in the absence of ATP, we measured the time to the first opening of the channel, after suddenly applying 2 mM ATP. Measurements were made both in high, 1.2 mM free  $Mg^{2+}$ , and in low, 5  $\mu M$  free  $Mg^{2+}$ , using 2 mM CDTA in these, and all subsequent experiments to buffer free  $[Mg^{2+}]$ . Figure 24A shows channel openings in three individual single-channel patches in response to sudden exposures to 2 mM ATP at 1.2 mM free  $Mg^{2+}$ . In each case, the first channel opening occurred within 5 s. With free  $[Mg^{2+}]$  buffered at 5  $\mu M$ , however, the time to first channel opening upon sudden addition of 2 mM ATP was markedly increased (Fig. 24 B,C). The latency ranged from 12 s to 45 s in the five separate ATP additions in the experiment depicted in panel B, and even longer, ~60 s and ~90 s in the two tests on another patch, depicted in panel C. And yet, in both experiments, the channels opened promptly (within 2.5 s) when free  $[Mg^{2+}]$  was raised to 1.2 mM (Fig. 24B, C).

Figure 25B summarizes 103 such measurements from 42 patches in 1.2 mM  $Mg^{2+}$  ( $\bullet$ ), and 23 from 9 patches in 5  $\mu M$   $Mg^{2+}$  ( $\blacktriangle$ ). Each point represents an individual measurement of the time to first channel opening.

**Fig. 24. Latency to first channel opening depends on  $[Mg^{2+}]$ .** **A.** Chart records of membrane currents from three single-channel patches, each showing a brief ( $\leq 5$  sec) delay to first channel opening following addition of 2 mM ATP to the solution bathing the cytosolic face of the patch. **B-C.** With free  $[Mg^{2+}]$  fixed at 5  $\mu$ M, the latency to first channel opening upon addition of 2 mM ATP is markedly increased.  $V_h = +10$  mV (E1/11, 7, 14, 15).







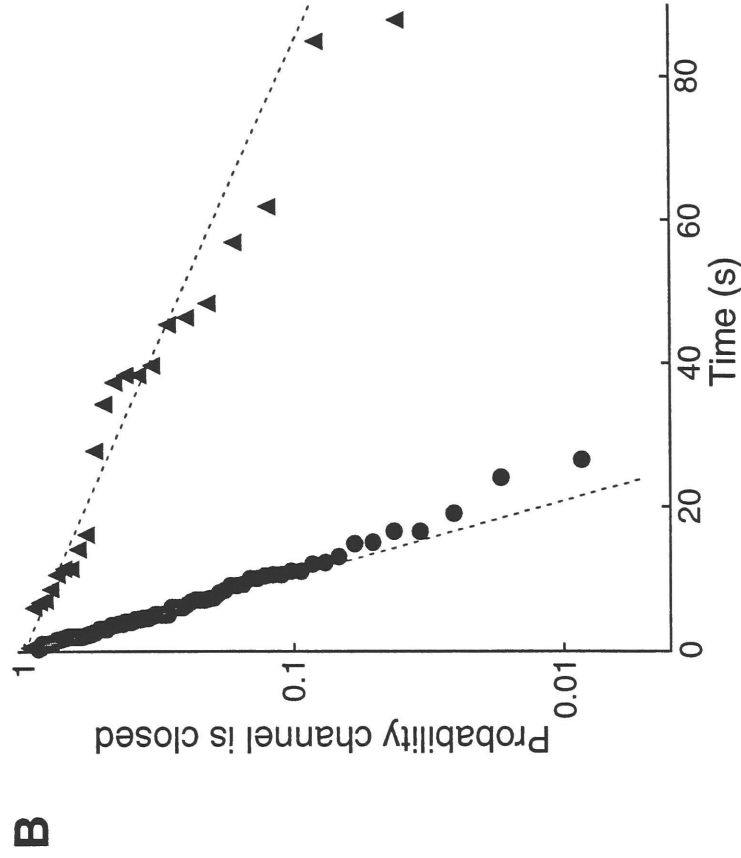
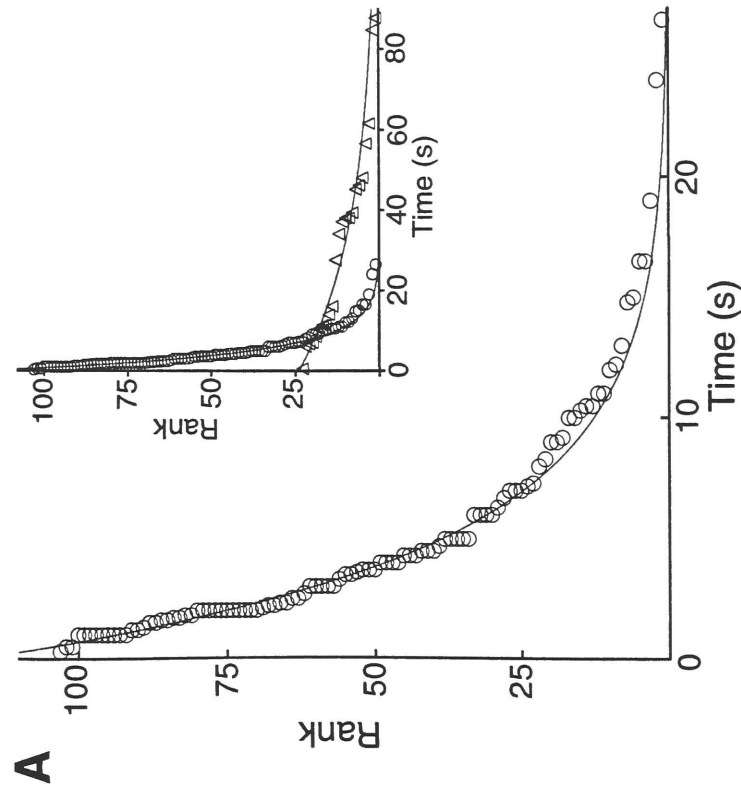


**Fig. 25. Summary of  $[Mg^{2+}]$  dependence of channel opening rate.** Summary of latencies to first channel opening from many single-channel patches, upon addition of 2 mM ATP, in either 5  $\mu M$   $Mg^{2+}$  or 1.2 mM  $Mg^{2+}$ . In 5  $\mu M$   $Mg^{2+}$ , 23 latencies were measured from 9 patches, and in 1.2 mM  $Mg^{2+}$ , 103 latencies were measured from 42 patches. **A.** Large plot shows latencies to first channel opening in 1.2 mM  $Mg^{2+}$  (○). Latencies were ranked in order of decreasing duration, plotted against rank number, and fitted to a single exponential by non-linear least squares (*smooth curve*). Latencies to first channel opening in 5  $\mu M$   $Mg^{2+}$  were similarly plotted and fit to a single exponential. **Inset** shows, on the same scale, latencies to first channel opening in 1.2 mM  $Mg^{2+}$  (○) and in 5  $\mu M$   $Mg^{2+}$  (Δ). The rank numbers were then normalized by the zero-time intercept to yield probability estimates, and the latencies were plotted against the log of these probabilities. The slopes (*dashed lines*) give the opening rates of channels in 1.2 mM  $Mg^{2+}$ ,  $0.22 \pm 0.003$  s $^{-1}$  (●), and in 5  $\mu M$   $Mg^{2+}$ ,  $0.03 \pm 0.003$  s $^{-1}$  (▲).



For each  $[Mg^{2+}]$ , these times were ranked in order of decreasing duration, plotted against rank number, and fitted to a single exponential by linear least squares (Fig. 25A). The rank numbers were then normalized by the zero-time intercept to yield probability estimates (see Methods), and the latencies were plotted against the log of these probabilities (Fig. 23B). The linear least squares fits give estimates for the channel opening rates:  $0.22 \pm 0.003 \text{ s}^{-1}$  at 1.2 mM free  $Mg^{2+}$ , and  $0.03 \pm 0.003 \text{ s}^{-1}$  at 5  $\mu\text{M}$  free  $Mg^{2+}$ . Thus, channel opening rate at 2 mM ATP is increased ~7-fold as free  $[Mg^{2+}]$  is raised from 5  $\mu\text{M}$  to 1.2 mM.

### C. $[Mg^{2+}]$ Dependence of Channel Closing Rate

As already observed (e.g., Figs. 23, 24BC), although channel opening rate is slowed when free  $[Mg^{2+}]$  is lowered to the low micromolar range, once opened, channels typically remain open for tens of seconds, even after all ATP has been rapidly withdrawn from the bath: but those open channels close promptly upon raising free  $Mg^{2+}$  to 1.2 mM (Fig. 23 *inset*). By analogy with the action of the non-hydrolyzable analog AMP-PNP to markedly stabilize channel openings in the presence of ATP, these findings suggest that, as in the case of GTP-binding proteins, binding of nucleotide stabilizes the active conformation of the protein (in this instance, stabilizing the channel in the open conformation), and subsequent nucleotide hydrolysis switches the protein from the active to the inactive conformation (closing the channel).

To test this, we availed ourselves of the ability to stabilize the channel in the open conformation by application of 2 mM ATP in low, 5  $\mu\text{M}$  free  $Mg^{2+}$  solutions. Once channels were stabilized in the open conformation,



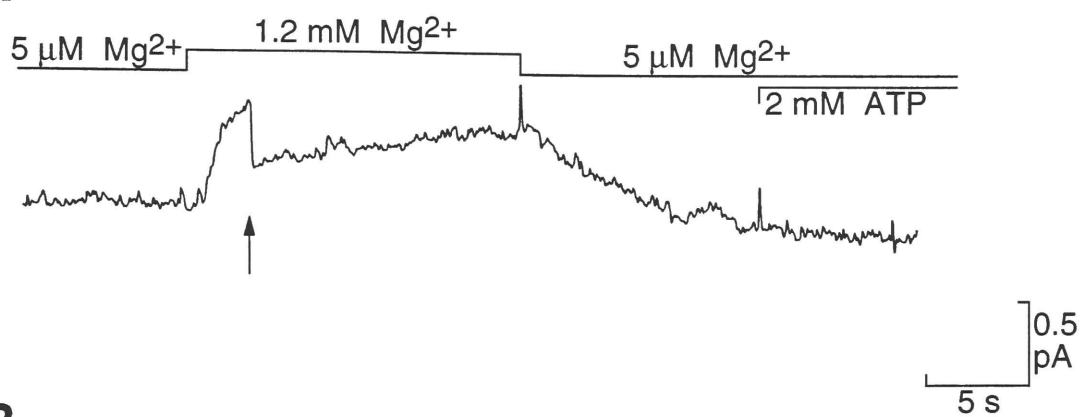
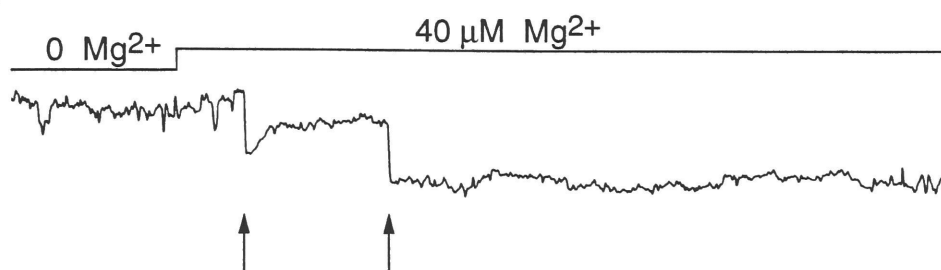
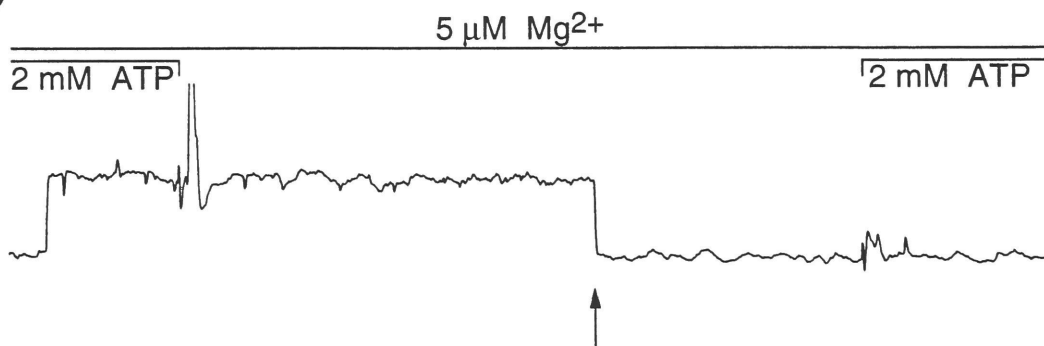
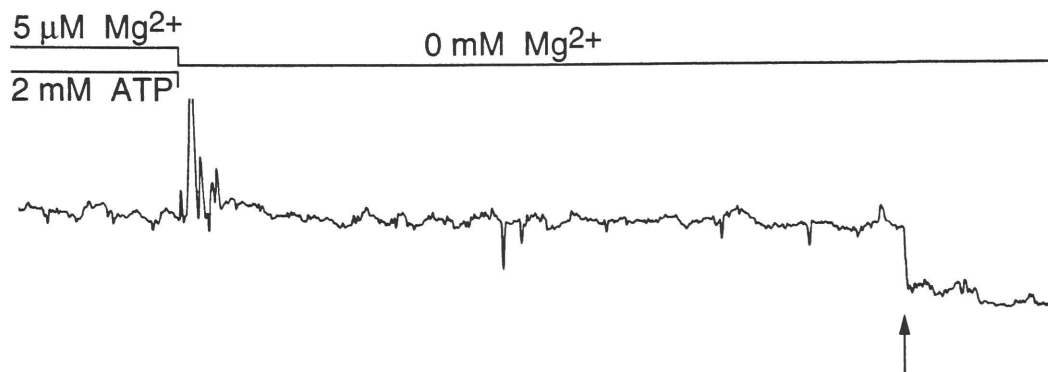
all nucleotide was removed from the bath, and then we readdded  $\text{Mg}^{2+}$  (at concentrations up to 1.2 mM) and measured the times to channel closure following the step change of free  $[\text{Mg}^{2+}]$ . Times to closure were measured from the time of nucleotide removal (for 0  $\mu\text{M}$  and 5  $\mu\text{M}$   $\text{Mg}^{2+}$ ), or from the time  $[\text{Mg}^{2+}]$  was raised from 0 or 5  $\mu\text{M}$  to the test  $\text{Mg}^{2+}$  concentration.

Figure 26 shows examples of this protocol from four separate patches. Panel A shows a current trace from a patch with at least three channels, which was stabilized in the open conformation in 2 mM ATP/5  $\mu\text{M}$   $\text{Mg}^{2+}$ . One of these channels remained open for over two minutes after withdrawal of all nucleotide from the bath, but closed rapidly (in 3 s) upon the sudden increase of  $[\text{Mg}^{2+}]$  to 1.2 mM. Panel B shows currents from another patch with three evident channels. Two channels remained open for at least 20 s following nucleotide removal, but closed soon (one in 3.5 s and the other, 10 s) after free  $[\text{Mg}^{2+}]$  was raised to 40  $\mu\text{M}$ . Panel C shows a current trace from a single-channel patch. Upon withdrawal of ATP, in 5  $\mu\text{M}$   $\text{Mg}^{2+}$ , the channel remained open for 20 s, until it finally closed. Panel D shows the current trace from a single-channel patch in which the channel closure, following withdrawal of all nucleotide and  $\text{Mg}^{2+}$ , was markedly prolonged, taking a further 35 s.

The times to closure, measured as described, at  $[\text{Mg}^{2+}]$  levels from 0 to 1.2 mM, are compiled in Figure 27A. Each point represents an individual time to closure of a channel at the given  $[\text{Mg}^{2+}]$ . For each  $[\text{Mg}^{2+}]$ , the times to closure were ranked in order of decreasing duration and fitted to a single exponential and the ranks were then normalized by the zero-time intercept to yield probability estimates, which were then plotted against time to closing in a semi-log plot, as in Figure 25. Channel closing rates determined from the slopes are:  $0.29 \pm 0.01 \text{ s}^{-1}$  in 1.2 mM  $\text{Mg}^{2+}$  ( $\blacktriangle$ ),  $0.21 \pm$

**Fig. 26. Channel closing depends on  $[Mg^{2+}]$ .** **A.** Current trace from a patch in which a channel was stabilized in the open conformation using 2 mM ATP/5  $\mu$ M  $Mg^{2+}$ ; the channel remained open for over 2 min after withdrawal of nucleotide, yet it closed promptly upon sudden increase in  $[Mg^{2+}]$  to 1.2 mM. Arrows mark channel closures. **B.** Current trace from another patch showing two channels remaining stabilized in the open conformation after nucleotide and  $Mg^{2+}$  removal, and closing upon raising free  $[Mg^{2+}]$  to 40  $\mu$ M. **C.** Current trace from a single-channel patch showing channel opened in 2 mM ATP/5  $\mu$ M  $Mg^{2+}$  solution, and closing with long delay, in 5  $\mu$ M  $Mg^{2+}$ , after withdrawal of nucleotide. **D.** Current trace from another single-channel patch showing extremely prolonged delay to channel closure when all  $Mg^{2+}$  was removed from the cytosolic bathing solution.



**A****B****C****D**



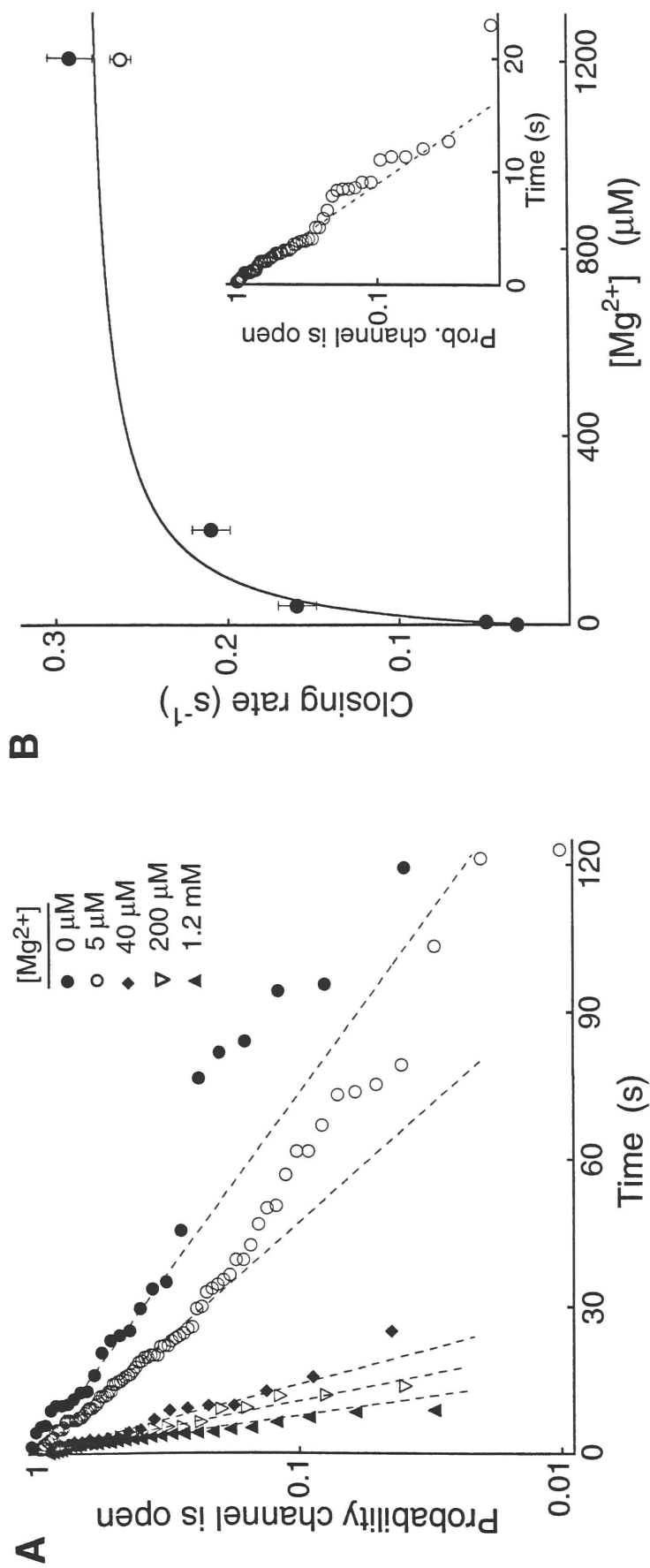


**Fig. 27. [Mg<sup>2+</sup>] dependence of channel closing rate.** **A.** Semi-log plot of times to channel closure, measured from time of nucleotide removal (for 0 and 5  $\mu$ M Mg<sup>2+</sup>), or from time [Mg<sup>2+</sup>] was raised from 5  $\mu$ M to the test concentration (for 40  $\mu$ M, 200  $\mu$ M, and 2 mM Mg<sup>2+</sup>). Channel closing rates (slopes of dashed lines):  $0.29 \pm 0.01$  s<sup>-1</sup> in 1.2 mM Mg<sup>2+</sup> (▲),  $0.21 \pm 0.01$  s<sup>-1</sup> in 200  $\mu$ M Mg<sup>2+</sup> (▽),  $0.16 \pm 0.01$  s<sup>-1</sup> in 40  $\mu$ M Mg<sup>2+</sup> (◆),  $0.05 \pm 0.001$  s<sup>-1</sup> in 5  $\mu$ M Mg<sup>2+</sup> (○), and  $0.03 \pm 0.002$  s<sup>-1</sup> in 0  $\mu$ M Mg<sup>2+</sup> (●). **B.** Closing rates from A were plotted versus free [Mg<sup>2+</sup>], and fit to equation 12;  $K_1 = 0.03$  (closing rate in 0 Mg<sup>2+</sup>),  $K_{\max} = 0.26 \pm 0.02$  s<sup>-1</sup>,  $K_{0.5} = 51 \pm 17$   $\mu$ M. **Inset:** Semi-log plot of 60 times to closure upon ATP withdrawal in 1.2 mM Mg<sup>2+</sup>, from 33 patches, fit to a single exponential as described (closing rate  $0.26 \pm 0.01$ ); plotted as ○, in B, for comparison.



0.01 s<sup>-1</sup> in 200 μM Mg<sup>2+</sup> (▽), 0.16 ± 0.01 s<sup>-1</sup> in 40 μM Mg<sup>2+</sup> (◆), 0.05 ± 0.001 s<sup>-1</sup> in 5 μM Mg<sup>2+</sup> (○), and 0.03 ± 0.002 s<sup>-1</sup> in 0 μM Mg<sup>2+</sup> (●). As free [Mg<sup>2+</sup>] is raised from 0 to 1.2 mM, there is an ~10-fold increase in channel closing rate. Figure 27B plots the closing rates determined in panel A versus [Mg<sup>2+</sup>]. The smooth curve represents the least squares fit of the equation:

$$K_{\text{eff}} = K_1 + \frac{K_2}{\left(1 + \frac{K_{0.5}}{[\text{Mg}^{2+}]}\right)} \quad (\text{eqn. 12})$$

showing that the closing rate is reasonably well fit by simple Michaelis-Menton kinetics, where K<sub>2</sub> (maximum closing rate) = 0.26 ± 0.02 s<sup>-1</sup>, K<sub>0.5</sub> = 51 ± 17 μM, and K<sub>1</sub> = 0.03 s<sup>-1</sup> (the channel closing rate in 0 Mg<sup>2+</sup>; see Chapter 5, Discussion). For comparison, also plotted is the closing rate upon ATP withdrawal in 1.2 mM Mg<sup>2+</sup> (○), obtained by fitting 60 times to closure following sudden removal of ATP, from 33 patches, to a single exponential (closing rate = 0.26 ± 0.01 s<sup>-1</sup>).

The interpretation of these results follows from the finding that AMP-PNP, in the presence of 1.2 mM free Mg<sup>2+</sup>, stabilizes the channel open state for several min, which suggests that hydrolysis of ATP is normally required for channel closing. The acceleration of channel closing caused by raising the free [Mg<sup>2+</sup>] can then be understood in terms of an increase in ATP hydrolysis rate as the free [Mg<sup>2+</sup>] is raised (Fig. 27B). Since channel closure was prompted by adding Mg<sup>2+</sup> ions alone, in the absence of ATP, and because channels cannot be opened without ATP, it appears that a second ATP molecule can remain tightly bound to an open CFTR channel, stabilizing the open conformation of the channel in the absence of Mg<sup>2+</sup> ions. The closing rate of a given channel upon readdition of Mg<sup>2+</sup> is then presumably governed by the probability that a Mg<sup>2+</sup> ion will bind and

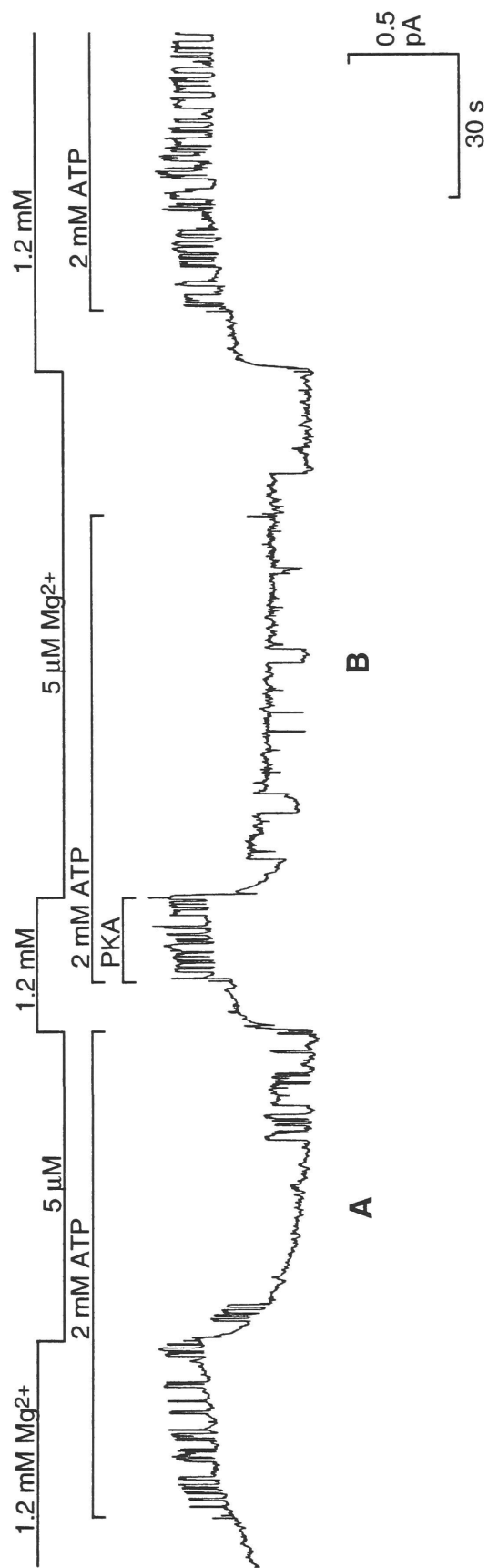
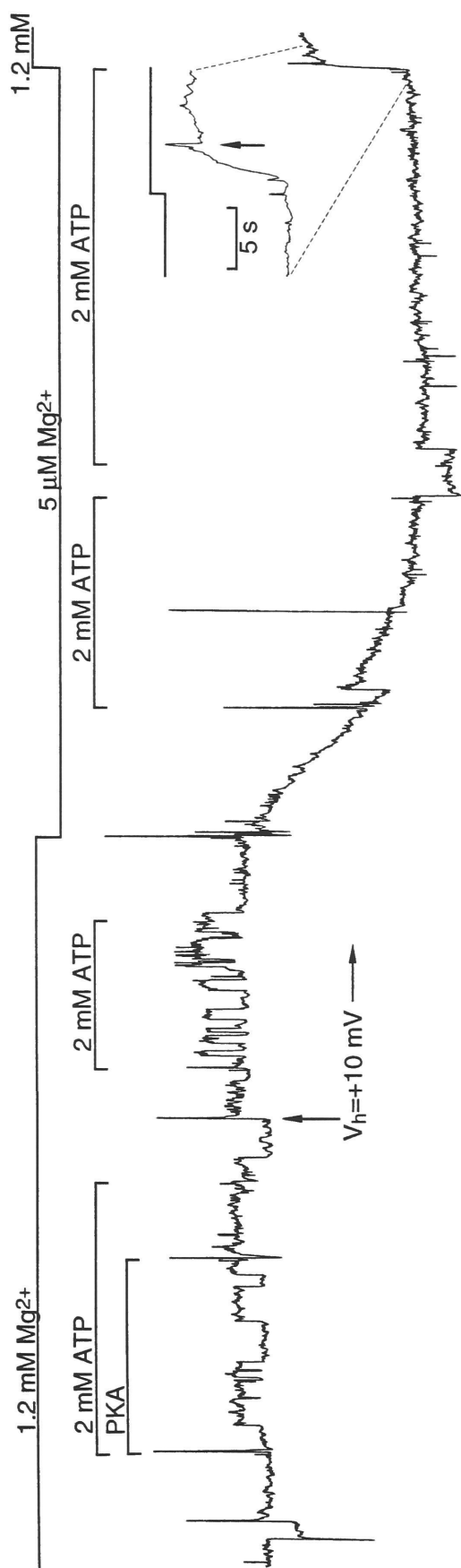


catalyze hydrolysis of that tightly bound ATP, whereupon the channel closes. This marked stabilization of the channel open state by tight binding of a nucleotide unable to undergo hydrolysis is thus closely analogous to the locking open by AMP-PNP of channels opened by ATP.

Intriguingly, the degree of channel phosphorylation by PKA appears to regulate the ability of lowered  $[Mg^{2+}]$  to slow channel closing in the presence of 2 mM [ATP]. Figure 28 shows the continuous current trace from an experiment in which application of ~100 nM PKA and 2 mM ATP revealed a single channel, which, upon subsequent reapplication of 2 mM ATP alone, opened and closed normally at high, 1.2 mM  $Mg^{2+}$ . But after free  $[Mg^{2+}]$  was lowered to 5  $\mu$ M, application of 2 mM ATP reopened the channel, which then stayed open for ~40 s. Reapplication of 2 mM ATP again opened the channel, which remained open for ~80 s, closing only after  $[Mg^{2+}]$  was raised to 1.2 mM (*inset, arrow*). With  $[Mg^{2+}]$  raised to 1.2 mM, the channel opened and closed normally, and yet, upon once again lowering  $[Mg^{2+}]$  to 5  $\mu$ M in the presence of ATP, the channel was not stabilized in the open conformation; in fact, it opened and closed 15 times, without once exhibiting a markedly prolonged opening (Fig. 28, section A; mean open time in the stretch =  $1.7 \pm 0.5$  s). However, a brief (~15 s) exposure to PKA restored the ability of low  $[Mg^{2+}]$  to greatly stabilize the open conformation: lowering free  $[Mg^{2+}]$  to 5  $\mu$ M in the presence ATP resulted in prolonged openings (Fig. 28, section B; mean open time =  $20.8 \pm 5.0$  s; 5 of 7 open times > 15 s in duration). Mean channel open time, in high, 1.2 mM  $Mg^{2+}$ , for the whole experiment, was  $1.4 \pm 0.1$  s ( $n = 152$ ). In all four patches in which the closing rate of at least one channel seemed unaffected by lowering  $[Mg^{2+}]$  to 5  $\mu$ M, temporary reapplication of PKA (to

**Fig. 28. Ability of low  $[Mg^{2+}]$  to slow channel closing depends on degree of channel phosphorylation.** Continuous chart record of membrane current from a patch containing a single evident channel.  $V_h$  switched from -10 mV to +10 mV at vertical arrow. Application of ~100 nM PKA and 2 mM ATP in high, 1.2 mM  $Mg^{2+}$  reveals a single channel, which, upon subsequent reapplication of 2 mM ATP alone, opened and closed normally. With  $[Mg^{2+}]$  lowered to 5  $\mu$ M, application of 2 mM ATP resulted in two channel openings whose closings were markedly delayed, the second closure occurring only after raising  $[Mg^{2+}]$  to 1.2 mM (*inset*). With  $[Mg^{2+}]$  raised to 1.2 mM, the channel opened and closed normally, yet, upon once again lowering  $[Mg^{2+}]$  to 5  $\mu$ M and applying ATP, the channel was not stabilized in the open conformation; it opened and closed 15 times, without once exhibiting a prolonged opening (mean open time =  $1.7 \pm 0.5$  s). However, after a brief (~15 s) exposure to PKA, lowering  $[Mg^{2+}]$  to 5  $\mu$ M and applying ATP resulted in prolonged openings (mean open time =  $20.8 \pm 5.0$  s; 5 of 7 open times > 15 s in duration). Mean channel open time in 1.2 mM  $Mg^{2+}$  for the whole experiment, was  $1.4 \pm 0.1$  s (n=152).  $R_s = 67$  G $\Omega$  (E1/I1,7,14,15).







enhance channel phosphorylation) caused the open time of all channels to become prolonged when  $[Mg^{2+}]$  was again lowered to  $\mu M$  levels.

#### **D. AMP-PNP Can Substitute for ATP at Nucleotide Binding Domain 2**

AMP-PNP, a hydrolysis-resistant analog of ATP, can prolong the open times of highly phosphorylated CFTR  $Cl^-$  channels already opened by ATP (Hwang et al., 1994). Since channel opening is believed to depend on ATP hydrolysis at NBD1 (e.g., Gadsby & Nairn, 1994; Carson et al., 1995) and AMP-PNP fails to open phosphorylated CFTR channels, AMP-PNP presumably acts at NBD2. To further probe the nature of nucleotide action at the NBDs, the ability of AMP-PNP to bind in place of ATP at NBD2 and lock channels in the open state was studied in detail by measuring both the rate at which channels became locked open, and the rate at which AMP-PNP-locked channels became unlocked.

Figure 29 shows a continuous current recording from a patch containing three channels. PKA was applied briefly to phosphorylate the channels just before the start of the record. Channels opened and closed normally during exposure to 1 mM ATP, and initially during the exposure to a mixture of 0.5 mM ATP and 0.5 mM AMP-PNP. But after ~52 s of cumulative channel open time (~80 s of running time) in the presence of the ATP/AMP-PNP mixture the first channel became locked open (*arrow*). A second channel became locked after only a further 0.5 s of channel open time (*arrow*), and both channels remained open, despite the removal of all nucleotide from the bath. Eventually, 13 min after washing out the nucleotides, one of the two locked channels closed. This channel could then open and close normally in response to 1 mM ATP.



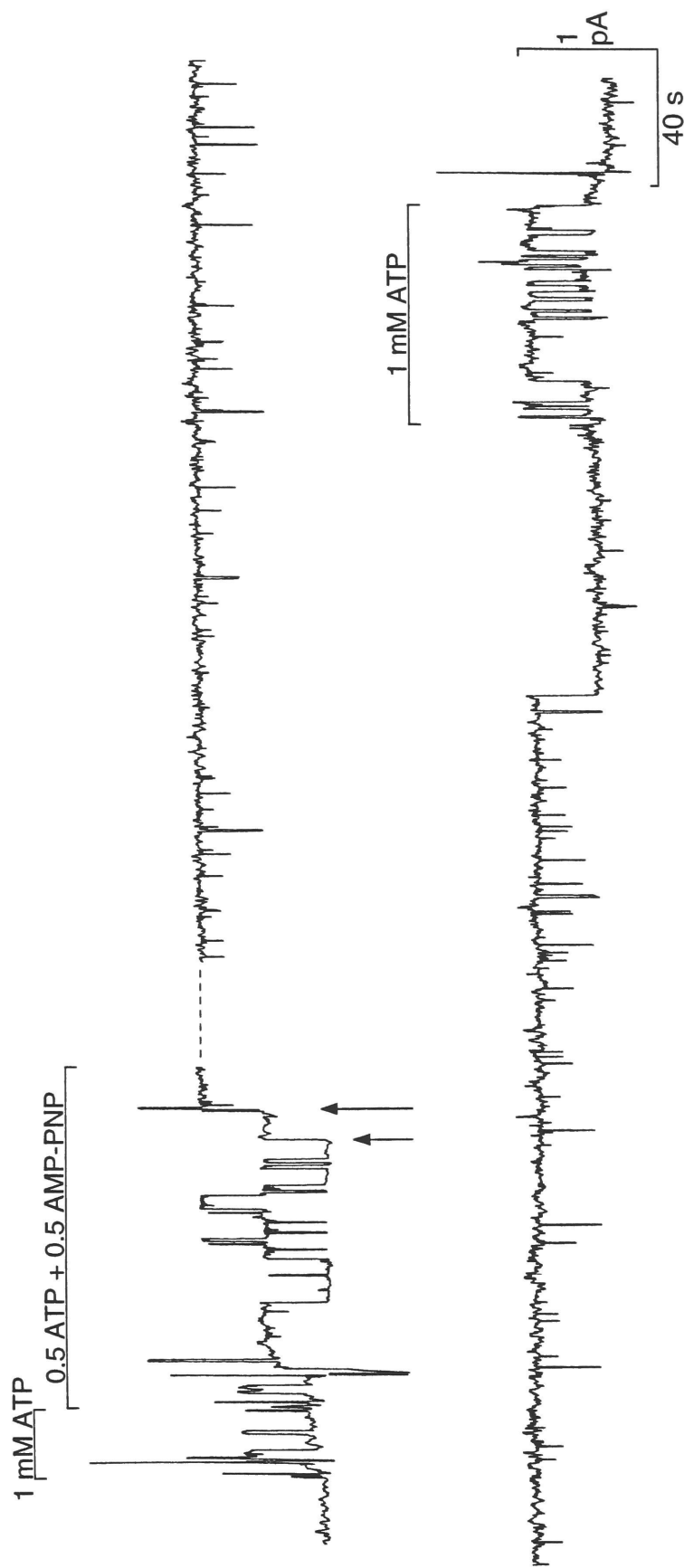


**Fig. 29. The ATP analog AMP-PNP can lock channels open.** Current trace from a patch containing two channels.  $V_h = +10$  mV. 125 nM PKA was applied for 40 s, just prior to start of record. Upper bars mark bath application of 1 mM ATP, or a mixture of 0.5 mM ATP and 0.5 mM AMP-PNP. Arrows mark channel locking events. Dashed line represents a 4.5 min break in the record, during which time two channels remained stably locked. 13 min after removal of all nucleotide from the bath solution, one of the two locked channels finally closed. Once closed, however, this channel could open and close normally in the presence of 1 mM ATP (E1/I6).



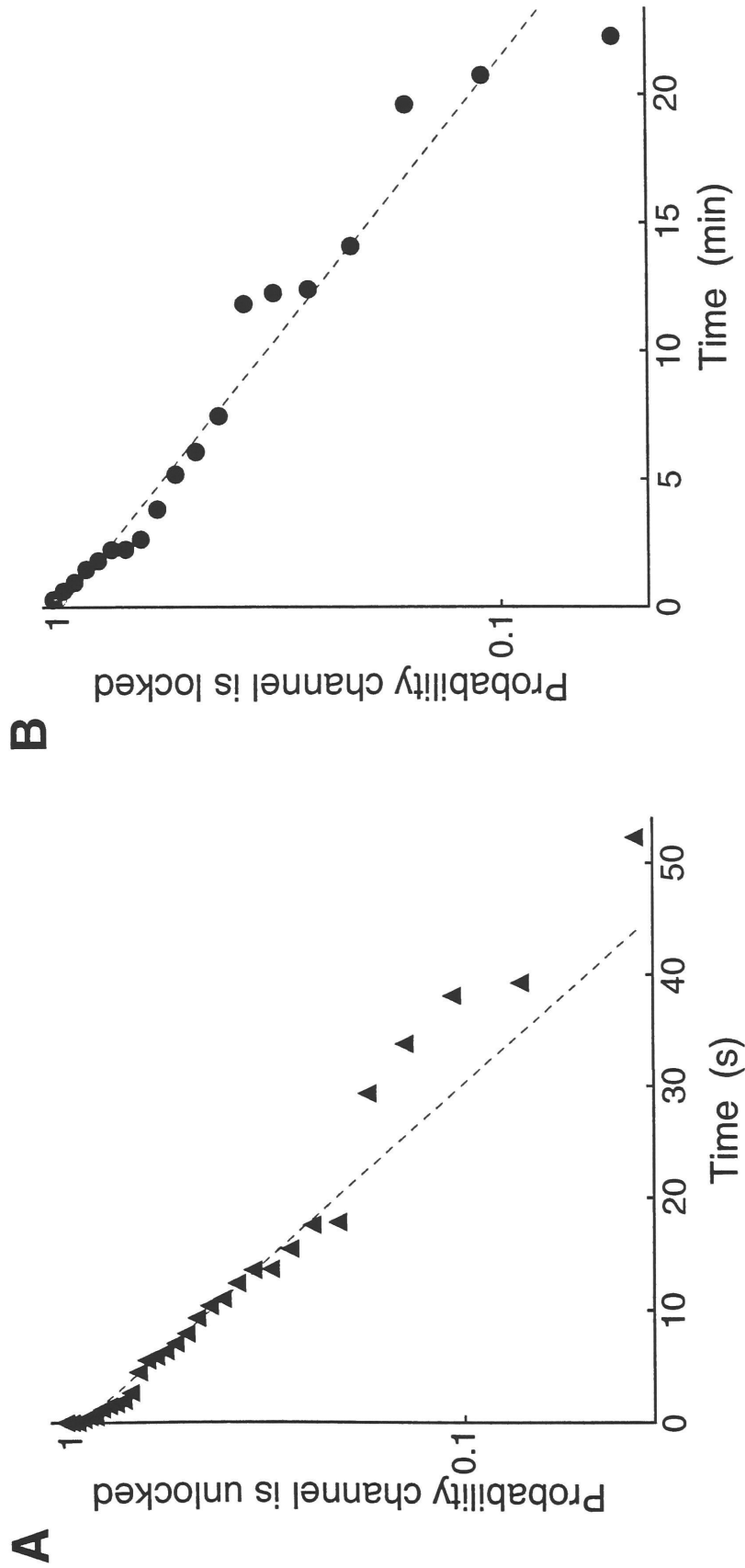


**Fig. 30. Channel locking and unlocking rates using the ATP analog AMP-PNP.** **A.** Summary of times to lock of 31 channels from 17 patches (▲), in the presence of 0.5 mM ATP plus 0.5 mM AMP-PNP. Times were measured as the cumulative open time before a channel locking event. Data were fitted to a single exponential and plotted against the log of the probability estimates, as before. Dashed line shows least squares exponential fit to the data. Channel locking rate was  $0.076 \pm 0.003 \text{ s}^{-1}$ . **B.** Summary of dwell times in the open state of 19 channels in 12 patches, stabilized by AMP-PNP (●). Times to closure were fitted to a single exponential and plotted against the log of the probability estimates, as before. Dashed line shows least squares exponential fit to the data. Channel unlocking rate was  $0.0018 \pm 0.0001 \text{ s}^{-1}$ .





Figure 30A summarizes 31 measurements (from 17 patches) of the time elapsed in the presence of 0.5 mM ATP and 0.5 mM AMP-PNP before a channel became locked open. Since AMP-PNP has no effect on closed channels, and acts only on channels that have already been opened by ATP, the relevant measure of time is time spent in the open state (cf. Baukrowitz et al., 1994). Accordingly, the times shown ( $\blacktriangle$ ) represent the cumulative open time from the first opening after adding AMP-PNP until the last channel closing, before the locking event occurred. Data were transformed to estimate probabilities that a channel was open, not locked, and plotted as in previous figures. The dashed line represents the least squares exponential fit to the data. These cumulative dwell times in the open state before locking are reasonably well fit by a single exponential, with a slope reflecting a locking rate of  $0.076 \pm 0.003 \text{ s}^{-1}$ .

Once locked in the open state by AMP-PNP, channels remain locked open for long periods. 19 measures of dwell times in the locked open state, from 12 patches, are plotted as before, and summarized in Figure 30B ( $\bullet$ ). The channel unlocking rate estimated from the exponential fit is  $0.0018 \pm 0.0001 \text{ s}^{-1}$ , implying a mean locked time of  $\sim 10 \text{ min}$ . This is likely to be a substantial underestimate of the true mean locked time, since, in the same 12 patches, 15 additional locking events induced by AMP-PNP were excluded from this analysis because the channels remained locked open when the experiment was terminated, usually because of seal breakdown.

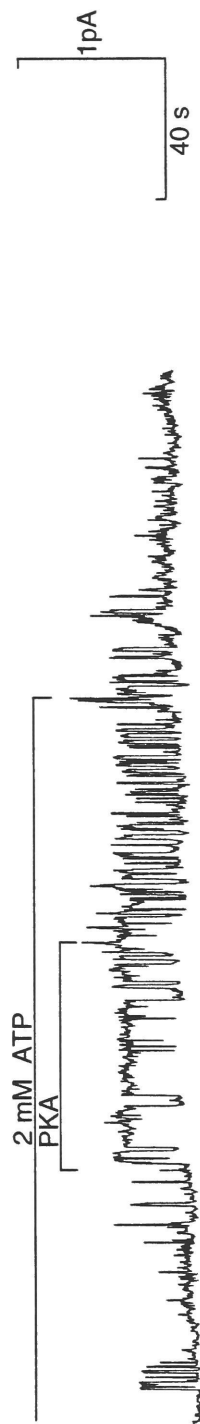
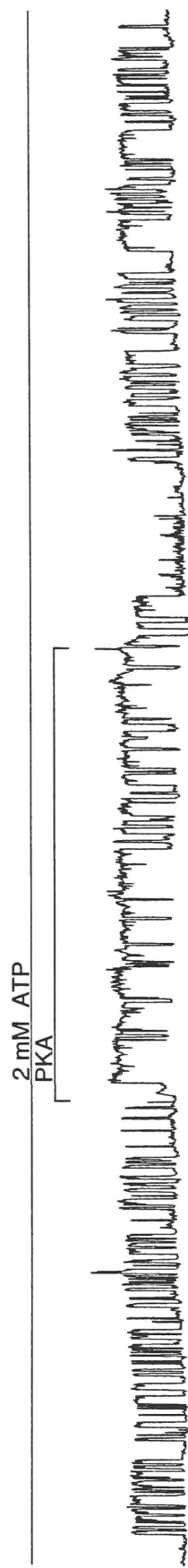
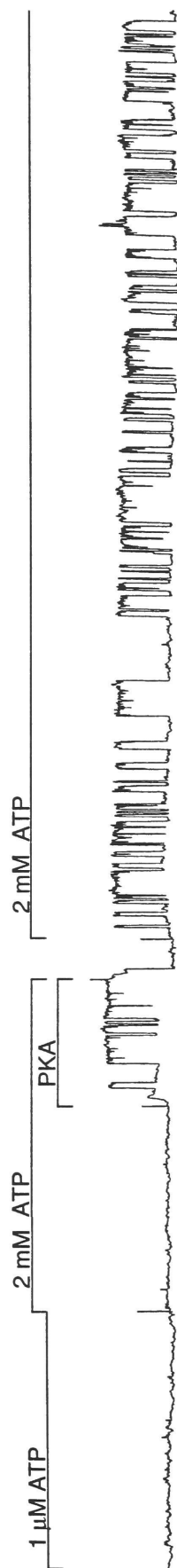
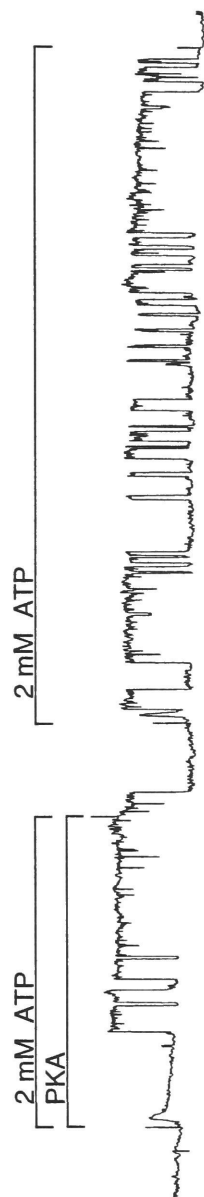


### **E. Phosphorylation Level of a Single Channel Molecule Governs Channel Open Time**

Figure 31 shows a continuous current trace from a patch containing a single CFTR Cl<sup>-</sup> channel, which was exposed to ~100 nM PKA, in the presence of 2 mM ATP on four separate occasions. During all four applications of PKA, channel activity was characterized by relatively prolonged open times (mean open time was  $5.1 \pm 0.8$  s). Upon withdrawal of PKA and reapplication of 2 mM ATP, the channel exhibited both brief and sustained channel openings in an apparently random manner. The failure to observe channel openings during application of 1  $\mu$ M ATP presumably reflects the low  $P_o$  (see Figs. 19, 20, above), but the subsequent failure of 2 mM ATP to elicit any channel openings possibly indicates that the channel had become dephosphorylated, since a second brief application of PKA resulted once again in prolonged channel openings, and channel activity in the presence of 2 mM ATP then continued for at least 8 min after removal of PKA. Channel behavior altered perceptibly, however, about 5 min after washing out PKA. Until then, the channel exhibited both brief and prolonged openings in the presence of 2 mM ATP, but thereafter, only brief openings were observed until the third PKA application again restored the mixture of brief and longer openings at 2 mM ATP.

Channel open probability ( $P_o$ ) in the presence of 2 mM ATP during all four PKA applications in the experiment averaged 0.72. Channel  $P_o$  during exposure to 2 mM ATP after washout of PKA averaged 0.49. However, channel  $P_o$  during 2 mM ATP applications after washing out PKA declined with time: within 5 min of PKA washout,  $P_o$  was 0.51, whereas > 5 min. after PKA withdrawal  $P_o$  averaged 0.39. The mean channel open time

**Fig. 31. Open time of a single channel molecule depends on degree of channel phosphorylation.** Continuous current trace from a patch containing a single channel.  $V_h = +10$  mV. Upper bars mark periods of bath application of 100 nM PKA and ATP at the concentrations indicated. During exposures to PKA, the channel consistently exhibited sustained open times. Within 5 min after PKA removal, the channel exhibited both sustained and brief openings; but > 5 min after PKA removal, the channel exhibited only brief openings.  $R_s = 40$  G $\Omega$  (E1/I1,2,7).





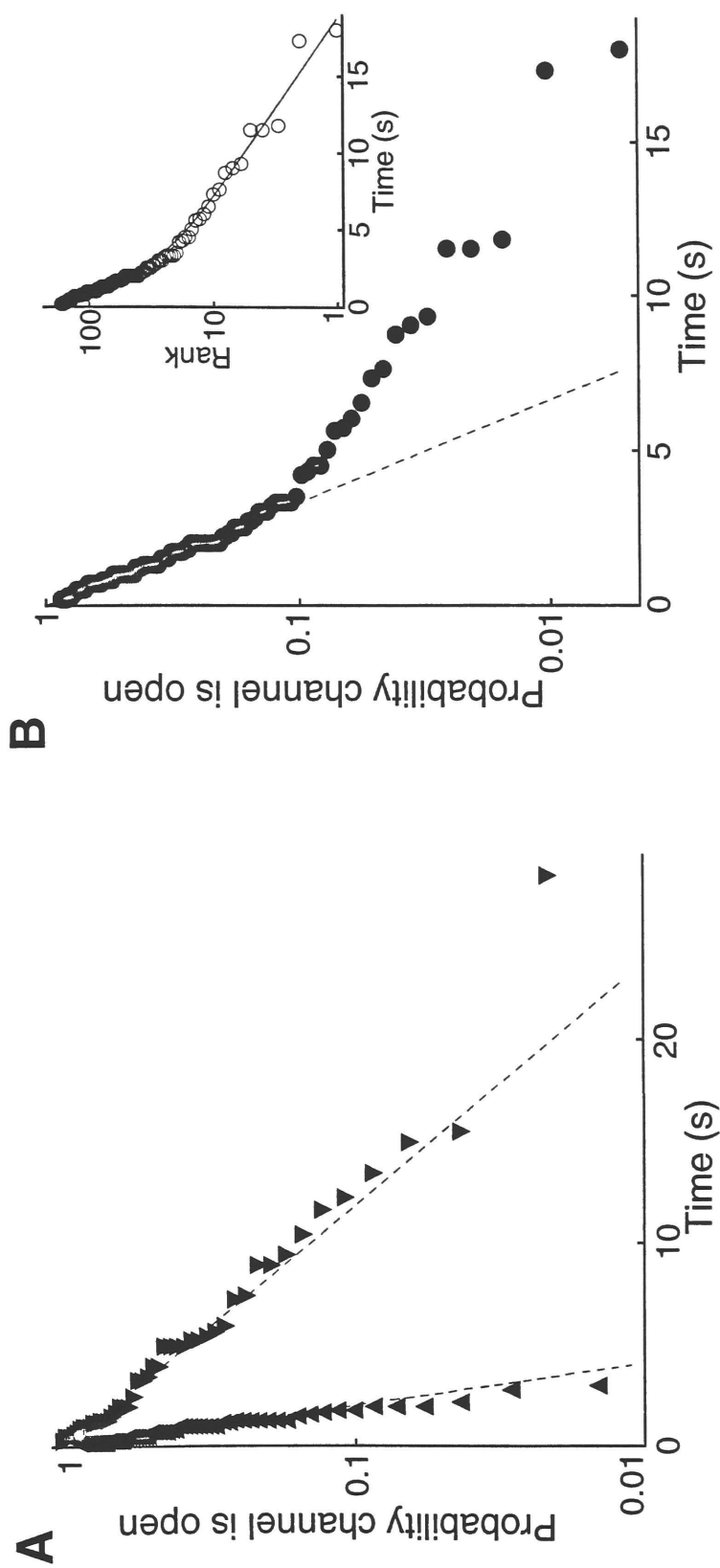


**Fig 32. Summary of phosphorylation dependence of open times of a single CFTR channel.** **A.** Plot of open times during PKA applications (▼), and > 5 min after PKA withdrawal (▲), for the experiment depicted in Figure 31. In each case, open times were ranked, fitted, and normalized to yield probability estimates which were then plotted against the open times as before. Dashed lines represent the best exponential fit to the data. Channel closing rate =  $0.19 \pm 0.01 \text{ s}^{-1}$  ( $n = 47$ ) during PKA applications (▼), and  $1.13 \pm 0.03 \text{ s}^{-1}$  ( $n = 62$ ) > 5 min after second PKA washout (▲). **B.** Channel open times within 5 min after PKA washout (●). With open times plotted and fit to a single exponential, as in A (*dashed line*), closing rate =  $0.70 \pm 0.01 \text{ s}^{-1}$  ( $n = 169$ ). ***Inset:*** Same data fit as described in text. Closing rates = 0.20 and  $0.97 \text{ s}^{-1}$ .





during all 2 mM ATP exposures in this experiment (excluding periods of PKA application) was  $1.75 \pm 0.21$  s.

Figure 32 summarizes the open times from the experiment depicted in Figure 31. Panel A plots the prolonged open dwell times during all PKA applications ( $\blacktriangledown$ ), and open times  $> 5$  min after PKA application ( $\blacktriangle$ ), as well as the predominantly brief open times observed  $> 5$  min after PKA washout. In each case, the dwell times were ranked, fitted to an exponential and the rank numbers normalized to yield probabilities, which were plotted semilogarithmically against the open times. Dashed lines show the least squares fits used to estimate the channel closing rates, which were  $0.19 \pm 0.01$  s<sup>-1</sup> ( $n = 47$ ) during PKA applications, but  $1.13 \pm 0.03$  s<sup>-1</sup> ( $n = 62$ )  $> 5$  min after PKA withdrawal. Figure 32B plots, in identical fashion, all channel open times at 2 mM ATP recorded within 5 min of washout of PKA ( $\bullet$ ). The dashed line represents the best fit of the data to a single exponential, which suggests a closing rate of  $0.70 \pm 0.01$  s<sup>-1</sup> ( $n = 169$ ). But, clearly, these open dwell times do not reflect a channel closing rate governed by a single kinetic process, but appear to reflect at least two processes. To address this, a single exponential was first fitted to dwell time  $\geq 3.5$  s, and then the entire data set was fitted to the sum of two exponentials, with the slow component fixed by the result of the first fit. The inset of Figure 32B shows this double exponential fit ( $\circ$ ) to the dwell times (here ranked, and simply plotted against rank) thus fit to two exponentials, which yielded the closing rates of  $0.97$  s<sup>-1</sup> for the faster component, and  $0.20$  s<sup>-1</sup> for the slower component, comparable to the rates obtained for the individual components in Fig. 32A.

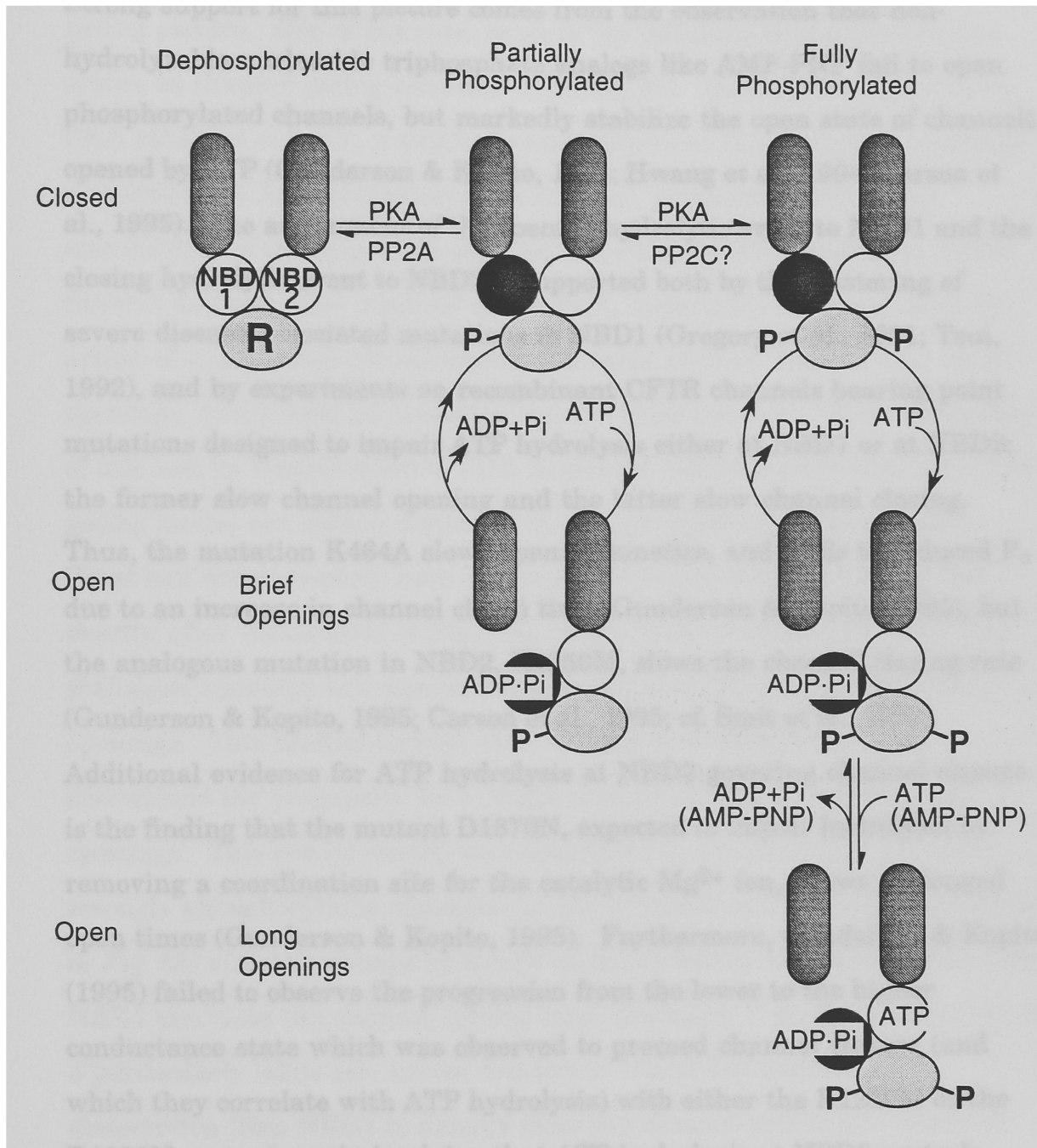


### **III. Discussion**

#### **A. Simplified Gating Scheme for CFTR Channels**

Figure 33 presents a cartoon that incorporates several essential features of the regulation of CFTR channel gating by PKA-mediated phosphorylation and ATP hydrolysis (Hwang et al., 1994). Despite its apparent complexity, this scheme is almost certainly a gross oversimplification, but it provides a convenient basis for discussion (for review, see Gadsby & Nairn, 1994). The major points, on which there is general agreement, are that all CFTR channels require phosphorylation before they can be opened, and that all openings depend on hydrolysis of ATP at NBD1. Partially phosphorylated channels are defined as those phosphorylated at R domain sites that must be dephosphorylated by phosphatase 2A, and phosphorylation of those sites is hypothesized to confer function only on NBD1: ATP hydrolysis at NBD1 permits opening of the channel which then closes after a brief interval upon dissociation of the hydrolysis products ADP plus  $P_i$ . Fully phosphorylated channels refer to channels additionally phosphorylated at sites that can be dephosphorylated by another phosphatase (possibly 2C), and phosphorylation of those additional sites is suggested to confer function also on NBD2, adding further complexity to channel gating. Thus, in a fully phosphorylated channel, ATP hydrolysis at NBD1 appears to both open the channel and permit binding of ATP at NBD2, whereupon the open conformation of the channel becomes stabilized (possibly by prevention of the dissociation of ADP from NBD1). That stabilization is manifest by prolonged channel openings, and is lost on hydrolysis of the ATP bound at NBD2.

**Fig. 33. Schematic model of the regulation of the two NBDs by incremental phosphorylation.** Upper row represents channels in closed conformations, middle row represents channels exhibiting brief openings, and lower row represents channels exhibiting longer openings. Vertical columns represent channel phosphorylation status. Partially phosphorylated channels allow hydrolyzable nucleoside triphosphate to interact only with NBD1; hydrolysis of the bound nucleotide leads to brief channel openings. Fully phosphorylated channels allow nucleotide to interact with both NBD1 and NBD2; hydrolysis at NBD1 leads to channel opening, bound nucleotide at NBD2 stabilizes the open state, and hydrolysis at NBD2 leads to channel closure.





In other words, in a fully phosphorylated channel, both channel opening and channel closing are believed to be governed by ATP hydrolysis. Strong support for this picture comes from the observation that non-hydrolyzable nucleoside triphosphate analogs like AMP-PNP fail to open phosphorylated channels, but markedly stabilize the open state of channels opened by ATP (Gunderson & Kopito, 1994; Hwang et al., 1994; Carson et al., 1995). The assignment of the opening hydrolytic event to NBD1 and the closing hydrolytic event to NBD2 is supported both by the clustering of severe disease-associated mutations in NBD1 (Gregory et al., 1991; Tsui, 1992), and by experiments on recombinant CFTR channels bearing point mutations designed to impair ATP hydrolysis either at NBD1 or at NBD2: the former slow channel opening and the latter slow channel closing. Thus, the mutation K464A slows opening kinetics, and leads to reduced  $P_o$  due to an increase in channel closed time (Gunderson & Kopito, 1995), but the analogous mutation in NBD2, K1250M, slows the channel closing rate (Gunderson & Kopito, 1995; Carson et al., 1995; cf. Smit et al., 1993). Additional evidence for ATP hydrolysis at NBD2 governing channel closure is the finding that the mutant D1370N, expected to impair hydrolysis by removing a coordination site for the catalytic  $Mg^{2+}$  ion, shows prolonged open times (Gunderson & Kopito, 1995). Furthermore, Gunderson & Kopito (1995) failed to observe the progression from the lower to the higher conductance state which was observed to precede channel closure (and which they correlate with ATP hydrolysis) with either the K1250M or the D1370N mutant, again implying that ATP hydrolysis at NBD2 controls channel closing.





## **B. Dependence of Channel Gating on Phosphorylation Status**

The experiments described here shed light on several aspects of this gating picture. One of the most basic is the influence of phosphorylation status on channel gating behavior (Figs. 30, 31). During the exposures to PKA catalytic subunit, a single channel displayed the prolonged openings expected for a fully phosphorylated channel, presumably reflecting stabilization of the open state after each opening by ATP binding at NBD2. Several minutes after washout of the PKA, apparently sufficient time for action of endogenous phosphatases, the same channel showed only brief openings, interpreted as reflecting loss of NBD2 function. The reversibility of this loss by reapplication of PKA confirmed that shifts between these two gating modes are indeed regulated by phosphorylation, as anticipated. What had not previously been envisaged, however, was the finding that shortly after withdrawal of PKA the single channel displayed occasional prolonged openings interspersed among the more frequent (~90%) brief openings. This finding implies that the degree of phosphorylation determines the propensity for a single channel to display brief or long openings. This can be readily accommodated in the scheme of Fig. 33 if strongly phosphorylated channels (in the presence of PKA, for the channel in Fig. 31) virtually always bind ATP at NBD2 before ADP dissociation from NBD1 can close the channel (giving long openings), if dephosphorylation of a particularly labile site spares function of NBD2 but permits ADP dissociation from NBD1 to usually close the channel before ATP binds at NBD2 (giving mostly brief, but some long, openings), and if further dephosphorylation abolishes function of NBD2 (permitting only brief openings; middle column, Fig. 33). The required amendment to the



scheme in Fig. 33, then, is that fully phosphorylated channels comprise (at least) two phosphoforms, raising the number of functionally distinct phosphoforms to three, corresponding to the three observed patterns of gating.

### **C. Influence of Free $[Mg^{2+}]$ on Channel Gating**

Straightforward consideration of the ATP hydrolytic events schematized in Fig. 33 suggests that a reduction of free  $[Mg^{2+}]$  sufficient to impair ATP hydrolysis at the two NBDs should slow both channel opening and channel closing. Data presented here (e.g., Figs. 23, 24, 28) indeed confirm that lowering the free  $[Mg^{2+}]$  to micromolar levels can prolong both channel closed times and channel open times. However, following the above discussion of gating patterns, although slowing ATP hydrolysis at low free  $[Mg^{2+}]$  must be expected to slow all channel openings, only the channel closings involving ATP hydrolysis at NBD2 (i.e., those preceded by longer open times) would be expected to be delayed. Fig. 24*B* shows precisely this kind of behavior, since at 5  $\mu M$  free  $[Mg^{2+}]$  only three of five open times are prolonged whereas all five openings are delayed. Moreover, in Fig. 28, the ability of lowered free  $[Mg^{2+}]$  to delay channel closing is more directly correlated with the phosphorylation status of the channel.

The marked slowing observed at micromolar free  $[Mg^{2+}]$  of channel opening following sudden application of a supramaximal concentration of ATP (2 mM) provides additional strong evidence that channel opening is rate-limited by hydrolysis of ATP at NBD1, rather than by ATP binding at NBD2, as has recently been suggested (Gunderson & Kopito, 1995). The observation that, at fixed 1.2 mM free  $Mg^{2+}$ , raising the  $[ATP]$  increases the channel opening rate (Fig. 20) further supports the conclusion that ATP



hydrolysis controls channel opening. These results also make it clear that it is the free  $[Mg^{2+}]$  (and hence the rate of ATP hydrolysis), rather than the concentration of a complex of  $Mg^{2+}$  and ATP, that governs channel opening, since, at 5  $\mu M$  free  $Mg^{2+}$  and 2 mM ATP, the measured channel opening rate is  $\sim 7$ -fold lower than that at 1.2 mM free  $Mg^{2+}$  (Fig. 25), yet the  $[Mg^{2+}ATP]$  is calculated under these conditions to be 113  $\mu M$ . However, Fig. 20 shows that the channel  $P_o$  (which predominantly reflects channel opening rate) is already  $\sim 75\%$  of maximal in the presence of 113  $\mu M$  ATP at 1.2 mM free  $Mg^{2+}$ . Thus, is the  $\sim 7$ -fold decrease in opening rate we see in the 5  $\mu M$   $Mg^{2+}$  solution were due to a decrease in the  $Mg^{2+}ATP$ , we would expect a  $\sim 7$ -fold decrease in  $P_o$ , which we do not.

#### **D. Stoichiometry of Coupling of ATP Hydrolysis to Channel Closing**

Perhaps the most striking findings of these experiments are that when both channel opening and closing are slowed by low micromolar free  $[Mg^{2+}]$ , channels can be readily trapped in the open state by sudden withdrawal of all nucleotides and all remaining  $Mg^{2+}$  ions. Those channels can subsequently remain open for a minute or two, but they can be closed by mere addition of  $Mg^{2+}$  ions, and they do so at a rate that varies in a saturable manner with increasing  $Mg^{2+}$  ion concentration (Figs. 26, 27). These results have a number of important implications. First, the titration of closing rate by free  $[Mg^{2+}]$  argues strongly that channel closing is governed by ATP hydrolysis. But, since all unbound nucleotides had been washed from the bath this means that, in turn, at least one ATP molecule must have remained tightly bound to the channel, stabilizing its open conformation. This marked stabilization of the channel open state by tight binding of a nucleotide unable to undergo hydrolysis resembles the locking



open by AMP-PNP of channels opened by ATP. We can infer that, like AMP-PNP, this tightly bound ATP molecule is bound at NBD2 and, since CFTR contains only two nucleotide binding sites and one ATP must have already been hydrolyzed to open the channel, we conclude that only a single ATP remains bound to each trapped-open channel. In that case, we can further conclude that hydrolysis of that one ATP is sufficient to close the channel. In other words the stoichiometry coupling ATP hydrolysis to channel closing is one ATP per closing.

#### **E. Resemblance of NBD Function to that of G Proteins**

The action of nucleotide binding at NBD2 to stabilize the channel open conformation until the nucleotide is hydrolyzed resembles the action of GTP binding to a G protein to stabilize its active conformation. This analogy extends to substantial sequence homology between CFTR's NBDs and the  $\alpha$  subunits of heterotrimeric G proteins, or small G proteins like p21 ras (Manavalan et al., 1995). High resolution X-ray crystallographic structures determined for these molecules reveal only a single catalytic  $Mg^{2+}$  ion binding site (e.g., Pai et al., 1990). The implication is that the closing of a trapped-open single CFTR channel upon readdition of  $Mg^{2+}$  requires simply the binding of a single  $Mg^{2+}$  ion to catalyze the hydrolysis of the single ATP molecule at NBD2. In this view, the delay in channel closing at low micromolar free  $[Mg^{2+}]$  is governed by the low probability of that  $Mg^{2+}$  ion locating, and binding at, the catalytic site.

The maximum rates for channel opening and channel closing at high free  $[Mg^{2+}]$  are both  $\sim 0.3\text{ s}^{-1}$ , presumably reflecting ATP hydrolysis rates at NBD1 and NBD2, respectively. These rates compare well with the GTPase





rates of G proteins (e.g., Gilman, 1987), but are low, e.g., for transport ATPases. If this interpretation is correct, our technique permits the microscopic measurement of characteristics of individual ATP hydrolysis cycles in a single molecule in its natural environment, in real time.

#### **F. High Affinity Binding of ATP at NBD2**

The long dwell time of trapped-open channels in the absence of nucleotides and  $\text{Mg}^{2+}$  ions implies an extremely high apparent affinity for ATP binding at NBD2, even in the absence of  $\text{Mg}^{2+}$ . This is remarkable, not least because  $\text{Mg}^{2+}$  ions contribute substantially to the binding energy of nucleotides in G proteins like p21 ras (e.g., John et al., 1993). However, the dissociation rate of AMP-PNP in the presence of  $\text{Mg}^{2+}$  is ~10 fold lower than that of ATP in the absence of  $\text{Mg}^{2+}$ . Since ATP dissociation cannot be measured if  $\text{Mg}^{2+}$  is added, because hydrolysis ensues, we attempted to learn whether withdrawal of  $\text{Mg}^{2+}$  would destabilize AMP-PNP binding ~10 fold, but saw no discernible effect in a few preliminary tests. A final possible explanation for the large difference in dissociation rates is that the closing rate of CFTR channels at 0 mM free  $\text{Mg}^{2+}$  reflects not dissociation of the bound ATP but some low rate of endogenous,  $\text{Mg}^{2+}$ -independent ATP hydrolysis. However, close inspection of the channel closing data at 5  $\mu\text{M}$  free  $\text{Mg}^{2+}$  (Fig. 27A) reveals that they can be reasonably well fit by the sum of two exponentials, yielding one closing rate of  $0.05 \text{ s}^{-1}$ , possibly reflecting a low rate of  $\text{Mg}^{2+}$ -dependent ATP hydrolysis, and a lower rate of  $0.03 \text{ s}^{-1}$ , identical to the single exponential obtained for 0 mM free  $\text{Mg}^{2+}$ . If two distinct closing rates were firmly established, it would suggest that there are two distinct open states from which the channel can close, one in the presence, and one in the absence, of free  $\text{Mg}^{2+}$ . Examination of the



temperature dependence of that closing rate might help further analysis. But, even if  $0.03 \text{ s}^{-1}$  is an upper limit for the dissociation rate of ATP, if the rate of ATP binding is high (i.e., approaching the diffusion limit), then the intrinsic binding affinity for ATP at NBD2 must be extremely high. An NBD2 binding affinity for ATP in the nM- $\mu$ M range would provide a satisfying explanation for the observation (Figs. 19-21) that the [ATP] dependence of channel  $P_o$  is well fit by Michaelis-Menten kinetics (Gunderson & Kopito, 1994; Venglarik et al., 1994; Winter et al., 1994) rather than some more complex function, and that only channel closed time varies with [ATP]. Thus, once the channel is opened by ATP hydrolysis at NBD1, the binding of ATP at NBD2 would not be limited by concentration, and the channel closing rate would be governed by the rate-limiting step in the NBD2 ATP hydrolysis cycle, or by dissociation of the hydrolysis products from NBD1.



## BIBLIOGRAPHY

- Almers, W., McCleskey, E.W. (1984) Non-selective conductance in calcium channels of frog muscle: calcium selectivity in a single-file pore. *Journal of Physiology* 353:585-608
- Ames, G.F., Lecar, F. (1992) ATP-dependent bacterial transporters and cyclic fibrosis: analogy between channels and transporters. *FASEB Journal* 6:2660-2666
- Andersen, O.S., Koeppe, R.E., II. (1992) Molecular determinants of channel function. *Physiological Reviews* 72:S89-S158
- Anderson, M.P., Berger, H.A., Rich, D.P., Gregory, R.J., Smith, A.E., Welsh, M.J. (1991a) Nucleoside triphosphates are required to open the CFTR chloride channel. *Cell* 67:775-784
- Anderson, M.P., Gregory, R.J., Thompson, S., Souza, D.W., Paul, S., Mulligan, R.C., Smith, A.E., Welsh, M.J. (1991b) Demonstration that CFTR is a chloride channel by alteration of its anion selectivity. *Science* 253:202-205
- Anderson, M.P., Welsh, M.J. (1991) Calcium and cAMP activate different chloride channels in the apical membrane of normal and cystic fibrosis epithelia. *Proc. Natl. Acad. Sci.* 88:6003-6007
- Anderson, M.P., Welsh, M.J. (1992) Regulation by ATP and ADP of CFTR chloride channels that contain mutant nucleotide-binding domains. *Science* 257:1701-1704
- Arreola, J., Melvin, J.E., Begenisich, T. (1995) Volume-activated chloride channels in rat parotid acinar cells. *Journal of Physiology* 484:677-687



- Bahinski, A., Nairn, A.C., Greengard, P., Gadsby, D.C. (1989a) Chloride conductance regulated by cyclic AMP-dependent protein kinase in cardiac myocytes. *Nature* 340:718-721
- Bahinski, A., Nairn, A.C., Greengard, P., Gadsby, D.C. (1989b) Chloride conductance regulated by protein kinase A in cardiac myocytes. *Journal of Physiology* 418:32P
- Bajnath, R.B., Groot, J.A., De Jonge, H.R., Kansen, M., Bijman, J. (1993) Synergistic activation of non-rectifying small-conductance chloride channels by forskolin and phorbol esters in cell-attached patches of the human colon carcinoma cell line HT-29cl.19A. *Pflügers Archiv* 425:100-108
- Barry, P.H., Diamond, J.M. (1970) Junction potentials, electrode standard potentials, and other problems in interpreting electrical properties of membranes. *Journal of Membrane Biology* 3:93-122
- Barry, P.H., Lynch, J.W. (1991) Liquid Junction Potentials and small cell effects in patch-clamp analysis. *Journal of Membrane Biology* 121:101-117
- Baukrowitz, T., Hwang, T.-C., Nairn, A.C., Gadsby, D.C. (1994) Coupling of CFTR Cl channel gating to an ATP hydrolysis cycle. *Neuron* 12:473-482
- Bean, C.P. (1972) The physics of porous membranes-neutral pores. In: *Membranes: A Series of Advances*. G. Eisenman, editor. Marcel Dekker Inc., New York
- Bear, C., Canhui, L., Kartner, N., Bridges, R.J., Jensen, T.J. (1992) Purification and functional reconstitution of the cystic fibrosis transmembrane conductance regulator (CFTR). *Cell* 68:809-818
- Bear, C.E., Duguay, F., Naismith, A.L., Kartner, N., Hanrahan, H.W., Riordan, J.R. (1991) Cl<sup>-</sup> channel activity in *Xenopus* oocytes expressing the cystic fibrosis gene. *Journal of Biological Chemistry* 266:19142-19145





- Begenisich, T. (1992) Ion channel selectivity, permeation, and block. *In: Methods in Enzymology*. B. Rudy and L.E. Iverson, editors. pp. 92-100. Academic Press, San Diego
- Belles, B., Malecot, C.O., Hescheler, J., Trautwein, W. (1988) "Rundown" of the Ca current during whole-cell recordings in guinea-pig heart cells: role of phosphorylation and intracellular calcium. *Pflügers Archiv* 411:353-360
- Benson, L.N., Newth, C.J.L., Desouza, M., Lobraico, R., Kartodihardjo, W., Corkey, C., Gilday, D., Olley, P.M. (1984) Radionuclide assessment of right and left ventricular function during bicycle stress in young patients with cystic fibrosis. *Am. Rev. Resp. Dis.* 130:987-992
- Berger, H.A., Andersen, M.P., Gregory, R.J., Thompson, S., Howard, P.W., Maurer, R.A., Mulligan, R., Smith, A.E., Welsh, M.J. (1991) Identification and regulation of the CFTR-generated chloride channel. *Journal of Clinical Investigation* 88:1422-1431
- Berger, H.A., Travis, S.M., Welsh, M.J. (1993) Regulation of the cystic fibrosis transmembrane conductance regulator by specific kinases and protein phosphatases. *Journal of Biological Chemistry* 268:2037-2047
- Bers, D.M. (1994) A practical guide to the preparation of  $\text{Ca}^{2+}$  buffers. *Methods in Cell Biology* 40:3-29
- Boat, T.F., Welsh, M.J., Beaudet, A.L. (1989) Cystic Fibrosis. *In: The Metabolic Basis of Inherited Disease*. W.S. Sly and D. Valle, editors. McGraw-Hill, Inc., New York
- Bormann, J., Hamill, O.P., Sakmann, B. (1987) Mechanism of anion permeation through channels gated by glycine and  $\gamma$ -aminobutyric acid in mouse cultured spinal neurones. *Journal of Physiology* 385:243-286



- Carson, M.R., Travis, S.M., Welsh, M.J. (1995) The two nucleotide-binding domains of cystic fibrosis transmembrane conductance regulator (CFTR) have distinct functions in controlling channel activity. *Journal of Biological Chemistry* 270:1711-1717
- Chabre, M. (1990) Aluminofluoride and beryllifluoride complexes: new phosphate analogs in enzymology. *Trends in Biological Sciences* 15:6-10
- Chang, X.-B., Tabcharani, J.A., Hou, Y.X., Jensen, T.J., Kartner, N., Alon, N., Hanrahan, J.W., Riordan, J.R. (1993) Protein kinase A (PKA) still activates CFTR chloride channels after mutagenesis of all 10 PKA consensus phosphorylation sites. *Journal of Biological Chemistry* 268:11304-11311
- Chao, A.C., de Sauvage, F.J., Dong, Y.-J., Wagner, J.A., Goeddel, D.V., Gardner, D.V. (1994) Activation of intestinal CFTR Cl<sup>-</sup> channel by heat-stable enterotoxin and guanylin via cAMP-dependent protein kinase. *EMBO Journal* 13:1065-1072
- Cheng, H.-C., Kemp, B.E., Pearson, R.B., Smith, A.J., Miscon, L., Van Patten, S.C., Walsh, D.A. (1986) A potent synthetic peptide inhibitor of the cAMP-dependent protein kinase. *Journal of Biological Chemistry* 261:989-992
- Cheng, S.H., Rich, D.P., Marshall, J., Gregory, R.J., Welsh, M.J., Smith, A.E. (1991) Phosphorylation of the R domain by cAMP-dependent protein kinase regulates the CFTR chloride channel. *Cell* 66:1027-1036
- Cliff, W.H., Frizzell, R.A. (1990) Separate Cl<sup>-</sup> conductances activated by cAMP and Ca<sup>2+</sup> in Cl<sup>-</sup> secreting epithelial cells. *Proc. Natl. Acad. Sci.* 87:4956-4960
- Cliff, W.H., Schoumacher, R.A., Frizzell, R.A. (1992) cAMP-activated Cl channels in CFTR-transfected cystic fibrosis pancreatic epithelial cells. *American Journal of Physiology* 262:C1154-C1160



- Cohen, B.N., Labarca, C., Davidsnon, N., Lester, H.A. (1992) Mutations in M2 alter the selectivity of the mouse nicotinic acetylcholine receptor for organic and alkali metal cations. *Journal of General Physiology* 100:373-400
- Cohen, P. (1988) Protein phosphorylation and hormone action. *Proceedings of the Royal Society of London, Series B* 234:115-144
- Collier, M.L., Warth, J.D., Geary, Y., Hart, P., Horowitz, B., Hume, J.R. (1996) Expression and regulation of cardiac (exon 5-) CFTR chloride channels in *Xenopus* oocytes by PKA and PKC. *Biophysical Journal* 70:A127
- Collins, A., Somlyo, A.V., Hilgemann, D.W. (1992a) The giant cardiac membrane patch method: stimulation of outward  $\text{Na}^+$ - $\text{Ca}^{2+}$  exchange current by MgATP. *Journal of Physiology* 454:27-57
- Collins, F.S. (1992b) Cystic Fibrosis: Molecular biology and therapeutic implications. *Science* 256:774-779
- Coronado, R., Miller, C. (1982) Conduction and block by organic cations in a  $\text{K}^+$ -selective channel from sarcoplasmic reticulum incorporated into planar lipid bilayers. *Journal of General Physiology* 79:529-547
- Cukierman, S., Yellen, G., Miller, C. (1985) The  $\text{K}^+$  channel of sarcoplasmic reticulum: a new look at  $\text{Cs}^+$  block. *Biophysical Journal* 48:477-484
- Dalemans, W., Barbry, P., Champigny, G. (1991) Altered chloride ion channel kinetics associated with the  $\Delta\text{F508}$  cystic fibrosis mutation. *Nature* 354:526-528
- Desilets, M., Baumgarten, C.M. (1986)  $\text{K}^+$ ,  $\text{Na}^+$ , and  $\text{Cl}^-$  activities in ventricular myocytes isolated from the rabbit heart. *American Journal of Physiology* 251:C197-208



- Diamond, J.M., Wright, E.M. (1969) Biological membranes: the physical basis of ion and nonelectrolyte selectivity. *Annual Review of Physiology* 31:581-646
- Dousmanis, A.G., Gadsby, D.C. (1994) Anion permeability sequence of the open cardiac CFTR Cl channel. *Biophysical Journal* 66:A361
- Dousmanis, A.G., Gadsby, D.C. (1996)  $[Mg^{2+}]$  governs CFTR  $Cl^-$  channel opening and closing rates, confirming hydrolysis of two ATP molecules per gating cycle. *Biophysical Journal* 70:A127
- Drumm, M.L., Wilkinson, D.J., Smit, L.S., Worrell, R.T., Strong, T.V., Frizzell, R.A., Dawson, D.C., Collins, F.S. (1991) Chloride conductance expressed by  $\Delta F508$  and other mutants CFTRs in *Xenopus* oocytes. *Science* 254:1797-1799
- Dulhanty, A.M., Riordan, J.R. (1994) Phosphorylation by cAMP-dependent protein kinase causes a conformational change in the R domain of the cystic fibrosis transmembrane conductance regulator. *Biochemistry* 33:472-4079
- Dwyer, T.M., Adams, D.J., Hille, B. (1980) The permeability of the endplate channel to organic metal cations in frog muscle. *Journal of General Physiology* 75:469-492
- Ehara, T., Ishihara, K. (1990) Anion channels activated by adrenaline in cardiac myocytes. *Nature* 347:284-286
- Ehara, T., Matsuura, H. (1993) Single-channel study of the cyclic AMP-regulated chloride current in guinea-pig ventricular myocytes. *Journal of Physiology* 464:307-320
- Eisenman, G., Dani, J.A. (1987) An introduction to molecular structure and permeability of ion channels. *Annual Review of Biophysics and Biophysical Chemistry* 16:205-226





- Eisenman, G., Horn, R. (1983) Ionic selectivity revisited: the role of kinetic and equilibrium processes in ion permeation through channels. *Journal of Membrane Biology* 76:197-225
- Fischmeister, R., Shrier, A. (1989) Interactive effects of isoprenaline, forskolin, and acetylcholine on  $\text{Ca}^{2+}$  current in frog ventricular myocytes. *Journal of Physiology* 417:231-239
- Franciolini, F., Nonner, W. (1987) Anion and cation permeability of a chloride channel in rat hippocampal neurons. *Journal of General Physiology* 90:453-478
- French, P.J., Bijman, J., Edixhoven, M., Vaandrager, A.B., Scholte, B.J., Lohmann, S.M., Nairn, A.C., De Jonge, H.R. (1995) Isotype-specific activation of cystic fibrosis transmembrane conductance regulator-chloride channels by cGMP-dependent protein kinase II. *Journal of Biological Chemistry* 270:26626-26631
- Gadsby, D.C., Nagel, G., Hwang, T.-C. (1995) The CFTR chloride channel of mammalian heart. *Annual Review of Physiology* 57:387-416
- Gadsby, D.C., Nairn, A.C. (1994) Regulation of CFTR channel gating. *Trends in Biochemical Sciences* 19:513-518
- Gilman, A.G. (1987) G proteins: transducers of receptor-generated signals. *Annual Review of Biochemistry* 56:615-649
- Gray, M.A., Pollard, C.E., Harris, A., Coleman, L., Greenwell, J.R., Argent, B.E. (1990) Anion selectivity and block of the small-conductance chloride channel on pancreatic duct cells. *American Journal of Physiology* 259:C752-C761



- Gregory, R.J., P, R.D., Cheng, S.H., Souza, D.W., Paul, S., Manavalan, P., Anderson, M.P., J, W.M., E, S.A. (1991) Maturation and function of cystic fibrosis transmembrane conductance regulator variants bearing mutations in putative nucleotide-binding domains 1 and 2. *Molecular and Cellular Biology* 11:3886-3893
- Gunderson, K.L., Kopito, R. (1995) Conformational states of CFTR associated with channel gating: the role of ATP binding and hydrolysis. *Cell* 82:231-239
- Gunderson, K.L., Kopito, R.R. (1994) Effects of pyrophosphate and nucleotide analogs suggest a role for ATP hydrolysis in cystic fibrosis transmembrane regulator channel gating. *Journal of Biological Chemistry* 269:19349-19353
- Halm, D.R., Frizzell, R.A. (1992) Anion permeation in an apical membrane chloride channel of a secretory epithelial cell. *Journal of General Physiology* 99:339-366
- Hanosh, A., Cutting, G.R. (1993) Genotype/phenotype relationships in cystic fibrosis. In: Cystic Fibrosis-Current Topics. J.A. Dodge, B.D.J. H, and J.H. Widdicombe, editors. pp. 69-89. John Wiley & Sons, West Sussex
- Harvey, R.D. (1993) Effects of stilbene-disulfonic derivatives on the cAMP-regulated chloride current in cardiac myocytes. *Pflügers Archiv* 422:436-442
- Harvey, R.D., Clark, C.D., Hume, J.R. (1990) Chloride current in mammalian cardiac myocytes. *Journal of General Physiology* 95:1077-1102
- Harvey, R.D., Hume, J.R. (1989) Autonomic regulation of a chloride current in heart. *Science* 244:983-985



- Harvey, R.D., Hume, J.R. (1990) Histamine activates the chloride current in cardiac ventricular myocytes. *Journal of Cardiovascular Electrophysiology* 1:309-317
- Haws, C., Krouse, M.E., Xia, Y., Gruenhardt, D.C., Wine, J.J. (1992) CFTR channels in immortalized human airway cells. *American Journal of Physiology* 263:L692-L707
- Herzig, S., Patil, P., Neumann, J., Staschen, C.-M., Yue, D.T. (1993) Mechanisms of  $\beta$ -adrenergic stimulation of cardiac  $\text{Ca}^{2+}$  channels revealed by discrete-time Markov analysis of slow gating. *Biophysical Journal* 65:1599-1612
- Hescheler, J., Kameyama, M., Trautwein, W. (1986) On the mechanism of muscarinic inhibition of the cardiac Ca current. *Pflügers Archiv* 407:182-189
- Hess, P., Tsien, R.W. (1984) Mechanism of ion permeation through calcium channels. *Nature* 356:441-443
- Higgins, C. (1992) ABC transporters: from microorganisms to man. *Annual Review of Cell Biology* 8:67-113
- Hilgemann, D.W. (1989) Giant excised cardiac sarcolemmal membrane patches: sodium and sodium-calcium exchange currents. *Pflügers Archiv* 415:247-249
- Hilgemann, D.W. (1990) Regulation of cardiac Na-Ca exchange in giant excised sarcolemmal membrane patches. *Nature* 344:242-245
- Hilgemann, D.W. (1995) The giant membrane patch. In: Single Channel Recording. B. Sakmann and E. Neher, editors. Plenum Press, New York



- Hilgemann, D.W., Nagel, G.A., Gadsby, D.C. (1991) Na/K pump current in giant membrane patches excised from ventricular myocytes. *In: The Sodium Pump: Recent Developments*. P. DeWeer and J.H. Kaplan, editors. pp. 543-547. Rockefeller University Press, New York
- Hille, B. (1972) The permeability of the sodium channel to metal cations in myelinated nerve. *Journal of General Physiology* 59:637-659
- Hille, B. (1973) Potassium channels in myelinated nerve: selective permeability to small cations. *Journal of General Physiology* 61:669-686
- Hille, B. (1975a) Ionic selectivity of Na and K channels on nerve membranes. *In: Membranes: A Series of Advances*. G. Eisenman, editor. pp. 255-323. Marcel Dekker, Inc., New York
- Hille, B. (1975b) Ionic selectivity, saturation, and block in sodium channels: a four barrier model. *Journal of General Physiology* 66:535-560
- Hille, B. (1992) *Ionic Channels of Excitable Membranes*. Sinauer Associates, Inc, Sunderland, MA
- Honkanen, R.E., Zwiller, J., Moore R.E., Daily S., Khatra, B.S., Dukelow, M., Boynton, A.L. (1990) Characterization of mrocystin-LR, a potent inhibitor of type 1 and type 2a protein phosphatases. *Journal of Biological Chemistry* 265:19401-19404
- Horie, M., Hwang, T.-C., Gadsby, D.C. (1992) Pipette GTP is essential for receptor-mediated regulation of Cl<sup>-</sup> current in dialysed myocytes from guinea-pig ventricle. *Journal of Physiology* 455:235-246
- Horowitz, B., Tsung, S.S., Hart, P., Levesque, P.C., Hume, J.R. (1993) Alternative splicing of CFTR Cl channels in heart. *American Journal of Physiology* 264:H2214-H2220





- Hwang, T.-C., Gadsby, D.C. (1994) Chloride ion channels in mammalian heart cells. *In: Current Topics in Membranes*. W.B. Guggino, editor. pp. 317-346. Academic Press
- Hwang, T.-C., Horie, M., Dousmanis, A.G., Gadsby, D.C. (1992a) Interactive modulation of PKA-regulated chloride current by forskolin, Gs, and Gi in guinea pig ventricular myocytes. *Biophysical Journal* 61:A395
- Hwang, T.-C., Horie, M., Dousmanis, A.G., Gadsby, D.C. (1992b) Regulation of PKA-activated Cl conductance in guinea pig ventricular myocytes: whole-cell studies. *Journal of General Physiology* 100:69a
- Hwang, T.-C., Horie, M., Gadsby, D.C. (1993) Functionally distinct phospho-forms underlie incremental activation of protein kinase-regulated Cl<sup>-</sup> conductance in mammalian heart. *Journal of General Physiology* 101:629-650
- Hwang, T.-C., Horie, M., Nairn, A., Gadsby, D.C. (1992c) Role of GTP-binding proteins in the regulation of mammalian cardiac chloride conductance. *Journal of General Physiology* 99:465-489
- Hwang, T.-C., Nagel, G., Nairn, A., Gadsby, D.C. (1994) Regulation of the gating of cystic fibrosis transmembrane conductance regulator Cl channels by phosphorylation and ATP hydrolysis. *Proc. Natl. Acad. Sci.* 91:4698-4702
- Isenberg, G., Klöckner, U. (1982) Calcium tolerant ventricular myocytes prepared by preincubation in a "KB Medium". *Pflügers Archiv* 395:6-18
- John, J., Rensland, H., Schlichting, I., Vetter, I., Borasio, G.D., Goody, R.S., Wittinghofer, A. (1993) Kinetic and structural analysis of the Mg<sup>2+</sup>-binding site of the guanine nucleotide-binding protein p21H-ras. *Journal of Biological Chemistry* 268:923-929



- Kaczmarek, L.K., Jennings, K.R., Strumwasser, F., Nairn, A.C., Wlatter, U., Wilson, F.D., Greengard, P. (1980) Microinjection of catalytic subunit of cyclic AMP-dependent protein kinase enhances calcium action potentials of bag cell neurons in cell culture. *Proc. Natl. Acad. Sci.* 77:7487-7491
- Kartner, N., Hanrahan, J.W., Jensen, T.J., Naismith, A.L., Sun, S., Ackerley, C.A., Reyes, E.F., Tsui, L.-C., Rommens, J.M., Bear, C.E., Riordan, J.R. (1991) Expression of the cystic fibrosis gene in non-epithelial invertebrate cells produces a regulated anion conductance. *Cell* 64:681-691
- Kerem, E., Corey, M., Kerem, B., Rommens, J., Markiewicz, D., Levison, H., Tsui, L.-C., Durie, P. (1990) The relation between genotype and phenotype in cystic fibrosis-analysis of the most common mutation ( $\Delta F508$ ). *New England Journal of Medicine* 323:1517-1522
- Levesque, P.C., Clark, C.D., Zakarov, S.I., Rosenshtraukh, L.V., Hume, J.R. (1993) Anion and cation modulation of the guinea-pig ventricular action potential during  $\beta$ -adrenergic stimulation. *Pflügers Archiv* 424:54-62
- Levesque, P.C., Hart, P.J., Hume, J.R., Kenyon, J.L., Horowitz, B. (1992) Expression of cystic fibrosis transmembrane regulator  $Cl^-$  channels in heart. *Circulation Research* 71:1002-1007
- Lin, M., Nairn, A.C., Guggino, S.E. (1992) cGMP-dependent protein kinase regulation of a chloride channel in T84 cells. *American Journal of Physiology* 262:C1304-1312
- Manavalan, P., Dearborn, D.G., McPherson, J.M., Smith, A.E. (1995) Sequence homologies between nucleotide binding regions of CFTR and G-proteins suggest structural and functional similarities. *FEBS Letters* 366:87-91



- Martell, A.E., Smith, R.M. (1989) Critical Stability Constants. Plenum Press, New York
- Marty, A., Neher, E. (1995) Tight-seal whole-cell recording. *In: Single-Channel Recording*. B. Sakmann and E. Neher, editors. pp. 31-52. Plenum Press, New York
- Matsuoka, S., Ehara, T., Noma, A. (1990) Chloride-sensitive nature of the adrenaline-induced current in guinea-pig cardiac myocytes. *Journal of Physiology* 425:579-598
- Nagel, G., Hwang, T.-C., Nastiuk, K.L., Nairn, A.C., Gadsby, D.C. (1992) The protein kinase A-regulated cardiac Cl<sup>-</sup> channel resembles the cystic fibrosis transmembrane conductance regulator. *Nature* 360:81-84
- Nakao, M., Gadsby, D.C. (1989) [Na] and [K] dependence of the Na/K pump current-voltage relationships in guinea-pig ventricular myocytes. *Journal of General Physiology* 94:539-565
- Ono, K., Fozzard, H.A. (1993) Two phosphatase sites on the Ca<sup>2+</sup> channel affecting different kinetic functions. *Journal of Physiology* 470:73-84
- Ono, K., Tareen, F.M., Yoshida, A., Noma, A. (1992) Synergistic action of cyclic GMP on catecholamine-induced chloride current in guinea-pig ventricular cells. *Journal Of Physiology* 453:647-661
- Overholt, J.L., Harvey, R.D. (1992) Ionic selectivity of cAMP dependent chloride channels in isolated ginea pig ventricular myocytes. *Biophysical Journal* 61:A442
- Overholt, J.L., Hobert, M.E., Harvey, R.D. (1993) On the mechanism of rectification of the isoproterenol-activated chloride current in guinea-pig ventricular myocytes. *Journal of General Physiology* 102:871-895



- Pai, E.F., Krengel, U., Petsko, G.A., Goody, R.S., Kabsch, W., Wittinghofer, A. (1990) Refined crystal structure of the triphosphate conformation of H-ras p21 at 1.35 Å resolution: implications for the mechanism of GTP hydrolysis. *EMBO* 9:2351-2359
- Parsons, T.D., Lagrutta, A., White, R.E., Hartzell, H.C. (1991) Regulation of Ca<sup>2+</sup> current in frog ventricular cardiomyocytes by 5'-guanylylimidodiphosphate and acetylcholine. *Journal of Physiology* 432:593-620
- Pearson, R.B., Kemp, B.E. (1991) Protein kinase phosphorylation site sequences and consensus specificity motifs: tabulations. *Methods in Enzymology* 200:62-81
- Picciotto, M., Cohn, J., Bertuzzi, G., Greengard, P., Nairn, A. (1992) Phosphorylation of the cystic fibrosis transmembrane conductance regulator. *Journal of Biological Chemistry* 267:12742-12752
- Prat, A.G., Xiao, Y.-F., Ausiello, D.A., Cantiello, H.F. (1995) cAMP-independent regulation of CFTR by the cytoskeleton. *American Journal of Physiology* 268:C1552-C1561
- Quinton, P.M. (1990) Cystic Fibrosis, a disease in electrolyte transport. *FASEB Journal* 4:2709-2717
- Quinton, P.M., Reddy, M.M. (1989) Cl<sup>-</sup> conductance and acid secretion in the human sweat duct. In: *Annals of the New York Academy of Sciences*. pp. 438-446
- Quinton, P.M., Reddy, M.M. (1992) Control of CFTR chloride conductance by ATP levels through non-hydrolytic binding. *Nature* 360:79-81
- Reddy, M.M., Bell, C.L., Quinton, P.M. (1991) Anion selectivity of Cl<sup>-</sup> conductance affected by cystic fibrosis as an in vitro diagnostic tool. *Pediatric Pulmonology* 6:A107





- Riordan, J.R., Rommens, J.M., Kerem, B.-S., Alon, N., Rozmahel, R., Grzelczak, Z., Zielenski, J., Lok, S., Plavsic, N., Chou, J.-L., Drumm, M.L., Iannuzzi, M.C., Collins, F.S., Tsui, L.-C. (1989) Identification of the cystic fibrosis gene: cloning and characterization of complementary DNA. *Science* 245:1066-1073
- Robinson, R.A., Stokes, R.H. (1965) *Electrolyte Solutions*. Butterworth, London
- Seamon, K.B., Daly, J.W. (1986) Forskolin: its biological and chemical properties. *In: Advances in Cyclic Nucleotide and Protein Phosphorylation Research*. pp. 1-150
- Sheppard, D.N., Welsh, M.J. (1992) Effect of ATP-sensitive K<sup>+</sup> channel regulators on cystic fibrosis transmembrane conductance regulator chloride currents. *Journal of General Physiology* 100:573-591
- Smit, L.S., Wilkinson, D.J., Mansoura, M.K., Collins, F.S., Dawson, D.C. (1993) Functional roles of the nucleotide-binding folds in the activation of the cystic fibrosis transmembrane conductance regulator. *Proc. Natl. Acad. Sci.* 90:9963-9967
- Soejima, M., Noma, A. (1984) Mode of regulation of the ACh-sensitive K<sup>+</sup> channel by the muscarinic receptor in rabbit atrial cells. *Pflügers Archiv.* 400:421-431
- Sullivan, M.M., Moss, R.B., Hindi, R.D., Lewiston, N.J. (1986) Supraventricular tachycardia in patients with cystic fibrosis. *Chest* 90:239-242
- Sullivan, S.K., Agellon, L.B., Schick, R. (1995) Identification and partial characterization of a domain in CFTR that may bind cyclic nucleotides directly. *Current Biology* 5:1159-1167



- Tabcharani, J.A., Chang, X.-B., Riordan, J.R., Hanrahan, J.W. (1991) Phosphorylation-regulated Cl<sup>-</sup> channel in CHO cells stably expressing the cystic fibrosis gene. *Nature* 352:628-631
- Tabcharani, J.A., Chang, X.-B., Riordan, J.R., Hanrahan, J.W. (1992) The cystic fibrosis transmembrane regulator chloride channel: iodide block and permeation. *Biophysical Journal* 62:1-4
- Tabcharani, J.A., Hanrahan, J.W. (1993) Permeation in the cystic fibrosis transmembrane regulator (CFTR). *Biophysical Journal* 64:A17
- Tabcharani, J.A., Low, W., Elie, D., Hanrahan, J.W. (1990) Low-conductance chloride channel activated by cAMP in the epithelial cell line T<sub>84</sub>. *FEBS Letters* 270:157-164
- Tabcharani, J.A., Rommens, J.M., Hou, Y.-X., Chang, X.-B., Tsui, L.-C., Riordan, J.R., Hanrahan, J.W. (1993) Multi-ion pore behaviour in the CFTR chloride channel. *Nature* 366:79-82
- Takai, A., Bialojan, C., Troschka, M., Rüegg, J.C. (1987) Smooth muscle myosin phosphatase inhibition and force enhancement by black sponge toxin. *FEBS Letters* 217:81-84
- Takano, M., Noma, A. (1992) Distribution of the isoprenaline-induced chloride current in rabbit heart. *Pflügers Archiv* 420:223-226
- Tareen, F.M., Ono, K., Noma, A., Ehara, T. (1991)  $\beta$ -Adrenergic and muscarinic regulation of the chloride current in guinea-pig ventricular cells. *Journal of Physiology* 440:225-241
- Taussig, L.M., Landau, L.I., Marks, M.I. (1984) Respiratory System. In: Cystic Fibrosis. L.M. Taussig, editor. Thieme Stratton, New York



- Tien, X.Y., Brasitus, T.A., Kaetzel, M.A., Dedman, J.R., Nelson, D.J. (1994) Activation of the cystic fibrosis transmembrane regulator by cGMP in the human colonic cancer cell line, Caco-2. *Journal of Biological Chemistry* 269:51-54
- Tominaga, M., Horie, M., Sasayama, S., Okada, Y. (1995) Glibenclamide, an ATP-sensitive K<sup>+</sup> channel blocker, inhibits cardiac cAMP-activated Cl<sup>-</sup> conductance. *Circulation Research* 77:417-423
- Tsui, L.-C. (1992) The spectrum of cystic fibrosis mutations. *Trends in Genetics* 8:392-398
- Tsui, L.-C., Markiewicz, D., Zielenski, J., Corey, M., Durie, P. (1993) Mutation Analysis in Cystic Fibrosis. In: Cystic Fibrosis-Current Topics. J.A. Dodge, D.J.H. Brock, and J.H. Widdicombe, editors. pp. 27-44. John Wiley & Sons, West Sussex
- Urbatsch, I.L., Al-Shawi, M.K., Senior, A.E. (1994) Characterization of the ATPase activity of purified chinese hamster P-glycoprotein. *Biochemistry* 33:7069-7076
- Urbatsch, I.L., Banumathi, S., Bhagat, S., Senior, A.E. (1995) Both P-glycoprotein nucleotide binding sites are catalytically active. *Journal of Biological Chemistry* 270:26956-26961
- Vaughn-Jones, R.D. (1979) Non-passive chloride distribution in mammalian heart muscle: micro-electrode measurement of the intracellular chloride activity. *Journal of Physiology* 295:83-109
- Venglarik, C.J., Schultz, B.D., Frizzell, R.A., Bridges, R.J. (1994) ATP alters current fluctuations of cystic fibrosis transmembrane conductance regulator: evidence for a three-state activation mechanism. *Journal of General Physiology* 104:123-146
- Walsh, K.B., Long, K.J. (1992) Inhibition of heart calcium and chloride currents by sodium iodide. *Journal of General Physiology* 100:847-865



- Warth, J.D., Hart, P., Horowitz, B., Hume, J.R. (1996a) Inhibition of CFTR gene expression reduces cAMP-dependent Cl<sup>-</sup> currents in cultured guinea-pig ventricular myocytes. *Biophysical Journal* 70:A127
- Warth, J.D., Collier, M., Hart, P., Geary, Y., Gelband, C.H., Chapman, T., Horowitz, B., Hume, J.R. (1996b) CFTR chloride channels in human and primate heart. *Cardiovascular Research* (in press)
- Welsh, M.J., Anderson, M.P., Rich, D.P., Berger, H.A., Denning, G.M., Ostedgaard, L.S., Sheppard, D.N., Cheng, S.H., Gregory, R.J., Smith, A.E. (1992) Cystic fibrosis transmembrane conductance regulator: a chloride channel with novel regulation. *Neuron* 8:821-829
- Welsh, M.J., Smith, A.E. (1993) Molecular mechanisms of CFTR chloride channel dysfunction in cystic fibrosis. *Cell* 73:1251-1254
- Wickman, K.D., Iniguez-Lluhi, J.A., Davenport, P.A., Tausig, R., Krapivinsky, G.B., Linder, M.E., Gilman, A.E., Clapham, D.E. (1994) Recombinant G-protein  $\beta\gamma$ -subunits activate the muscarinic-gated atrial potassium channel. *Nature* 368:255-257
- Winter, M.C., Sheppard, D.N., Carson, M.R., Welsh, M.J. (1994) Effect of ATP concentration on CFTR Cl<sup>-</sup> channels. *Biophysical Journal* 66:1398-1403
- Wright, E.M., Diamond, J.M. (1977) Anion selectivity in biological systems. *Physiological Reviews* 57:109-157
- Yellen, G. (1987) Permeation in potassium channels: implications for channel structure. *Annual Review of Biophysics and Biophysical Chemistry* 16:227-246
- Yount, R.G. (1975) ATP analogs. *Enzymology* 43:1-56







**End**